Materials for Hydrogen Storage and Synthesis of New Materials by Hydrogenation

Serhiy Luzan

Doctoral Thesis
Department of Physics
Umeå University
Umeå 2012

ISBN: 978-91-7459-463-8
Printed by KBC Service Center
Umeå, Sweden, 2012

Abstract

The search for new materials for hydrogen storage is important for the development of future hydrogen energy applications. In this Thesis, it is shown that new materials with interesting properties can be synthesized by the reaction of hydrogen with various nanocarbon precursors. The thesis consists of two parts. The first part is devoted to studies of hydrogen storage in some metal-organic frameworks (MOFs) and nanostructured carbon materials, while the second part describes synthesis of new materials by the reaction of hydrogen gas with various carbon materials (i.e. fullerene C_{60}, single-walled carbon nanotubes (SWCNTs), and fullerene C_{60} encapsulated inside SWCNTs (C_{60}@SWCNTs)).

Hydrogen adsorption was measured for a set of Zn- and Co-based MOFs at near ambient temperatures. MOFs synthesized using different metal clusters and organic connecting ligands allowed to study effects of different surface area, pore volume, and pore shapes on hydrogen storage parameters. Hydrogen adsorption values in the studied MOFs correlated well with surface area and pore volume but did not exceed 0,75wt.%. Therefore, new methods to improve the hydrogen storage capacity in MOFs were investigated. The addition of metal catalysts was previously reported to improve significantly hydrogen storage in MOFs. In this thesis the effect of Pt catalyst addition on hydrogen adsorption in MOF-5 was not confirmed. Contrary to previous reports, hydrogen adsorption in MOF-5 mixed/modified with Pt catalysts had fast kinetics, correlated well with surface area, and was on the same level as for unmodified MOF-5. New nanostructured carbon materials were synthesized by the reaction between fullerene C_{60} and coronene/anthracene. Despite negligible surface area these materials adsorbed up to 0,45wt.% of hydrogen at ambient temperatures.

The reaction of fullerene C_{60} with hydrogen gas was studied at elevated temperatures and hydrogen pressures. *In situ* gravimetric monitoring of the reaction was performed in a broad temperature interval with/without addition of metal catalysts (i.e. Pt and Ni). The reaction resulted in synthesis of hydrogenated fullerenes $C_{60}H_x$ (with $x \leq 56$) followed by fullerene cage fragmentation and collapse upon prolonged duration of hydrogen treatment. Possible mechanisms of C_{60} hydrogenation and fragmentation were discussed. It is demonstrated that reaction of SWCNTs with hydrogen gas at elevated temperatures and hydrogen pressures can be used for nanotube opening, purification from amorphous carbon, side-wall hydrogenation, and partial unzipping of SWCNTs. Some graphene nanoribbons (GNRs) were synthesized as the result of SWCNTs unzipping. A surprising ability of hydrogen to penetrate inside SWNTs and to react with encapsulated fullerene C_{60} was demonstrated.

Sammanfattning

Sökandet efter nya material för vätelagring är viktigt för utveckling av framtida väteenergitillämpningar. I denna avhandling visas att nya material med intressanta egenskaper kan syntetiseras genom reaktion av väte med olika nanokolprekursorer. Avhandlingen består av två delar. Den första delen ägnas åt studier av vätelagring i vissa metall-organiska fackverk (så kallade MOFs) och nanostrukturerade kolmaterial medan den andra delen beskriver syntes av nya material genom reaktion av vätgas med olika kolmaterial (dvs. fulleren C_{60}, enkelväggiga kolnanorör (SWCNTs) och fulleren C_{60} kapslat i SWCNTs (C_{60} @ SWCNTs)).

Väteadsorptionen mättes för ett antal Zn- och Co-baserade MOFs vid rumstemperatur. MOFs syntetiserades med hjälp av olika metallkluster och organiska ligander för att studera effekterna av olika yta, porvolym och porformer på vätelagringsparametrarna. Väteadsorptionsvärden i de studerade MOFs korrelerade väl med yta och porvolym, men översteg inte 0,75wt.%. Därför undersöktes nya metoder för att förbättra kapaciteten för vätelagring i MOFs. Tillsättning av metallkatalysatorer har tidigare rapporterats avsevärt förbättra vätelagring i MOFs. I denna avhandling kunde effekten av en tillsats av Pt-katalysator på väteadsorption i MOF-5 inte bekräftas. I motsats till tidigare rapporter hade väteadsorption i MOF-5 blandad/modifierad med Pt-katalysatorer snabb kinetik och korrelerade väl med arean, men var på samma nivå som för omodifierad MOF-5. Nya nanostrukturerade kolmaterial syntetiserades genom reaktion mellan fulleren C_{60} och coronene/antracene. Trots försumbar yta adsorberade dessa material upp till 0,45wt.% väte vid rumstemperatur.

Reaktionen av fulleren C_{60} med vätgas studerades vid förhöjda temperaturer och vätetryck. *In situ* gravimetrisk övervakning av reaktionen utfördes i ett brett temperaturintervall med/utan tillsats av metallkatalysatorer (dvs. Pt och Ni). Reaktionen resulterade i syntes av hydrogenerade fullerener $C_{60}H_x$ (med $x \leq 56$) följt av fragmentering och kollaps av fullerenstrukturen vid förlängd varaktighet av vätebehandlingen. Möjliga mekanismer för hydrering och fragmentering av C_{60} diskuteras. Det har visats att reaktionen mellan SWCNTs och vätgas vid förhöjda temperaturer och vätetryck kan användas för öppning av nanorör, borttagning av amorft kol, funktionalisering av sidoväggar och partiell "blixtlåsöppning" av SWCNTs. Reaktionen kan också syntetisera grafen-nanoband (GNRs) som en följd av att SWCNTs öppnas på längden. En överraskande stor förmåga för väte att tränga in i SWNT och där reagera med inkapslade fullerenmolekyler C_{60} demonstrerades.

List of publications

The thesis is based on the following publications which are reprinted with the kind permission of the publishers:

1. Thermal Decomposition of $C_{60}H_{18}$.
   Luzan S.M., Cataldo F., Tsybin Y.O., Talyzin A.V. *J. Phys. Chem. C*, **2009**, *113*, 13133-13138.
2. Hydrogen storage in Co- and Zn-based metal-organic frameworks at ambient temperature.
   Luzan S.M., Jung H., Chun H., Talyzin A.V. *Int. J. Hydrogen Energy*, **2009**, *34*, 9754-9759.
3. High-temperature reactions of C_{60} with polycyclic aromatic hydrocarbons.
   Martin N.M., Luzan S.M., Talyzin A.V. *Chem. Phys.*, **2010**, *368*, 49-57.
4. Hydrogen adsorption in Pt catalyst/MOF-5 materials.
   Luzan S.M. and Talyzin A.V. *Micropor. Mesopor. Mater.*, **2010**, *135*, 201-205.
5. Reaction of C_{60} with Hydrogen Gas: In Situ Monitoring and Pathways.
   Luzan S.M., Tsybin Y.O., Talyzin A.V. *J. Phys. Chem. C*, **2011**, *115*, 11484-11492.
6. Hydrogenation, Purification, and Unzipping of Carbon Nanotubes by Reaction with Molecular Hydrogen: Road to Graphene Nanoribbons.
   Talyzin A.V., Luzan S.M., Anoshkin I.V., Nashibulin A.G., Jiang H., Kauppinen E.I., Mikoushkin V.M. Shnitov V.V., Marchenko D.E., Noreus D. *ACS Nano*, **2011**, *5*, 5132-5140.
7. Effect of Catalysts on the Reaction of C_{60} with Hydrogen.
   Luzan S.M. and Talyzin A.V. *Fullerenes, Nanotubes, and Carbon Nanostructures*, **2012**, 20, 319-323.
8. Hydrogen-Driven Collapse of C_{60} Inside Single-Walled Carbon Nanotubes.
   Talyzin A.V., Luzan S.M., Anoshkin I.V., Nashibulin A.G., Jiang H., Kauppinen E.I. *Angew. Chem. Int. Ed.*, **2012**, 51, 4435-4439.

Besides, some interesting results can be found in the following papers which were not included in the thesis:

9. Pressure-Induced Insertion of Liquid Acetone into the Graphite Oxide Structure.
   Talyzin A.V. and Luzan S.M. *J. Phys. Chem. C*, **2010**, *114*, 7004-7006.
10. Comment to the "Response to "Hydrogen adsorption in Pt catalyst/MOF-5 materials" by Li et al [1]".
    Luzan S.M. and Talyzin A.V. *Micropor. Mesopor. Mater.*, **2011**, *139*, 216-218.
11. Coronene Fusion by Heat Treatment: Road to Nanographenes.
    Talyzin A.V., Luzan S.M., Leifer K., Akhtar S., Fetzer J., Cataldo F., Tsybin Y.O., Tai C.W., Dzwilewski A., Moons E. *J. Phys. Chem. C*, **2011**, *115*, 13207-13214.
12. Temperature dependent structural breathing of hydrated graphite oxide in H_2O.
    Talyzin A.V., Luzan S.M., Szabo T., Chernyshev D., Dmitriev V. *Carbon*, **2011**, *49*, 1894-1899.
13. Hydration of Graphite Oxide in Electrolyte and Non-Electrolyte Solutions.
    Luzan S.M. and Talyzin A.V. *J. Phys. Chem. C*, **2011**, *115*, 24611-24614.
14. Phase Transitions in Graphite Oxide Solvates at Temperatures Near Ambient.
    You S., Luzan S.M., Yu J., Sundqvist B., Talyzin A.V. *J. Phys. Chem. Letters*, **2012**, 3(7), 812-817.
15. Effect of synthesis method on solvation and exfoliation of graphite oxide.
    You S., Luzan S.M., Talyzin A.V. Submitted to *Carbon***.**

Table of contents

List of Abbreviations:

ACs	–	Activated carbons
AC	–	Alternating current
APPI FT-ICR	–	Atmospheric pressure photoionization Fourier transform ion cyclotron resonance
BCC	–	Body-centered cubic
BET	–	Brunauer-Emmett-Teller
BJH	–	Barrett, Joyner, and Halenda
BTB	–	Benzene tribenzoate
CCD	–	Charge coupled device
CNTs	–	Carbon nanotubes
CNTH	–	Carbon nanotube hydrogenated
CVD	–	Chemical vapour deposition
DFT	–	Density functional theory
DMF	–	N,N'-dimethylformamide
DOE	–	Department of energy
DSC	–	Differential scanning callorimetry
DTA	–	Differential thermal analysis
FCC	–	Face-centered cubic
FT-IR	–	Fourier transform infrared
GAI	–	Generalized adsorption isotherm
GCMC	–	Grand canonical Monte Carlo
GNFs	–	Graphite nanofibers
GNRs	–	Graphene nanoribbons
HCl	–	Hydrochloric acid
HPLC	–	High-performance liquid chromatography
IR	–	Infrared
IRMOFs	–	Isoreticular metal-organic frameworks
IUPAC	–	International union of pure and applied chemistry
MALDI TOF	–	Matrix-assisted laser desorption ionization time-of-flight
MOFs	–	Metal-organic frameworks
MS	–	Mass spectrometry
NMR	–	Nuclear magnetic resonance
PAHs	–	Polycyclic aromatic hydrocarbons
Pt/AC	–	Platinum catalyst supported on activated carbon
RT	–	Room temperature
SEM	–	Scanning electron microscopy
SWCNTs	–	Single-walled carbon nanotubes
TEM	–	Transmission electron microscopy
TGA	–	Thermo-gravimetric analysis
XPS	–	X-ray photoelectron spectroscopy
XRD	–	X-ray diffraction
1D/3D	–	1 dimensional/3 dimensional

1 Introduction

1.1 An overview of hydrogen storage: problems and targets

New alternative energy sources are required to replace fossil fuels, for example by wind and solar energy. One of the actively explored concepts is to convert solar energy directly to hydrogen and then to use hydrogen as an energy carrier and a fuel for e.g. cars. Considering that water covers about 71% of the Earth surface we have almost an unlimited source of hydrogen which is an ideal energy carrier. It has an extremely high gravimetrical energy density (142MJ/kg) which is at least three times larger than the equivalent value for liquid hydrocarbons (47MJ/kg). Hydrogen as the fuel is also environmentally friendly as the only exhaust product in both combustion and fuel cell engines is water vapour. Therefore, hydrogen is an attractive candidate for replacement of petrol or diesel in cars or other vehicles.

Hydrogen can be used as a fuel in cars with slightly modified combustion engines. However, combustion engines are not a sustainable solution due to relatively low efficiency of ~25%. On another hand, cars can be powered by fuel cells, electrochemical devices, which combine hydrogen and oxygen to produce electricity. Fuel cells convert hydrogen in electricity with an efficiency of 50-60% and release only water and heat as side products. The main obstacle for widespread application of fuel cells is the absence of sufficiently good and compact, light-weight hydrogen storage systems which are capable of delivering hydrogen gas to a fuel cell at nearly room temperature and at pressures not much higher than atmospheric pressure.

An average modern car equipped with a combustion engine needs approximately 30-35 liters of petrol or diesel to travel 500km. The combined weight of the fuel and the tank is about 80kg. A car equipped with a fuel cell engine would need about 5kg of hydrogen to travel the same distance. The problem is that 5kg of hydrogen at normal conditions (room temperature and atmospheric pressure) occupies ~56 000 liters of space which is equivalent to a balloon of 5m diameter[1, 2].

One possible solution is to pressurize hydrogen and to store it in high-pressure tanks. This relatively simple solution was already successfully tested on the market. City busses which are run by hydrogen were launched in Germany, Japan, and UK (see **Figure 1.1**). However, even if the pressure inside of tanks is increased up to 600bar the density of hydrogen is too low for automotive applications. Another option is to use liquid hydrogen. It increases a mass/volume ratio but a lot of energy is required to liquefy hydrogen and evaporation of hydrogen from storage container is unavoidable.

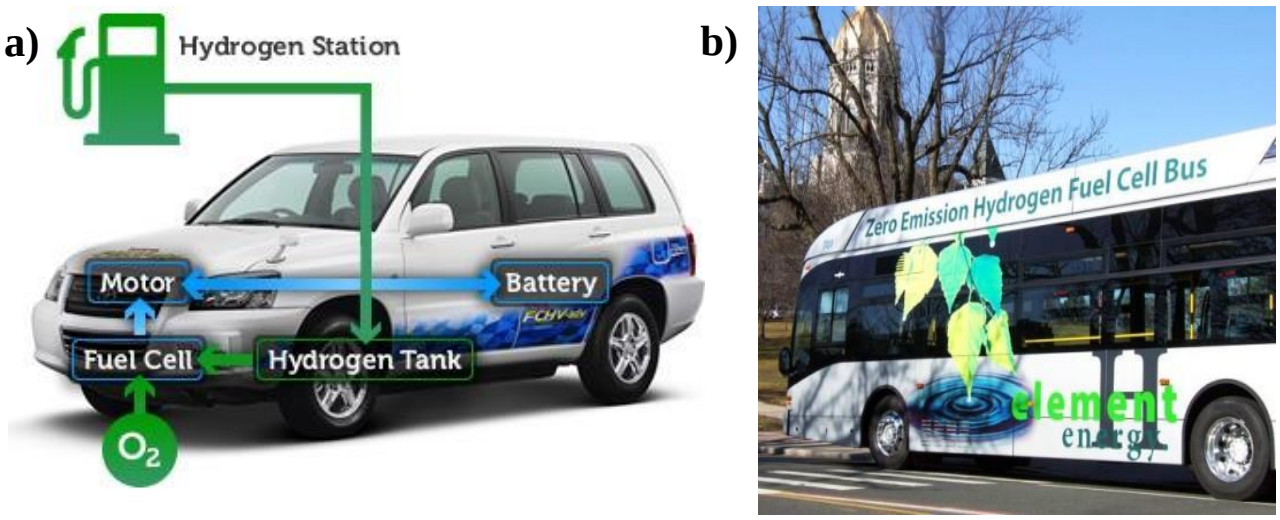

Figure 1.1. a) Schematic representation of a fuel cell vehicle[3]; b) a city bus with a fuel cell engine and hydrogen as a fuel[4].

Another possibility is to use some solid material which could adsorb and store hydrogen with high gravimetric and volumetric densities. It is well known that some metal hydrides exhibit hydrogen densities higher than in liquid hydrogen.

Storage Parameter	Units	2017	Ultimate
Gravimetric Capacity	wt.%	5,5	7,5
Volumetric Capacity	gH_2/L	40	70
Operating ambient temperature	ºC	-40/60	-40/60
Min/max delivery temperature	ºC	-40/85	-40/85
Cycle life (1/4 tank to full)	cycles	1500	1500
Min delivery pressure from storage system *	bar	5	3
Max delivery pressure from storage system *	bar	12	12
System fill time (for 5kg of H_2)	min	3,3	2,5

Table 1.1. Technical system targets for on-board hydrogen storage (information from the U.S. DOE web-page[5]).

*- for fuel cell driven vehicles.

Main target parameters of the required hydrogen storage materials were formulated within the US Department of Energy program (see **Table 1.1**) and have become widely accepted by the

international scientific community. Current gravimetrical targets for hydrogen storage were set by DOE in 2009 to reach 5,5wt.% by 2017.

Hydrogen storage materials could be divided into two classes depending on the mechanism of hydrogen sorption: materials where adsorption is due to *physisorption* or due to *chemisorption*. In case of *physisorption*, molecular hydrogen is weakly bound to the surface of the material by van der Waals or hydrogen bonds. In case of *chemisorption*, H_2 molecules dissociate into atomic hydrogen which is then absorbed into the bulk forming stronger ionic or covalent bonds with the material. In the next sections we will review various materials studied for hydrogen storage, discuss their advantages and drawbacks, and list factors affecting hydrogen storage in those materials.

1.2 Materials for hydrogen storage

1.2.1 Hydrogen storage via physisorption

The physisorption mechanism suggests adsoption of molecular hydrogen on a surface via relatively weak van der Waals bonding. Several characteristic features of physisorption can be noted. The adsorption process is fast, i.e. the saturation is achieved within minutes after hydrogen pressure is stabilized, and fully reversible. Hydrogen is released when pressure is lowered and is adsorbed when pressure is increased again. Surface area is the main factor which controls hydrogen adsorption capacity of the material. The more surface area which is accessible for sorbate molecules the more sorbate molecules will be adsorbed on the sorbent surface. The most frequently studied sorbents are activated carbons, carbon nanostructured materials (e.g. fullerenes, carbon nanotubes, nanographene flakes), and metal-organic frameworks.

Carbon materials

Activated Carbons: activated carbons (ACs) is one of the most studied gas adsorption materials and also shows some of the best performances for storage of hydrogen. ACs are synthesized by carbonization of organic precursors followed by an activation step using e.g. annealing in an oxidizing atmosphere or chemical treatment. Such synthesis procedure results in materials with very high surface area (up to 3300m^2/g) which have superior hydrogen adsorption properties at 77 K. ACs were reported to adsorb about 6,0 wt.% of H_2 at 40 bar pressure at 77 K[6]. This experimental value is close to the maximal theoretically possible hydrogen adsorption value of 6,6 wt.% calculated for ACs[1]. Calculations were performed considering the maximum possible theoretical concentration of hydrogen molecules on a graphene sheet (~0,4H/C) and considering double side coverage of a graphene sheet by hydrogen. At ambient temperatures hydrogen adsorption in ACs normally does not exceed 1wt.% [7].

Carbon nanotubes: carbon nanotubes (CNTs) discovered in 1991[8] attracted a lot of attention as a promising material for hydrogen storage applications (see **Figure 1.2a**). Prior to hydrogen adsorption measurements nanotubes are typically subjected to some treatment to make the inner part accessible for gas penetration and to increase the accessible surface area. At liquid nitrogen temperatures CNTs adsorb up to 8,0wt.% of H_2[9]. However, at ambient temperatures CNTs were shown to store less than 1wt.% of H_2 at pressures up to 100bar[10, 11]. Experimental results are in good agreement with the most recent theoretical calculations which showed that hydrogen adsorption in those materials should not exceed 1wt.% at ambient temperature and moderate pressures[12].

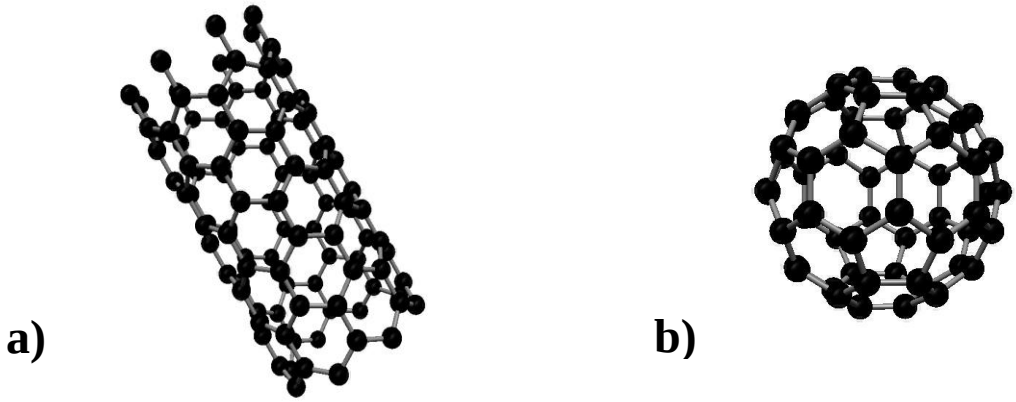

Figure 1.2. a) Single-walled carbon nanotube; b) buckminsterfullerene C_{60}.

A lot of research effort was recently concentrated on modification of CNTs with the aim of improving their hydrogen storage properties. For example, it was shown both theoretically[13] and experimentally[14] that defects induced on side-walls of CNTs improve their hydrogen adsorption capacity. Several methods were suggested in order to make defect CNTs, for example acid treatment[15], ball milling[16], plasma etching[17], and heat treatment in various environments (e.g. ammonia, oxygen, open air)[18, 19] were used.

It should be noted that many of early studies of hydrogen storage in CNTs (and some other carbon materials) reported significantly overestimated values for gravimetric capacity which later were proved to be erroneous due to various experimental errors. For example, Dillon *et al* (1997) reported hydrogen adsorption in low purity single-walled CNTs at ambient temperature in the range of 5-10wt.%[20]. For graphite nanofibers (GNFs), one of the reports claimed values as high as 67wt.% at 25ºC and 120bar of H_2 pressure[21]. This value of hydrogen adsorption is three times higher than the hydrogen content in methane CH_4 and suggests that about 12 hydrogen atoms are adsorbed on

one carbon atom on the CNT surface which is, of course, impossible. The latter example emphasizes that hydrogen adsorption measurements, which are performed according to procedures which are very simple at a first glance, is a very delicate experiment which requires a lot of considerations to avoid many different types of errors[22].

Fullerenes: in contrast to other carbon materials such as CNTs, ACs and graphite nanofibers (GNFs), bulk fullerene C_{60} powder shows negligible values of BET surface area (see **Figure 1.2b**)[23]. Nevertheless, solid C_{60} (fullerite) is able to store some hydrogen but the mechanism of this storage is more similar to intercalation than to physisorption. The face-centered cubic (FCC) structure of C_{60} has two kinds of interstitial sites: octahedral (d=4,12Å) and tetrahedral (d=2,24Å). The kinetic diameter of a hydrogen molecule is 2,9Å[24] which is less than the size of the octahedral holes. Hydrogen molecules diffuse into the lattice of C_{60} without dissociation and occupy octahedral holes. The kinetics of the diffusion process is more slow (could take tens of minutes) compared to normal physisorption where equilibrium is achieved within minutes. Another typical feature is the absence of a strong correlation of hydrogen storage capacity with temperature variations. The hydrogen storage capacity of C_{60} is limited to one H_2 molecule per octahedral void which results in about 0,1-0,2wt.% of H_2 observed over broad ranges of temperatures and pressure[25-27]. Using high-energy ball milling hydrogen adsorption was increased up to 0,7wt.% at room temperature and 300bar of hydrogen pressure[28]. It should be noted that along with improvement of hydrogen uptake authors observed an increase of the surface area of ball-milled fullerene C_{60} from less than $1m^2/g$ (below the detection limit) up to $255m^2/g$ after 48 hours of treatment and partial collapse of fullerene cage structure.

Graphene: graphene is another possible candidate as a hydrogen storage material. At the moment the only method which can be employed for synthesis of bulk amounts of powdered graphene-like material is the thermal exfoliation of graphite oxide[29]. It should be noted that materials produced by this method consist mostly of graphite sheets with a thickness of 2-15 graphene layers. This material is very similar to ACs but has a smaller surface area of the order of $600\text{-}1000m^2/g$. The hydrogen adsorption in a graphene-like material with a surface area of $640m^2/g$ was estimated as 0,72wt.% at 100bar and 298K which is on the same level as for ACs with comparable surface area[30].

Metal-Organic Framework Materials (MOFs)

Probably the most promising materials for hydrogen adsorption via physisorption are MOFs. MOFs are crystalline coordination polymers which consist of metal clusters connected by organic linkers (see **Figure 1.3**)[24]. Hydrogen adsorption properties of more than 200 MOFs were studied[31].

MOFs show some advantages as hydrogen adsorbents compared to other porous solids. They have an extremely high surface area with record values registered for MOF-200 and MOF-210 (a Langmuir surface area of 10400 m^2/g)[32]. Combining different organic ligands and ion clusters it is possible, in principle, to synthesize MOFs with an almost infinite number of geometrical and chemical variations of the structure. Additional hydrogen adsorption sites can be introduced into the structure of MOFs by post-synthetic modifications improving their hydrogen adsorption properties[33,34].

MOFs exhibit superior hydrogen adsorption properties at cryogenic temperatures (77K). For instance, MOF-210 has the highest hydrogen excess uptake of 8,6wt.% ever reported for physisorption. The record high values of the total uptake which takes into account the amount of hydrogen pressurized inside voids of the MOF's structure was 17,6wt.% at 77K and 80bar [35].

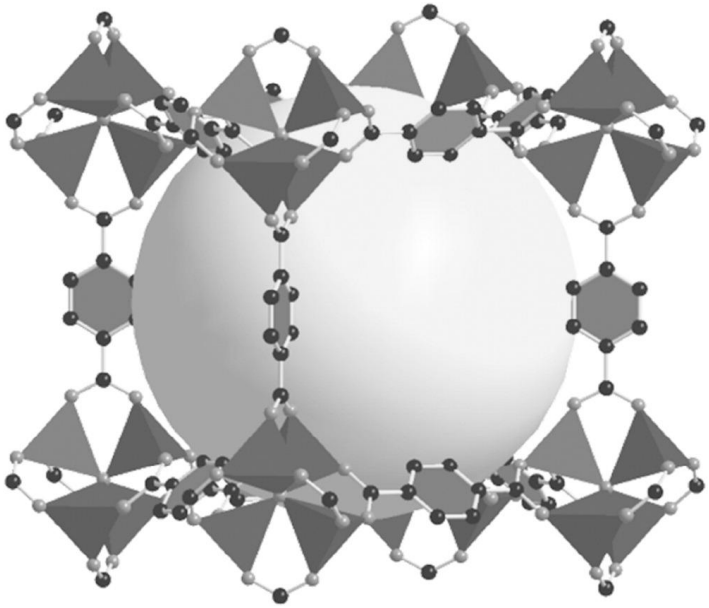

Figure 1.3. Structure of the well-known material MOF-5. Eight clusters, which contain four ZnO_4 tetrahedra units each, build up a unit cell and enclose a large cavity which can fit the yellow sphere with diameter of 18,5Å (carbon atoms: black, oxygen atoms: grey)[36]. Reprinted from the Journal of Membrane Science, Vol.328, Perez E.V., Balkus K.J., Ferraris J.P., and Musselman I.H."Mixed-matrix membranes containing MOF-5 for gas separation", pp.165-173, 2009, with kind permission from Elsevier.

Even higher adsorption values were reported for MOF-177. MOF-177 consists of octahedral ZnO_4 clusters connected by benzene tribenzoate (BTB) ligands and was reported to adsorb 11,0 wt.% of H_2 in terms of excess adsorption or 19,67wt.% in terms of absolute adsorption (volumetric hydrogen density of 46g L^{-1}) at 77K and 100 bar of hydrogen pressure[37].

At ambient temperatures, hydrogen adsorption in MOFs is relatively low and usually does not exceed 1 wt.%[24]. However, even with values of gravimetric storage capacity on the level of 1 wt.% MOFs are among the best of the materials which store hydrogen by the physisorption mechanism. The gravimetric capacity of MOFs is as good as that of the best ACs [7] and CNTs [10], but their volumetric properties are far superior. In MOFs a high surface area is combined with a bulk density comparable to the real density which is a strong advantage compared to ACs. The ratio between the real and bulk density shows the accessibility of the structure for guest molecules. In ACs, extremely high dispersion results in a low bulk density, tens of times below the real density of graphite. Therefore, a real tank filled with crystalline MOF powder will be able to store more hydrogen compared to highly dispersed activated carbons.

Very strong research efforts have been recently focused on improving hydrogen storage in MOFs at ambient temperatures which requires an understanding of the main factors influencing hydrogen adsorption. Some factors are the same as for most other materials where hydrogen is stored due to physisorption while other factors are inherent only for MOFs.

Hydrogen bonding strength: possibly the most crucial factor is the bonding strength of H_2 molecules to the adsorbent surface which is proportional to the isosteric heat of adsorption. H_2 molecules interact with the surface of MOFs via the weak van der Waals force which results in low isosteric heat of adsorption in the range of 4-7 kJ*mol^{-1} [31]. According to calculations an isosteric heat of hydrogen adsorption in the range of 22-25 kJ*mol^{-1} is needed to store ~7wt.% of hydrogen at 298K and 30bar of hydrogen pressure[38]. Therefore, in order to achieve the desired hydrogen uptake in MOFs hydrogen bonding strength should be enhanced by a factor of 3-4. Several recently suggested ideas on how to improve the strength of hydrogen interaction with MOFs are the following: reducing pore size, introducing unsaturated metal adsorption sites, doping MOFs with alkali metals, changing organic ligands and metal clusters, and using the hydrogen spillover effect. All those methods have their cons and pros which will be discussed in later sections.

Surface area: an important factor influencing hydrogen adsorption in porous materials is surface area. Hydrogen adsorption in MOFs is higher for MOFs with larger BET surface area (see **Figure 1.4**). The relation between hydrogen uptake and BET surface area in MOFs is almost linear at 77K and high hydrogen pressures. A similar linear relation between hydrogen uptake and BET surface area of MOFs is also observed at room temperatures, but to observe it MOFs need a proper activation. The proper activation procedure is needed to remove solvent molecules and to produce unsaturated open metal sites which are important for hydrogen adsorption at room temperatures[39].

Pore volume: another important factor which influences hydrogen adsorption due to physisorption is pore volume. Hydrogen adsorption in MOFs correlates with total pore volume though this correlation is more pronounced at 77K[24, 40]. Theoretical calculations performed for a

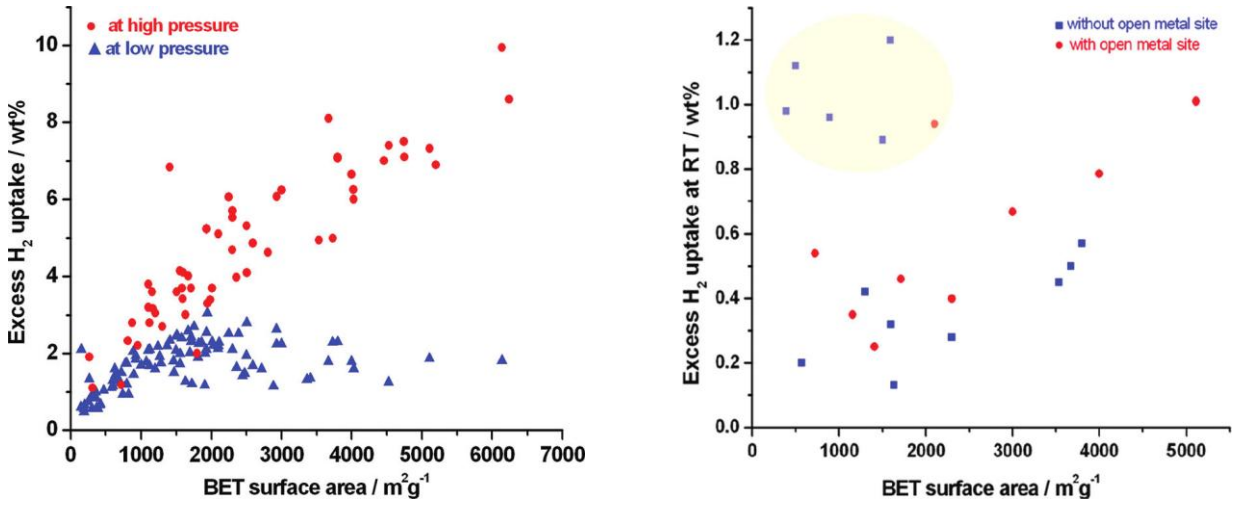

Figure 1.4. Excess hydrogen uptake in MOFs at 77K (left figure) and at room temperatures (right figure) plotted versus BET surface area[39]. Reprinted with permission from Chemical Reviews, Vol.112, Suh MP., Park HJ., Prasad TK. et al. "Hydrogen storage in metal-organic frameworks", pp. 782-835, Copyright 2012 American Chemical Society.

family of MOFs with the same framework topology and the same surface chemistry but with different pore sizes showed that three different adsorption regimes exist at 77K: at low pressure, hydrogen uptake correlates with the heat of adsorption; at intermediate pressure, uptake correlates with the surface area; while at the highest pressures uptake correlates with pore volume[41]. A good example of how different factors determine hydrogen adsorption in different pressure ranges can be seen in **Figure 1.5**.

Pore geometry: the shape and size of pores are also crucial for hydrogen adsorption. Due to the overlap of the potential fields from both sides of the pore walls, small pores should have higher affinity towards hydrogen and thus higher hydrogen uptake capacity comparing to pores with larger diameter. This theoretical assumption was confirmed by experimental results. Using thermal desorption measurements Panella *et al* showed that hydrogen desorbs from MOFs with smaller pore sizes at higher temperatures than from MOFs with larger pore sizes[42]. According to theoretical calculations, carbon-based materials with a pore width of 6Å (for slit pore geometry) have higher hydrogen uptake at very low pressures while materials with a larger pore width of 9Å are more

appropriate for hydrogen storage at higher pressures (the kinetic diameter of a hydrogen molecule is 2,9Å)[24]. There are few possible methods to reduce pore sizes in MOFs. One method is to introduce

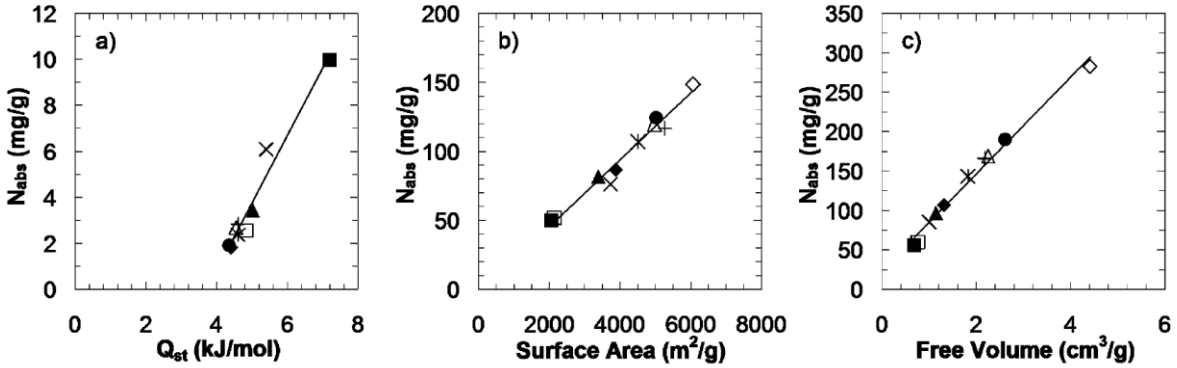

Figure 1.5. Theoretical values of hydrogen uptake calculated for different MOFs: a) at 0,1bar plotted versus isosteric heat of adsorption; b) at 30bar plotted versus accessible surface area; c) at 120bar plotted versus pore volume[41]. Reprinted with permission from the Journal of Physical Chemistry B, Vol.110, Frost H., Duren T., Snurr R.Q. "Effects of surface area, free volume, and heat of adsorption on hydrogen uptake in metal-organic frameworks", pp. 9565-9570, Copyright 2006 American Chemical Society.

bulky groups into organic ligands. However, in this case the improved gravimetric adsorption properties are accompanied by an increased density of the framework which results in only a negligible improvement of hydrogen uptake[43]. Another method to reduce pore sizes is catenation, or penetration, of two or more identical frameworks[44]. This technique was proven to work at low pressure and 77K[43], but GCMC simulations predicted that it would not work at high pressures due to a reduced free volume[45]. Via impregnation of MOFs with organic molecules such as fullerene C_{60}, free volume within pores can be reduced and additional hydrogen adsorption sites can be introduced inside the framework. Theoretical calculations performed for IRMOF-8 and IRMOF-10 impregnated with C_{60} showed that those materials have higher hydrogen uptake at 77K and pressures up to 10bar comparing to pristine MOFs[46]. In fact, synthesis of MOF-177 impregnated with C_{60} was reported in the literature but no hydrogen adsorption data is available for this material[47].

Adsorption sites in MOFs: inelastic neutron scattering and neutron diffraction studies revealed that MOFs have two groups of hydrogen adsorption sites: inorganic clusters and organic ligands[48, 49]. At lower pressures hydrogen adsorption starts on metal clusters and when these sites are saturated (at higher pressures) adsorption continues on organic linkers. This was verified experimentally in MOFs with different compositions of metal clusters and variations of surface area[50]. For example, a study by Hirscher and Panella revealed that at low pressures (up to approx. 6 bar) a Cu-based MOF material has a greater hydrogen uptake than a Zn-based MOF-5 material due

to a stronger interaction with hydrogen. At higher pressures the adsorption behavior is changed, and due to its higher surface area MOF-5 exhibits a greater hydrogen storage capacity (see **Figure 1.6**). The importance of inorganic metal clusters for hydrogen adsorption was also demonstrated by Botas *et al* using MOF-5 with part of the Zn substituted by Co atoms[51].

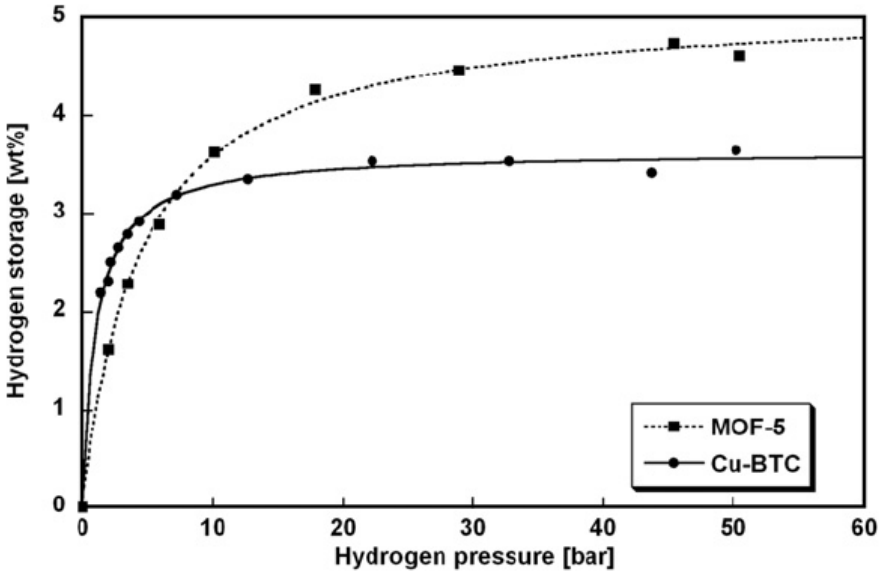

Figure 1.6. Hydrogen adsorption isotherms of MOF-5 (squares) and Cu-BTC (dots) at 77K. The experimental data were fitted with a Langmuir-type equation[50]. Reprinted from Scripta Materialia, Vol.56, Hirscher M. and Panella B. "Hydrogen storage in metal-organic frameworks", pp.809-812, 2007, with kind permission from Elsevier.

It is important to note that adsorption sites on metal clusters need to be carefully activated by complete removal of the solvent molecules which contaminate the material after synthesis[52].

Another group of hydrogen adsorption sites is associated with organic ligands. There is no single opinion on how the structure and the chemical composition of organic ligands influence hydrogen adsorption in MOFs. Some theoretical studies showed that larger aromatic ligands can improve hydrogen adsorption[53] while some other theoretical studies showed that the increased weight of MOFs due to introduction of heavy organic ligands would have a negative effect on hydrogen adsorption[54]. The latter assumption was confirmed by experimental data. Rowsell *et al* performed hydrogen uptake measurements on a series of MOFs obtained from MOF-5 by addition of functional groups (such as -Br, $-NH_2$, $-C_2H_4-$) to connecting ligands[43]. They did not observe any correlations between functionalities introduced into ligands and hydrogen uptake.

Summarizing this section, the most important factors which define hydrogen storage capacity of MOFs at ambient temperature are surface area and pore volume while other factors are mostly important at cryogenic temperatures.

1.2.2 Hydrogen storage via spillover

The hydrogen spillover effect suggests dissociation of molecular hydrogen into atomic hydrogen over metal catalyst particles and subsequent migration of atomic hydrogen to support materials. The hydrogen spillover process is a well-known phenomenon in catalysis reactions[55]. Transition metals with nearly filled d-shells (e.g. Ni, Pt, Pd) are normally used as catalysts to initiate hydrogen spillover[56]. For the first time hydrogen spillover was observed in hydrogenation of ethylene which proceeded much faster if the Pt/SiO_2 catalyst was used[57]. In later studies hydrogen spillover was observed in hydrogenation of the Pt-doped activated carbon[58]. It should be noted that the hydrogen spillover effect is typically observed at elevated temperatures in the range of 150-400ºC.

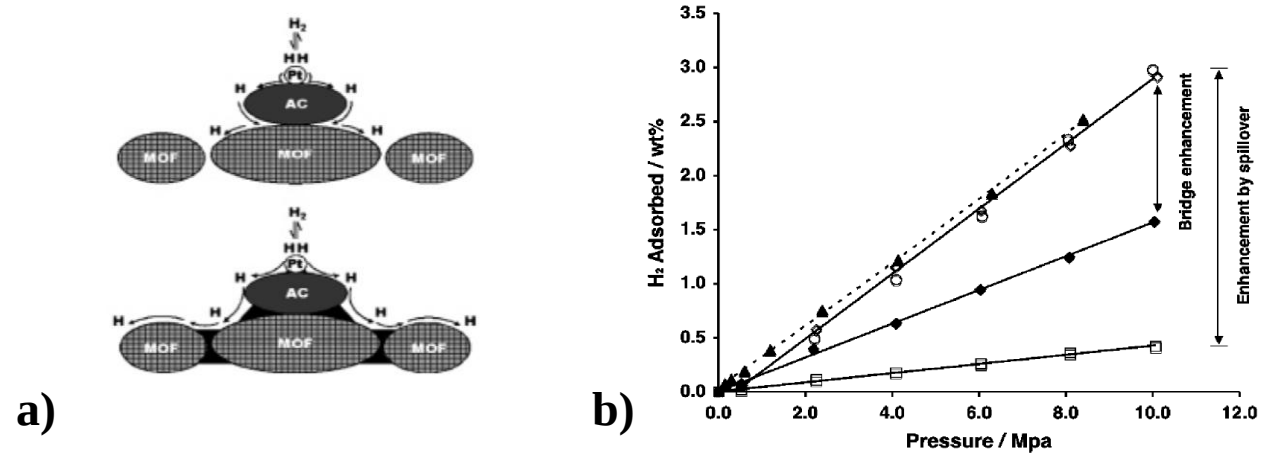

Figure 1.7. a) Schematic representation of the hydrogen spillover process in MOFs mixed (top picture) or bridged (bottom picture) with Pt/AC catalyst; b) hydrogen adsorption measured for pristine MOF-5(empty squares), MOF-5 mixed with Pt/AC catalyst (filled diamonds), and MOF-5 bridged with Pt/AC catalyst (filled triangles)[59]. Reprinted with permission from the Journal of American Chemical Society, Vol.128, Li Y. and Yang RT. "Hydrogen storage in metal-organic frameworks by bridged hydrogen spillover", pp. 8136-8137, Copyright 2006 American Chemical Society.

In the early 90s a few reports were published in which hydrogen spillover in catalytic reactions was observed at near ambient temperatures, e.g. in hydrogenation of benzene and in hydrogenation of TiO_2 samples[60, 61]. In recent years the concept of hydrogen spillover was actively introduced into the hydrogen storage field by the group of Prof. R.T Yang for various adsorbents doped with metal

catalysts (see **Figure 1.7a**). They reported the improvement of hydrogen adsorption by the factor of 1,5-4 in ACs[62], CNTs[63], GNFs[56], zeolites[64], and graphene[65] doped with metal catalysts.

In 2006 this group reported a remarkable increase of hydrogen adsorption for MOF materials with catalyst added by simple grinding[66], and the next study from the same group reported an even further increased hydrogen adsorption by improving the contact between the metal catalyst and the adsorbent[67]. To improve the contact a precursor (usually glucose or sucrose) is carbonized forming carbon bridges between the source of spillover and the adsorbent. Using this relatively simple "bridging" technique the group of Prof. R.T. Yang reported a hydrogen adsorption of 3wt.% measured in MOF-5 modified with Pt/AC catalyst (at ambient temperatures and 100bar of H_2 pressure). This represents an impressive improvement of hydrogen adsorption by a factor of 7,5 comparing to pristine MOF-5[59] while an improvement by a factor of ~3,3 was reported for the simple mixture of MOF-5 with Pt/AC catalyst[66].

These studies demonstrated some unique features of spillover related to hydrogen adsorption/desorption which make it rather different compared to hydrogen adsorption via physisorption, and the difference was considered to be specific for the spillover mechanism. Hydrogen adsorption in catalyst doped MOFs exhibited linear isotherms (for pressures at least up to 100bar, see **Figure 1.7b**)[59], slow adsorption kinetics (see **Figure 1.8**)[68], and showed no correlation between hydrogen uptake and surface area/pore volume of the adsorbent[68].

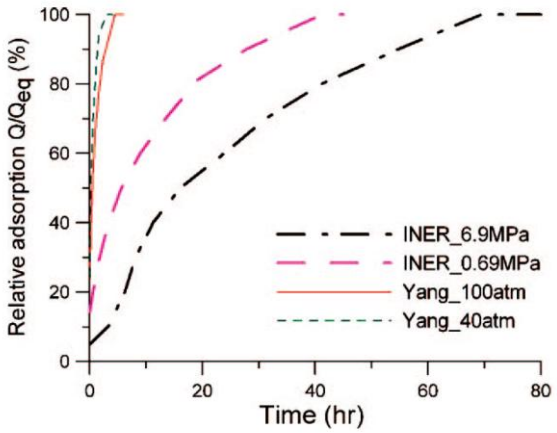

Figure 1.8. Kinetics of hydrogen adsorption in different IRMOF-8 samples bridged with Pt/AC catalyst at room temperature (adsorption via hydrogen spillover)[68]. Reprinted with permission from the Journal of American Chemical Society, Vol.131, Tsao C.-S., Yu M.-S., Wang C.-Y., et al. "Nanostructure and hydrogen spillover of bridged metal-organic frameworks", pp. 1404-1406, Copyright 2009 American Chemical Society.

In a recent article the group of Prof. R.T. Yang claimed that the metal catalyst was not needed at all to observe hydrogen spillover in exfoliated graphite oxide (called graphene in this study)[69]. An enhancement of hydrogen adsorption compared to activated carbons with similar surface area together with slow adsorption kinetics was explained by hydrogen spillover on edge sites or structural vacancies in graphene sheets. However, several other studies performed on exfoliated graphite oxide did not confirm this effect[30, 70].

Moreover, very few reports with independent confirmation of increased hydrogen adsorption in metal doped MOFs are available after 6 years following the initial report[68, 71-73]. That is somewhat surprising taking into account the very high levels of reported hydrogen adsorption which meet current DOE targets. However, in 2009 another independent study[68] confirmed the reports from Prof. R.T. Yang's group and provided us with motivation to reproduce and further develop hydrogen storage materials based on MOFs and the spillover mechanism.

In some part the later study seems to contradict the earlier one. For example, the group of Prof. R.T. Yang reported that the enhancement and the total values of hydrogen adsorption via spillover in various carbon materials are proportional to the surface area of those materials, i.e. materials with higher surface area have higher hydrogen adsorption via the spillover mechanism[63]. On the contrary, Tsao *et al* reported that materials with a more defective structure, i.e. with smaller surface area, have higher hydrogen adsorption via spillover compared to the same type of materials with larger surface area[68].

Following the initial claims on the significant increase of hydrogen adsorption in MOFs via spillover[59, 66, 73] more and more reports appear in the literature where authors have failed to observe any spillover features measuring hydrogen adsorption in materials prepared according to seemingly the same synthesis procedures[74, 75]. The reproducibility of hydrogen adsorption on carbon materials was also seriously questioned in some recent studies. For example, the group of Prof. R.T. Yang claimed that hydrogen spillover is a reversible process[62, 66]. During desorption hydrogen atoms were assumed to migrate back to metal catalyst particles where they supposedly recombined into molecular hydrogen (i.e. reverse "spillover"), and desorbed[76]. In later studies it was shown that new C-H bonds were indeed formed during hydrogen adsorption in some carbon materials doped with metal catalysts, but elevated temperatures in the interval of 250-300ºC were needed to break those bonds and to desorb hydrogen[56, 77]. Therefore, according to those reports hydrogen spillover at ambient temperatures led to the irreversible hydrogen storage, and the reversible hydrogen storage was entirely due to physisorption of molecular hydrogen.

The theoretical model proposed by the group of Prof. R.T. Yang in order to explain reversible hydrogen adsorption in MOFs via the spillover mechanism was also subjected to strong criticism[76,78,79]. Psofogiannakis and Froudakis showed that H atoms must overcome a tremendous energy barrier (>60kcal/mol) in order to migrate from Pt to the graphite surface and therefore this process is very unlikely to happen at room temperature[80]. This theoretical result agrees well with some experimental data which showed that there was no transfer of atomic hydrogen from metal catalyst particles to the adsorbent surface during hydrogen adsorption measurements in Pt-doped GNFs[81]. Moreover, it was shown that the net hydrogen adsorption measured on Pd-loaded activated carbons was the sum of atomic hydrogen chemisorbed on Pd clusters and molecular hydrogen physisorbed on the activated carbon surface[82].

Summarizing this chapter, many intriguing results in the field of hydrogen storage were reported for various adsorbents (MOFs, ACs, zeolites, CNTs, GNFs etc) doped with metal catalysts, and some attempts were made to explain those results using the concept of hydrogen spillover[83]. It should be noted that some hydrogen adsorption results reported in this field are very close to DOE targets, e.g. hydrogen adsorption of 4wt.% was reported for Pt-modified IRMOF-8[59]. However, very few independent confirmations of these hydrogen adsorption results were available at the moment when we started to work in this field, some experimental results being questioned and actively debated. The factors affecting hydrogen adsorption via the spillover mechanism as well as the very existence of this effect at room temperatures were not clear. Therefore, more studies in this field were required to clarify many questions. In particular, we intended to verify the effect of metal catalyst nanoparticles on hydrogen storage in MOF materials and to clarify the possibility of using the room temperature spillover mechanism for hydrogen adsorption/desoprtion.

1.2.3 Hydrogen storage via chemisorption

1.2.3.1 Metal hydrides and complex hydrides

Metal hydrides are among the most common materials for hydrogen storage and represent an extremely broad research field at the moment. Hydrogen can chemically react with some solids forming covalent or ionic bonds, i.e. be stored via chemisorption. Most common materials considered for hydrogen storage are various metal hydrides (e.g. hydrides of elemental metals and complex hydrides). Hydrides of light metals such as Li, Be, Na, Mg, B, and Al are especially attractive due to their high gravimetric capacity for hydrogen storage. One of the most studied metal hydrides, magnesium hydride, MgH_2, shows a high gravimetric H_2 capacity of 7,7 wt.% and good reversibility[84]. However, the main disadvantages of MgH_2 as well as of most other metal hydrides

are the high temperature of hydrogen release, slow desorption, and a high reactivity towards air and oxygen. For instance, release of hydrogen from MgH_2 was observed upon heating at 300ºC and 1bar H_2[85]. It is possible to lower the hydrogen release temperature (by ~40-100ºC) using e.g. strongly dispersed material[84,86].

Some of the most interesting materials studied for hydrogen storage during the last decade are complex hydrides. Sodium, lithium, and beryllium, which are the only metallic elements lighter than magnesium, can form solid-state compounds with hydrogen with extremely high hydrogen content (e.g. 18 wt.% for $LiBH_4$). Alanates and borohydrides of various compositions are the most typical representatives of this group. Disadvantages of hydrogen storage in complex hydrates are relatively high temperatures of hydrogen release, slow kinetics, and problems with re-hydrogenation.

Summarizing this section, metal hydrides and complex hydrides have high contents of hydrogen, but high hydrogenation/dehydrogenation temperatures, slow kinetics, and degradation upon successive adsorption/desorption cycling are the main problems which needs to be solved for hydrogen storage applications.

1.2.3.2 Hydrogen storage in fullerene C_{60} via chemisorption

Fullerene C_{60} has also been considered as a possible material for hydrogen storage applications. For example, the reaction of fullerene C_{60} with hydrogen gas was actively studied within the program sponsored by USA DOE[87, 88].

The C_{60} molecule has a ball-shaped cage structure (see **Figure 1.2**) as discovered by Kroto and Smalley in 1985[89]. Hydrogen can react with fullerene C_{60} by the opening C=C double bonds and formation of covalent C-H bonds. As a result, hydrogenated fullerenes (also called *fulleranes*) with composition $C_{60}H_x$ are formed where X is always an *even* number of hydrogen atoms.

Theoretically, a maximum of 60 hydrogen atoms could be attached both to the inner (endohedrally) and outer (exohedrally) surfaces of the fullerene cage. The composition $C_{60}H_{60}$ would correspond to 7,7wt.% of H_2, but it was never observed experimentally. Experimental observations of C_{60} hydrogenation are also limited only to exohedral attachment of hydrogen atoms while experimental evidence for the endohedral type of covalent functionalization is yet to be found.

Fulleranes can be synthesized by numerous methods such as hydroboration[90], hydrozirconation[91], transfer hydrogenation[92], electrochemical reduction[93], reduction by Zn-HCl in toluene solution[94], chemical reduction with diimides[95], hydrogen radical-induced hydrogenation[96], and photo-induced electron transfer[97]. However, the most important method for production of

fulleranes in bulk amounts is a direct reaction of fullerene C_{60} with hydrogen gas at elevated temperatures and pressures[98].

Hydrogenation of C_{60} by hydrogen gas was observed for the first time by Petrie *et al*[99]. As it was believed that only ionized fullerenes could react with hydrogen gas, iodoethane was used to promote ionization of C_{60}[96]. In later studies it was shown that hydrogenation of C_{60} using hydrogen gas does not require any catalyst if the reaction is performed at elevated conditions. The typical temperature range required for hydrogenation of C_{60} is 350-450ºC[100-107] at a hydrogen pressure range of 5-120bar[100-107].

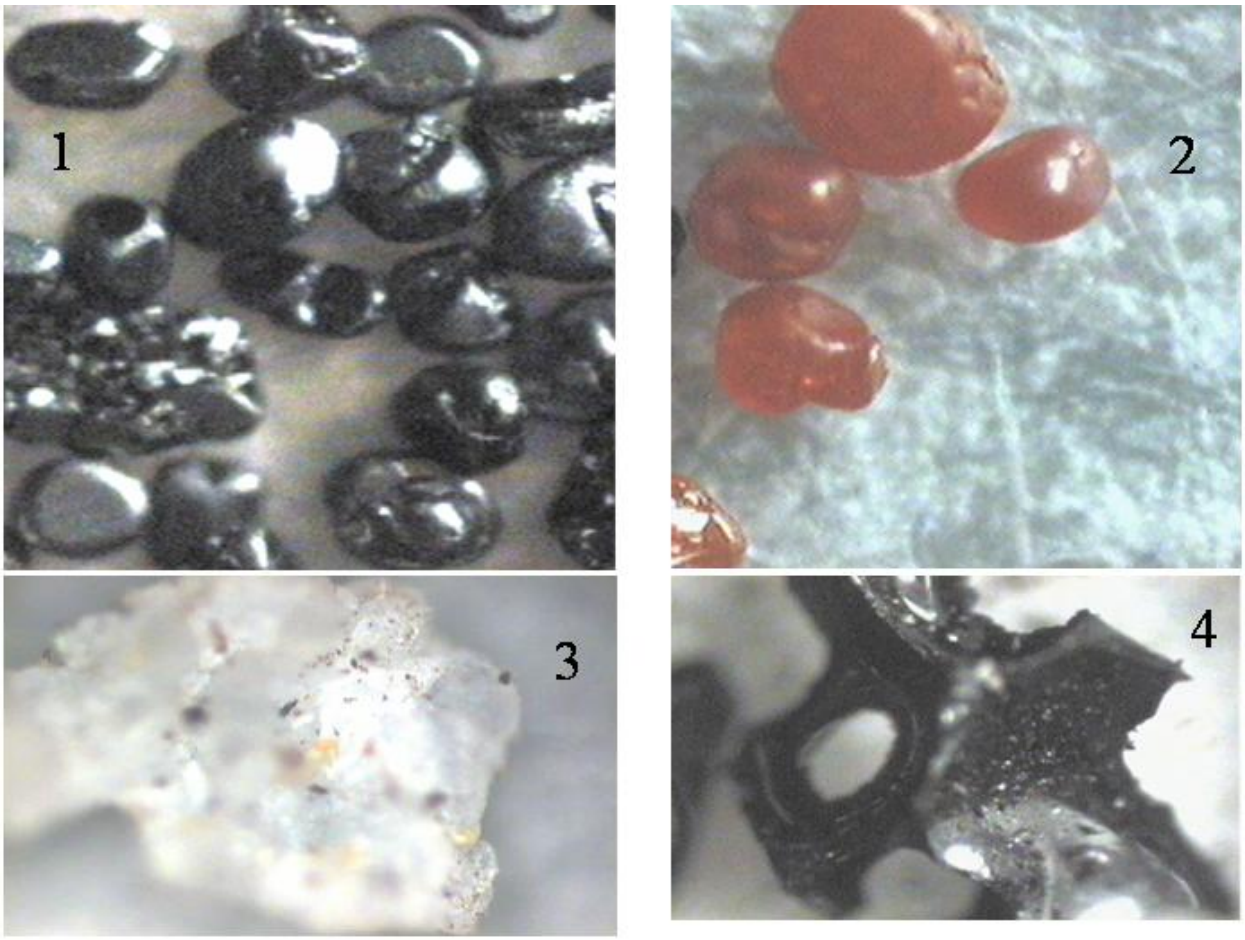

Figure 1.9. Fullerene C_{60} with different degree of hydrogenation: pristine C_{60} (1); medium degree of hydrogenation (2); highly hydrogenated C_{60} (3); products of hydrogenation-induced collapse of fullerene molecules (4) [108]. Reprinted from the book by Cataldo F. and Iglesias-Groth S. "Fulleranes: the hydrogenated fullerenes", pp.89, 2010, with kind permission from Springer Science and Business Media.

Hydrogenation of C_{60} results in drastically changed physical properties: pristine C_{60} is black in color and opaque, while highly hydrogenated fullerenes become white and transparent (see **Figure**

1.9)[108]. Pristine C_{60} is a semiconductor whereas highly hydrogenated fullerenes are insulators[108, 109]. Fulleranes are also chemically more inert compared to pristine C_{60} due to saturation of the C=C double bonds suitable for functionalization. Moreover, the addition of H atoms results in significant changes in the shape of the fullerene molecule (see **Figure 1.10**).

The high gravimetric and volumetric capacity of hydrogen is an advantage of fulleranes. However, the relatively high temperatures required for hydrogenation and hydrogen release, as well as slow kinetics of hydrogenation, are the main obstacles for application of fulleranes as hydrogen storage materials[100]. Using proper catalysts could be a possible way to solve these problems. Various metals such as Ni, Pd, Pt, or intermetallic compounds were tested previously in attempts to lower the hydrogenation temperature for C_{60}[100,110,111]. Using these catalysts the hydrogenation temperature of C_{60} can be lowered by ~50-100ºC. Moreover, addition of metal catalysts significantly improves hydrogenation kinetics, e.g. addition of Pt catalysts was found to improve the reaction rate by approximately ten times for a reaction performed at 400ºC and 50 bar H_2 pressure[112, 113]. However, the temperature of hydrogenation remains to be too high even if catalysts are used.

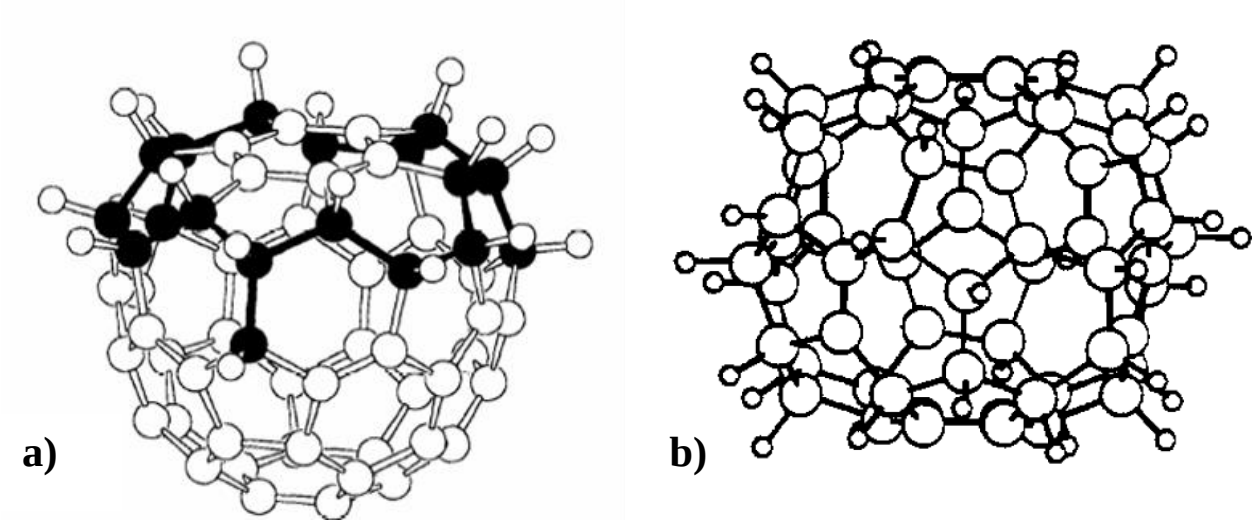

Figure 1.10. Hydrogenated fullerenes:

a) C_{3v} isomer of $C_{60}H_{18}$[114]. Reprinted with permission from Organic Letters, Vol.7, Wågberg T. et al. "Selective synthesis of the C3v isomer of $C_{60}H_{18}$", pp. 5557-5560, Copyright 2005 American Chemical Society.

b) C_{3i} isomer of $C_{60}H_{36}$ [115]. Reprinted with permission from the Journal of Physical Chemistry B, Vol.97, Hall L.E., McKenzie D.R., Attala A.M. et al. "The structure of hydrogenated fullerene ($C_{60}H_{36}$)", pp. 5741-5744, Copyright 1993 American Chemical Society.

Nevertheless, hydrogenation of C_{60} remains to be a very intensively developing research field. Recently, Schur *et al* reported synthesis of fulleranes with an extremely high hydrogen content of 8,2wt.% where 7,7wt.% (corresponds to an average composition of $C_{60}H_{60}$) of hydrogen was covalently bonded to the C_{60} cage and 0,5wt.% of hydrogen was adsorbed in voids of the structure[116]. It should be noted that these authors did not consider possible fullerane fragmentation which is likely to happen upon extensive hydrogenation and would lead to formation of a mixture of polycyclic aromatic hydrocarbons (PAHs)[103, 104].

Materials which are considered for hydrogen storage applications must release hydrogen during dehydrogenation. However, dehydrogenation of fulleranes is much less studied compared to hydrogenation of C_{60}. Highly hydrogenated fulleranes ($C_{60}H_x$, where $x > 36$) are relatively unstable and partial collapse of the structure is observed already upon extensive hydrogenation. Therefore, it is expected that dehydrogenation would lead to even more pronounced fullerane decomposition. This assumption was confirmed by experimental results [106, 117]. However, dehydrogenation was mainly studied for very complex mixtures of $C_{60}H_x$ which consisted of fulleranes with a broad variation of hydrogen content[87]. Fulleranes with a lower content of hydrogen, e.g. $C_{60}H_{18}$, are expected to have higher stability against thermally induced decomposition. For instance, a hydrofullerene mixture containing approximately 3,5wt.% of hydrogen was reported to release hydrogen reversibly [100]. In order to verify reversibility of hydrogenation for fulleranes with lower hydrogen content dehydrogenation experiments must be carried out on samples containing a single isomer of $C_{60}H_x$ (where $18<x<36$).

Very promising results which will possibly revive interest in fullerenes as hydrogen storage material were recently published by Teprovich *et al* who studied hydrogen storage in C_{60} mixed with lithium hydride[118]. The new composite material had a reversible hydrogen storage of up to 5wt.% depending on the C_{60}/Li molar ratio. Moreover, hydrogenation had much faster kinetics and lower desorption temperatures (~270ºC comparing to 500-600ºC reported for ordinary fulleranes). Those results open possibilities for synthesis of new materials for hydrogen storage which are based on simple mixtures of metal hydrides with C_{60}.

Hydrogenation of C_{60} was extensively studied over the past 20 years. The research in this field resulted in the synthesis of many new and interesting materials which could be of interest from many different points of view and their importance is not limited only to hydrogen storage applications There is also a general fundamental interest in more detailed studies of the hydrogenation of fullerenes which is the subject of next section.

1.3 Synthesis of new materials by hydrogenation of C_{60} and CNTs

1.3.1 Isolation of new hydrogenated fullerenes

Besides hydrogen storage applications, there is a general interest in more detailed studies of fullerene C_{60} hydrogenation which could lead to synthesis of new materials. Hydrogenation of C_{60} normally results in a very complex mixture of fulleranes with different content of hydrogen[103] while only few fulleranes, mostly with low hydrogen content, were so far isolated and characterized[114,119,120]. The two most studied fulleranes synthesized successfully are $C_{60}H_{18}$ and $C_{60}H_{36}$ [92, 114, 121]. No other fulleranes $C_{60}H_x$ with x>18 were so far isolated in a pure state. Another problem in synthesis and separation of highly hydrogenated fullerenes is the high number of possible isomers with the same $C_{60}H_x$ composition. For instance, the number of possible $C_{60}H_{36}$ isomers is $6*10^{14}$ [122] out of which over 100 isomers were summarized by Clare and Kepert[123]. In fact, $C_{60}H_{36}$ was usually obtained as a mixture of several isomers[124].

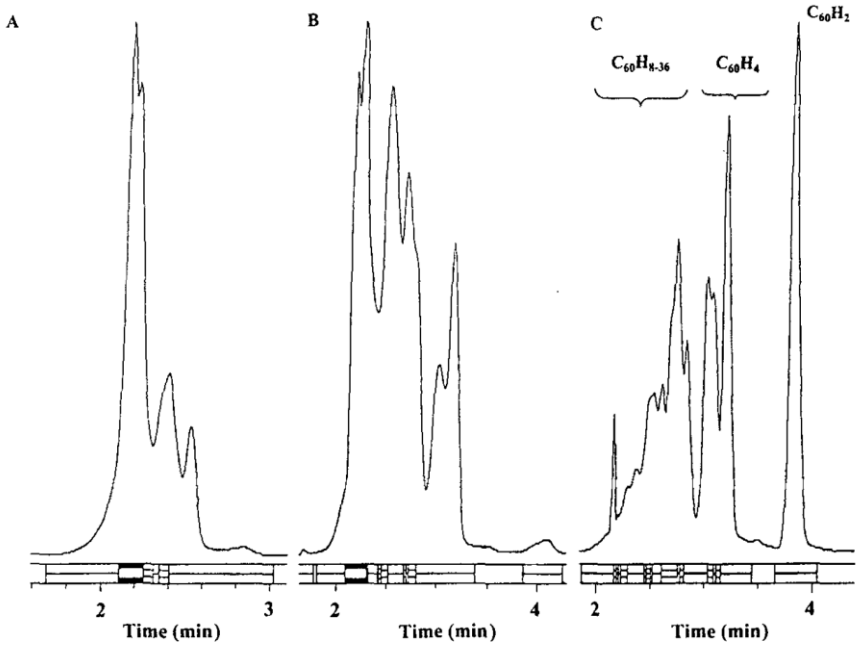

Figure 1.11. HPLC separation of a fulleranes mixture using acetonitrile-toluene mixed with different ratios as a mobile phase: a) 15:85; b) 25:75; c) 35:65[125]. Reprinted from Chromatographia, Vol.48, Bucsi I., Szabo P., Aniszfeld R., et al. "HPLC separation of hydrogenated derivatives of buckminsterfullerene", pp.59-64, 1998, with kind permission from Springer Science and Business Media.

Liquid chromatography is a very efficient tool to separate different fullerenes (e.g. C_{60}. C_{70}, C_{82} etc) from pristine mixtures obtained e.g. by arc discharge method. However, fulleranes are

usually produced as even more complicated mixtures with tens of various molecules of slightly different compositions. Only few attempts to isolate fulleranes other than $C_{60}H_{18}$ and $C_{60}H_{36}$ are available in literature. It is known that fulleranes are separated in a high-performance liquid chromatography (HPLC) column according to the number of H atoms attached to the cage: highly hydrogenated C_{60} elute first while fulleranes with lower hydrogen content show longer retention time[125]. Due to high complexities of fulleranes mixtures (consist of fulleranes with various degrees of hydrogenation or of different isomers of the same $C_{60}H_x$ composition) the chromatographic bands overlap making isolation of pure fractions impossible (see **Figure 1.11**).

Optimization of HPLC separation seem to be a very promising method for isolation of pure fulleranes. However, it is desirable also to synthesize less complex mixtures of fulleranes to ensure easier separation. The ideal solution would be to find methods for direct synthesis of fulleranes with a certain composition, e.g. by variation of synthesis conditions (temperature, hydrogen pressure, hydrogenation time). For instance, synthesis of a C_{3v} isomer of $C_{60}H_{18}$ with 95% purity was achieved in our group earlier by direct hydrogenation of C_{60} at 400ºC and 100bar of hydrogen pressure and a certain duration of treatment (see **Figure 1.10**)[114]. Synthesis of highly hydrogenated fulleranes can be expected in the future choosing appropriate synthesis conditions and combining them with advanced HPLC methods.

1.3.2 Synthesis of fragmented fullerenes and fullerene fragments

Recent studies performed in our group revealed that prolonged hydrogenation at extreme conditions leads to fullerane break up by removal of several carbon atoms off the cage thus forming fragmented fulleranes. Formation of fragmented fulleranes is possible due to saturation of dangling bonds by hydrogen atoms and stabilization of the fragmented structure by hydrogen[103]. Even more prolonged hydrogenation leads to complete collapse of the fullerane structure and to formation of PAHs mixtures. Hydrogen driven collapse of fullerene C_{60} was proposed by Talyzin *et al* as a new method to synthesize various unusual PAHs[126]. One possible example of such an unusual molecule is the "buckybowl", cup-like non-planar hydrocarbon molecules which recently attracted strong attention [127]. Those unusual molecules could possibly be used as precursors for the synthesis of CNTs with certain chiralities, e.g. pentaindenocorannulene $C_{44}H_{18}$ was proposed as an attractive precursor for synthesis of "armchair" [5,5] SWCNTs (see **Figure 1.12**)[128].

Buckybowls are synthesized by bottom-to-top approach using planar precursor molecules[129]. This synthesis procedure is complicated, does not have high yield, and result in the synthesis of microgram amounts of buckybowls. On the other hand, buckybowls can be considered as large

fragments of fullerene C_{60} molecules. Understanding of hydrogen driven collapse of C_{60} and using it in a controlled way would open a possibility for synthesis of buckybowl molecules in bulk amounts.

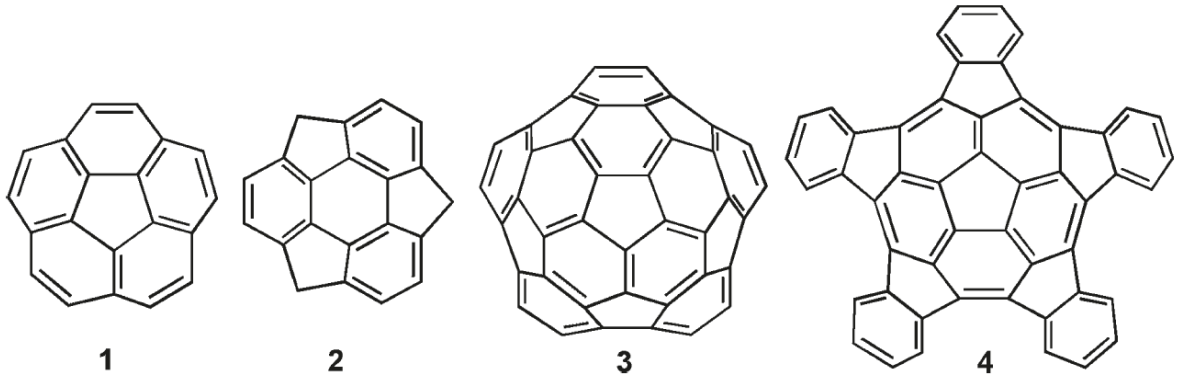

Figure 1.12. Examples of some buckybowl molecules: 1) corranulene $C_{20}H_{10}$[130]; 2) sumanene $C_{21}H_{12}$[127]; 3) a $C_{40}H_{10}$ molecule which can be considered as the simplest capped carbon nanotube[129]; 4) pentaindenocorannulene $C_{44}H_{18}$[128]. Reprinted with permission from the Journal of American Chemical Society, Vol.133, Wu T.-C., Hsin H.-J., Kuo M.-Y., et al. "Synthesis and Structural Analysis of a Highly Curved Buckybowl Containing Corannulene and Sumanene Fragments", pp. 16319-16321, Copyright 2011 American Chemical Society.

1.3.3 Hydrogenation of carbon nanotubes: functionalization and unzipping

Hydrogenation at extreme temperature and hydrogen pressure conditions is also very interesting to apply for reaction with carbon nanotubes. For example, functionalization of CNTs with hydrogen can be used as an efficient tool for improving their dispersion properties. Hydrogenated CNTs were reported to disperse well in common organic solvents such as methanol, ethanol, chlorophorm, and benzene[131]. Moreover, hydrogenation can be used to increase the band gap, i.e. decrease conductivity, of CNTs due to transformation of sp^2-bonds into sp^3-bonds which lead to localization of π-electrons[132]. Therefore, hydrogenation may help to obtain purely semiconducting CNTs samples if all metallic nanotubes become semiconducting after hydrogenation.

Initially, it was assumed that CNTs do not react with molecular hydrogen, and therefore atomic hydrogen should be used for hydrogenation. Nikitin *et al* reported synthesis of hydrogenated CNTs by hydrogenation with atomic hydrogen where 65 ± 15 at.% of carbon atoms were hydrogenated. Hydrogenation was reversible and all hydrogen was released upon heating at 600ºC[133]. In later studies it was shown that the degree of CNTs hydrogenation depends on the CNTs

diameter[134]. For CNTs with an average diameter of ~2nm almost 100% hydrogenation with a relatively low desorption temperature of 200-300ºC was achieved.

CNTs can also be used as a precursor for the synthesis of GNRs[135]. GNRs of a specific width, 2π times the diameter of the parent nanotubes, can be produced by unzipping of CNTs. At the moment the most common method for unzipping CNTs is oxidation[135, 136]. Hydrogenation, which was successful for opening of C_{60} molecules, had not been tested for CNTs unzipping prior to our experiments. Successful unzipping of CNTs by hydrogenation will lead to synthesis of oxygen-free GNRs which is impossible when GNRs are synthesized by CNTs oxidation[137,138].

One of the initial aims of our experiments with hydrogenation of carbon nanotubes was to verify the possibility of their opening using annealing in hydrogen. CNTs are normally closed by fullerene-like cups after synthesis and these are usually removed by chemical or mechanical treatments to make the inner space of the CNTs available e.g. for encapsulation of other molecules[139]. Based on our experimental data on hydrogen driven C_{60} collapse[101, 103] we expected that extensive hydrogenation would lead to removal of the fullerene-like CNT tips. Therefore, we tested hydrogenation as a tool for CNTs opening, and possibly CNTs unzipping.

1.3.4 Hydrogenation of molecules (C_{60}) encapsulated inside SWCNTs

One more interesting opportunity is to apply gas phase hydrogenation to some molecules encapsulated inside of CNTs. It is known that the inner space of CNTs can be filled with various molecules to study their chemical reactions in 1D-confined space. There are reports on CNTs filled with coronene[140], anthracene[141], ferrocene[142], adamantane[143], and GNRs[144]. One of the best studied examples of encapsulated CNTs is peapods (C_{60}@CNTs) which are obtained by insertion of C_{60} molecules into CNTs (see **Figure 1.13**)[141]. Experiments performed earlier in our group showed that hydrogen gas could penetrate into the inner space of C_{60}@CNTs and react with C_{60}. Formation of fulleranes with small hydrogen content (~$C_{60}H_{12-14}$) was observed upon exposure of C_{60}@CNTs to hydrogen gas while the CNTs walls remained non-hydrogenated[145]. Therefore, we decided to check how peapods will react with hydrogen in a broader temperature interval and at various durations of hydrogenation.

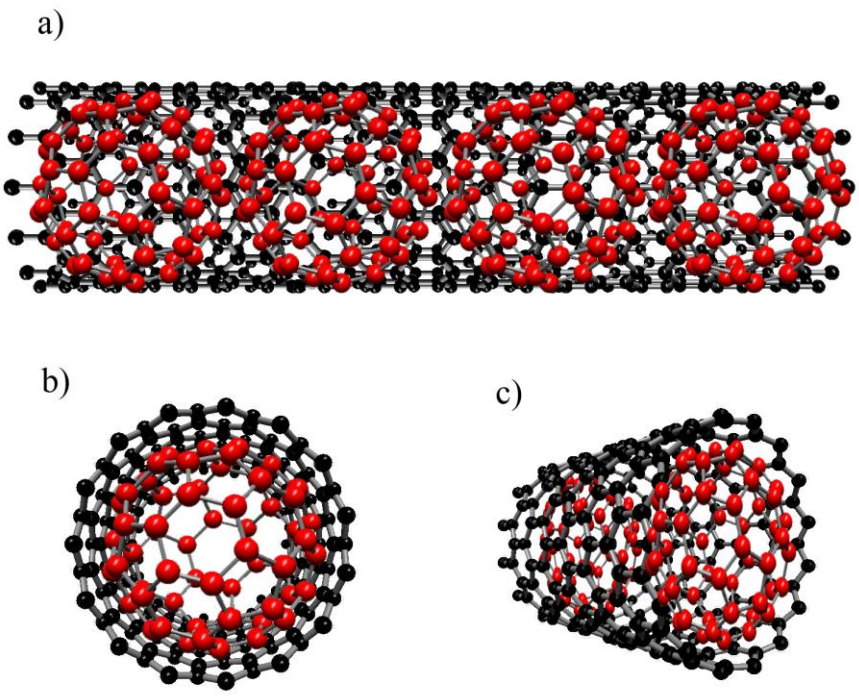

Figure 1.13. Schematic picture of C_{60}@SWCNTs peapods: a) side view; b) front view; c) tilted view.

2 Motivation for this work

This thesis consists of two major parts. In the first part I summarize our results on hydrogen storage in various materials. In particular, we studied hydrogen adsorption for a set of Zn- and Co-based MOFs which have different surface area and pore geometry. We also verified the effect of structural stability on hydrogen adsorption in MOFs. Looking for new possibilities to improve hydrogen adsorption in MOFs we studied a set of Pt-doped and Pt-modified (via the "bridging" technique) MOF-5 samples where the hydrogen "spillover" effect was expected.

Carbon materials are attractive candidates for hydrogen storage due to their light weight and high availability. In this thesis we studied hydrogen storage in novel nanocarbon materials synthesized by the reaction between fullerene C_{60} and anthracene/coronene.

We also studied hydrogenation of C_{60} in a broad temperature interval using a gravimetric method which allows to monitor C_{60} hydrogenation in situ. Using a gravimetric balance we tried to optimize hydrogenation conditions and to synthesize fullerane mixtures with relatively simple $C_{60}H_x$ compositions. The HPLC technique was used aiming to separate highly hydrogenated fulleranes. We examined the effect of metal catalyst (Pt and Ni) addition on kinetics of C_{60} hydrogenation and composition of hydrogenation products. The composition of every hydrogenated sample was studied with atmospheric pressure photoionization Fourier transform-ion cyclotron resonance (APPI FT-ICR) and matrix-assisted laser desorption/ionization time-of-flight (MALDI-TOF) mass spectrometry which shed light on the mechanism of hydrogenation and fragmentation of C_{60} induced by extensive hydrogenation.

In order to use C_{60} for hydrogen storage the reversibility of the hydrogenation process must be verified, especially for mildly hydrogenated fulleranes which have higher stability comparing to highly hydrogenated species. In this work we studied dehydrogenation of a sample which consists of 95% purity C_{3v} isomer of $C_{60}H_{18}$.

Hydrogenation is a powerful tool for synthesis of new materials or for modifying physical properties of existing materials as was earlier shown for hydrogenation of C_{60}[108]. In this work we explore hydrogenation of CNTs with molecular hydrogen which according to our previous experience with C_{60} should lead to opening of CNTs. Opened CNTs could be later impregnated with various molecules, e.g. C_{60}, and hydrogenation of C_{60} can be studied in the 1D-confined space of CNTs. In this work we studied hydrogenation of C_{60}@CNTs in a broad temperature interval and compared it with hydrogenation of bulk C_{60}.

3 Experimental section

3.1 Synthesis of the materials

3.1.1 MOF-5 (synthesis of the raw material, mixed and "bridged" with Pt catalyst)

MOF-5 was synthesized by the "one pot" method. According to this method a source of metal clusters (zinc nitrate hexahydrate: $Zn(NO_3)_2*H_2O$, 98%, Sigma Aldrich) and a source of organic ligands (terephtalic acid: H_2BDC, 98%, Sigma-Aldrich) were dissolved in N,N'-dimethylformamide (DMF, ≥99,8%, A.C.S. reagent, Sigma Aldrich) under mild stirring. In order to promote deprotonation of terephatlic acid triethylamine was dropwise added to the solution. After 2h of stirring the solution was filtered off, washed three times with DMF, and dried in an oven maintained at 105ºC during 20h. In order to cause hydrogen spillover MOF-5 was mixed with platinum 5wt.% on activated carbon (or 10wt.% Pt/AC) in a weight ratio 9:1 using an agate mortar and pestle. To facilitate spillover the contact between the catalyst and MOF-5 was improved using carbon bridges. In order to build them a ternary physical mixture of sucrose (A.C.S. reagent, Sigma–Aldrich), Pt/AC catalyst, and MOF-5 (the weight ratio 1:1:8) was first heated to 200ºC with a ramp of 1ºC/min and kept for 3 h in a helium atmosphere (the melting point of sucrose is 186ºC). During the first step sucrose is supposed to melt thoroughly and to fill spaces between catalyst particles and MOF-5. Then the temperature was increased to 300ºC, and held for 12 h. During this step sucrose carbonized, supposedly forming carbon bridges between Pt-catalyst and MOF-5. After the bridging process was completed, samples were cooled down to room temperature with a ramp of 1ºC/min.

3.1.2 Hydrogenation of fullerene C_{60}, SWCNTs, and C_{60}@SWCNTs

C_{60} powder (sublimed, >99,9% pure, purchased from MER Corp., USA) was loaded into a stainless steel container. The hydrogenation reaction was performed in a sealed chamber under a static hydrogen pressure of 50bar and in the temperature interval of 350-440ºC. The weight change of the fullerene C_{60} powder during hydrogenation was measured in situ by the Rubotherm gravimetric system (see **Chapter 3.2.3** for more details).

To study the effect of metal catalyst addition on C_{60} hydrogenation we mixed C_{60} powder with Ni catalyst (supported on Al_2O_3/SiO_2, 65wt.% of Ni) and Pt catalyst (supported on carbon black, 60wt.% of Pt) using agate mortar and pestle. Ni catalyst was mixed with C_{60} powder in a 1:1 (Ni:C) ratio. Pt catalyst was mixed with C_{60} powder in a 3:1 (Pt:C) ratio.

SWCNTs were provided by the group of Prof. Kauppinen from Aalto University. They synthesized SWCNTs by an aerosol chemical vapour deposition (CVD) method using CO

decomposition on Fe particles[146]. Hydrogenation of SWCNTs was performed in alumina crucibles placed in a sealed chamber under a static hydrogen pressure of 50bar and in the temperature interval of 400-550ºC. Typical duration of the hydrogenation experiment was 72hours.

C_{60}@SWCNTs was synthesized by the C_{60} gas phase encapsulation method in vacuum as described elsewhere[147]. Hydrogenation of C_{60}@SWCNTs was performed in alumina crucibles placed in a sealed chamber under a static hydrogen pressure of 50bar and temperatures of 450, 500, and 550ºC. Typical duration of the hydrogenation experiment was 72hours.

3.1.3 Reactions of fullerene C_{60} with anthracene/coronene

The reaction between C_{60} and anthracene/coronene was conducted under argon atmosphere in the temperature interval of 290–800ºC for 20–24 h. The powder C_{60} (99.5%, SES Research, Huston, USA) was mixed with coronene (97%, Aldrich, Germany) or anthracene (96.9%, Fluka, Sigma–Aldrich, Germany) using agate mortar and pestle, loaded into a stainless steel reactor (inner volume ca. 0.6 cm^3) and closed under argon. Experiments were performed for powders mixed in a ratio of one molecule of C_{60} per one molecule of anthracene/coronene. Several additional experiments were performed for fullerene C_{60} mixed with anthracene in a ratio of 2:1, but the difference was insignificant.

3.2 Characterization techniques

3.2.1 X-ray diffraction analysis

X-ray diffraction (XRD) technique is an important technique which is commonly used for the structural characterization of materials. All atoms in crystalline materials are considered as sets of parallel crystallographic planes which are characterized by Miller indices (*h k l*). Diffraction maxima occur when a certain set of crystallographic planes fulfill conditions for constructive interference provided by the Bragg law (see **Figure 3.1**):

$$2d\sin\theta = n\lambda \quad (1).$$

where θ is the angle between the incident beam and the crystallographic plane, *d* is the distance between two successive crystallographic planes, λ is a radiation wavelength, and *n* is an integer number. In other words, the interference occurs if the path difference of the beams diffracted from two adjacent planes $\Delta L = 2d\sin\theta$ equals to an integer number of wavelength λ.

XRD patterns are recorded by an X-ray diffractometer. The major parts of every X-ray diffractometer are a X-ray tube, a sample desk, and a detector. The X-ray tube generates X-ray radiation and consists of a tungsten filament and a water cooled Cu cup. The filament is connected

to a source of AC current (usually of the order of 10 A). Electrons are emitted from the surface of the filament and are accelerated by a potential difference applied between the tungsten wire and the copper cup (normally 40kV). Upon the collision of electrons with the cup part of their energy is converted into radiation which leaves the X-ray tubes through windows usually made of beryllium. Outgoing X-ray radiation is filtered, so that only $CuK_{\alpha 1}$ and $CuK_{\alpha 2}$ lines (1,5405 and 1,5443Å correspondingly with a mean value of 1,542Å) are used. Incident radiation is diffracted by the sample, which is placed in the middle of the goniometer circle (see **Figure 3.2**), and recorded by a detector. The intensity of diffracted radiation is normally measured by a scintillation counter which could detect radiation with a wavelength of 0,5 - 2,7Å.

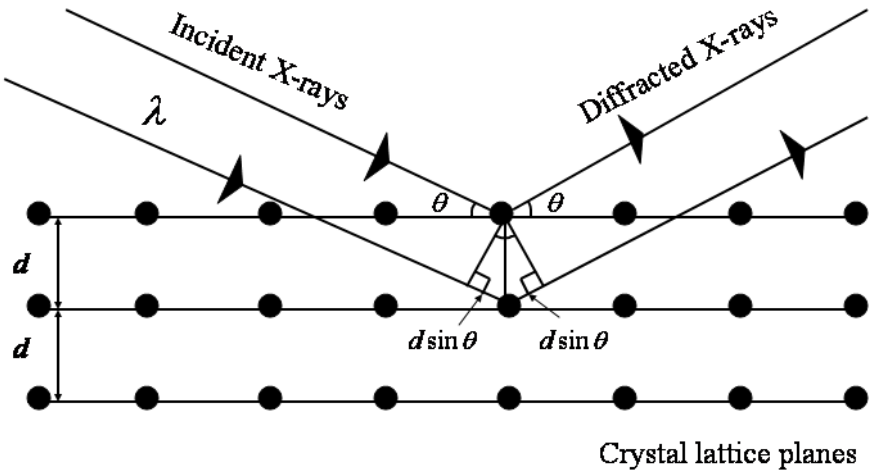

Figure 3.1. Diffraction of incident X-rays from the family of parallel atomic planes.

The X-ray diffractometer used in this work operates in the Bragg-Brentano mode. In this mode the X-ray tube, the detector, and the sample are located on the focusing circle. The X-ray tube is fixed, and the detector moves along the goniometer circle with an angular speed which is two times higher than the angular speed of the sample (the rotational axes of the sample and of the detector coincide). During the XRD analysis the detector is always at 2θ angle and the sample surface is always at θ angle in respect to the incident X-ray beam. The detector scans around the sample in the specified 2θ interval and records the angle and the intensity of diffracted radiation. The angle θ when incident radiation is diffracted and the intensity of diffracted radiation form a two dimensional

pattern. Each reflection on this pattern corresponds to the set of parallel crystallographic planes (*h k l*). X-ray diffraction measurements in this thesis were performed using Siemens D5000 diffractometer with CuK_{α} radiation.

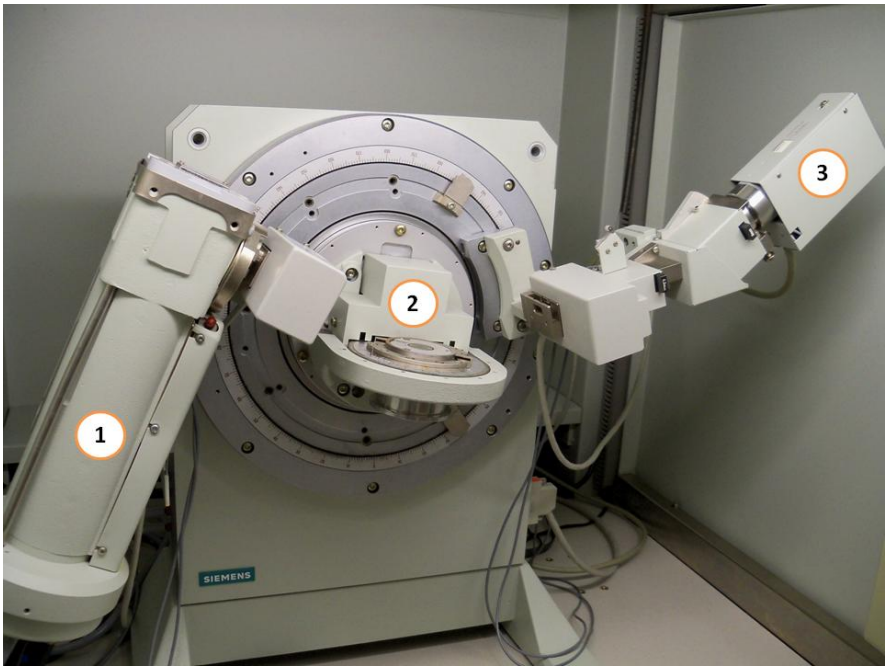

Figure 3.3. Siemens D5000 diffractometer with its main constituent parts: 1) X-ray tube, 2) sample holder, 3) detector.

3.2.2 Nitrogen sorption analysis

Nitrogen sorption analysis is a powerful tool for investigations of the material porosity. The basic principle of this technique is to measure the amount of nitrogen adsorbed by the material at certain conditions and applying some theoretical models to convert this amount into such properties of the material as surface area, pore volume, micropore volume, total pore volume, or pore size distribution function etc.

The amount of nitrogen *n* adsorbed by the material depends on temperature *T*, equilibrium pressure *p*, and on the nature of the nitrogen-sorbent system:

$$n = f(p, T, system) \quad (2).$$

If a specific nitrogen-material system is maintained at a constant temperature *T*, which is below the nitrogen critical temperature, the nitrogen adsorption isotherm for this specific system is

$$n = f\left(\frac{p}{p_0}\right)_T \quad (3)$$

where p_0 is nitrogen saturation pressure at temperature *T*. Nitrogen adsorption isotherm is a relation between the amount nitrogen adsorbed and relative pressure p/p_0 at a known temperature (in case of

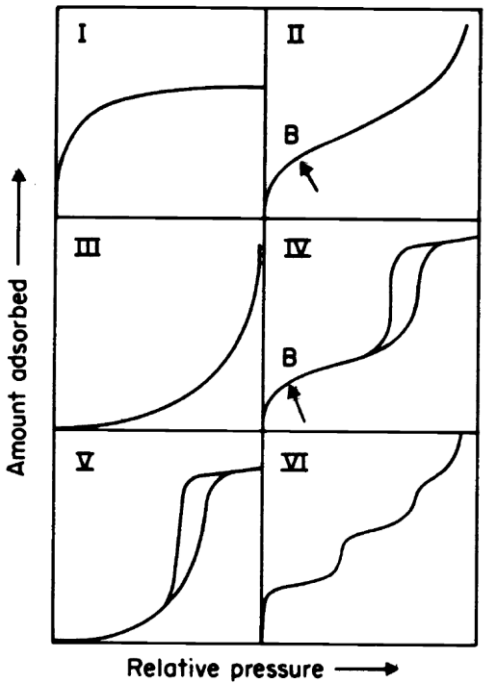

Figure 3.4. Types of adsorption isotherms[148]. Reprinted from the Journal of Pure&Applied Chemistry, Vol.57, Sing KSW., Everett DH., Haul RAW., et al. "Reporting physisorption data from gas/solid systems with special reference to the determination of surface area and porosity", pp.603-619, 1985 with permission from IUPAC.

nitrogen adsorption T= –196ºC). Looking at the shape of the isotherm one can predict the type of material porosity, i.e. to understand whether the sorbent is a microporous, mesoporous, or non-porous material. The classification of nitrogen adsorption isotherms according to IUPAC is shown in **Figure 3.4**. For instance, *Type I* isotherms are normally measured on microporous adsorbents, e.g. MOFs, AC. *Type II* isotherms are measured on non-porous or macroporous adsorbents. *Type III* and *Type V* isotherms do not show any transition point between monolayer-multilayer adsorption (marked by point B in case of *Type II* isotherms). Materials with *Type III* or *V* isotherms do not adsorb nitrogen by layers but nitrogen molecules are clustered around some favorable adsorption sites. Typically, *Type III* or *V* isotherms are observed for materials which have relatively weak interaction with nitrogen molecules. Mesoporous adsorbents normally exhibit *Type IV* isotherms where the monolayer-multilayer adsorption on mesopore walls is followed by capillary condensation. *Type VI* isotherms with clear layer-by-layer adsorption are measured on materials which have highly uniform surface.

Figure 3.5. Nitrogen sorption analyzer and its main constituent parts: 1) sample cells, 2) an open-ended Dewar with liquid nitrogen, 3) a sample cell placed in the heater in process of vacuum degassing, 4) a sample cell placed in the heater in process of nitrogen flow degassing, 5) a keyboard control unit, 6) a temperature controller.

The amount of nitrogen adsorbed by the material is measured by either a *volumetric* or a *gravimetric* method. The volumetric method measures the pressure drop caused by nitrogen removal from the gas phase. The gravimetric method measures the weight change of the material during nitrogen adsorption. The typical design of a nitrogen sorption analyzer (based on the volumetric method) with its main constituent parts is shown in **Figure 3.5**.

Different models (methods) are applied to interpret nitrogen adsorption isotherm data. *The Brunauer-Emmett-Teller (BET) method* is normally used to estimate surface area of the material. This method is based on the following equation:

$$\frac{1}{n\left(\frac{p}{p_0}-1\right)}=\frac{1}{n_m C}+\frac{C-1}{n_m C}\frac{p}{p_0} \quad (4),$$

where n is the amount of nitrogen adsorbed at pressure p, n_m is the amount of nitrogen forming a monolayer of surface coverage, and C is a constant which is related to the adsorption energy in the first adsorbed monolayer ($C \approx 50 - 250$) . If one plots $\frac{1}{n\left(\frac{p}{p_0}-1\right)}$ versus $\frac{p}{p_0}$ to get a slope $\frac{C-1}{n_m C}$ and an intercept $\frac{1}{n_m C}$ of the line one can calculate a n_m parameter. The n_m parameter can be then converted into surface area S using the following equitation:

$$S=\frac{n_m}{M_r}N_A\sigma \quad (5),$$

where M_r is a molecular weight of nitrogen, N_a is the Avogadro constant, and σ is the nitrogen cross-sectional area. The linearity range of the $\frac{1}{n(\frac{p}{p_0}-1)}$ vs. $\frac{p}{p_0}$ sequence is different for different types of materials and should be carefully considered when calculating the n_m value. The BET isotherm linearity range differs from 0,05-0,30 for most mesoporous and macroporous materials down to 10^{-3} - 10^{-4} for microporous materials.

Dubinin's theory is commonly used to describe pore filling in microporous materials. This theory is described by a general equation for fractional micropore filling:

$$\frac{n}{n_p}=e^{-\left(\frac{A}{bE_0}\right)^2} \quad (6)$$

where n_p is micropore volume, A is an expression for the "adsorption potential" (see **Equation 7**), E_0 is the "characteristic" energy for a standard vapor (normally benzene) and b is a constant[149].

$$A=-RT\ln\left(\frac{p}{p_0}\right) \quad (7).$$

The main disadvantages of Dubinin's method are that this method assumes a homogeneous surface of the material and is not specific towards the pore shape. Other methods were developed which are specific towards the pore geometry. For instance, the Horvath and Kowazoe method assumes slit-like pores[150], the Saito and Foley method assumes cylindrical pores[151], and the Cheng and Yang method assumes spherical pores[152].

Nitrogen sorption analysis also provides information about the pore size distribution in the mesopore range if the model proposed by Barrett, Joyner, and Halenda (BJH) is applied to the nitrogen adsorption data. This model is described by the modified version of the Kelvin equation[153]:

$$r_k = -\frac{2\gamma V_M \ln\left(\frac{p}{p_0}\right)}{RT} \quad (7),$$

where r_k is the Kelvin pore radius, γ is the surface tension of nitrogen at its boiling point, V_M is the molar volume of liquid nitrogen, T is the nitrogen boiling temperature, and $\frac{p}{p_0}$ is nitrogen relative pressure. The equation describes successive emptying of pores with radius r_k by lowering relative pressure $\frac{p}{p_0}$.

However, the best results are achieved if Density Functional Theory (DFT) or methods of molecular simulations (Monte Carlo simulation) are used for pore analysis[154, 155]. Using molecular calculations one can model nitrogen adsorption in a pore with a certain width. Summarizing results of molecular simulations for nitrogen adsorption in pores with various widths and comparing it with experimental data one could deduce the pore size distributions function. This approach is described by a Generalized Adsorption Isotherm (GAI) equation:

$$N(\frac{p}{p_0}) = \int_{W\min}^{W\max} (N(\frac{p}{p_0}, W) f(W) dW \quad (10),$$

where W is a pore width, $N\left(\frac{p}{p_0}\right)$ represents the experimental sorption isotherm data, $N\left(\frac{p}{p_0}, W\right)$ represents a calculated sorption isotherm for the pore with width W, $f(W)$ is a pore size distribution function, and pores which are considered for nitrogen adsorption have a width within the interval (W_{min}, W_{max}).

All measurements in this thesis were performed by the Quantachrome Nova 1200e nitrogen analyzer which is a volumetric instrument (see **Figure 3.5**). The pressure transducer is the main factor limiting the width of micropores which can be measured by the volumetric instrument. The Quantachrome Nova 1200e sorption analyzer allows to conduct measurements in the $\frac{p}{p_0}$ relative pressure range of 10^{-3} – 1. Prior to the measurements all samples were degassed under the vacuum

(or under the nitrogen flow) and at appropriate temperatures. All calculations were performed using the standard NOVAWin-P version 10.0+ software.

3.2.3 Rubotherm gravimetric system

Hydrogen adsorption measurements were performed using a Rubotherm gravimetric system equipped with a magnetic suspension balance. The magnetic suspension balance measures *in situ* the weight change of the sample. The sample is placed in a sample chamber which is isolated from the external atmosphere. The sample weight is measured via interaction of a permanent magnet (connected to the sample inside the sample chamber) with an electromagnet (located outside of the sample chamber), see **Figure 3.6**. The sample chamber can be filled with different gases (e.g. hydrogen, helium) and the sample weight can be measured at various temperatures and pressures. The possibility to measure the sample weight at not-ambient conditions (atmosphere, temperature, pressure) is the main advantage of the Rubotherm gravimetric balance compared to other conventional gravimetric balances.

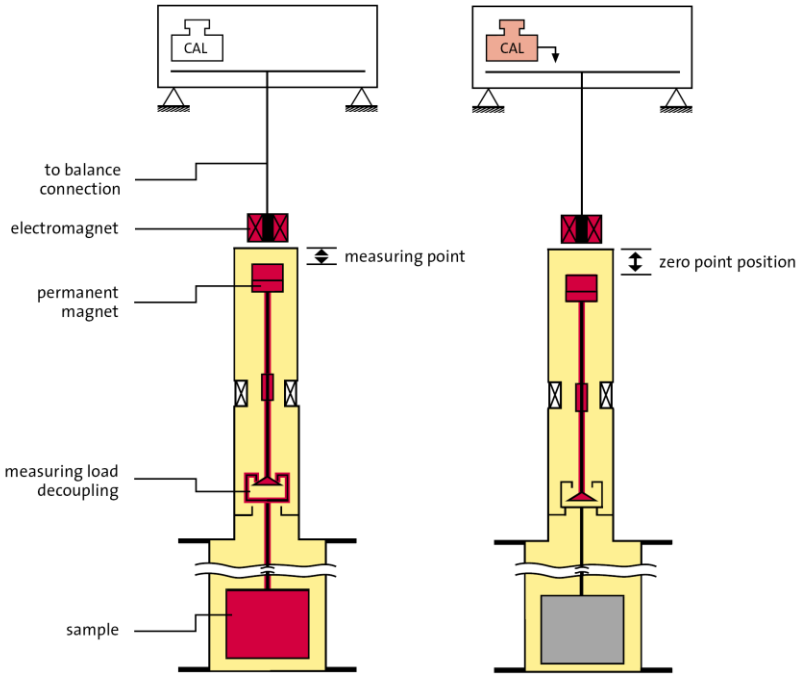

Figure 3.6. Schematic representation of the Rubotherm gravimetric balance: in the measuring mode (to the left); in the taring and calibration mode (to the right). Reprinted from the" Rubotherm magnetic suspension balances" brochure with permissions from Rubotherm GmbH.

Typical duration of a hydrogen adsorption experiment is about 1–3 days. The gravimetric system provides possibility to make an internal calibration every 2-3 minutes which is extremely

important for long measurements (see **Figure 3.6**). The sample settles down on a support, and only weight of the suspension magnet coupled with an empty balance pan is transmitted to the balance (i.e. "zero point" position). The weight of the suspension magnet at the "zero point" position is used for the internal calibration which is repeated throughout the entire experiment with automatic corrections of the weight difference.

The gravimetric balance performs sample weight measurements (sample weights up to 10g) with a resolution of 0,01mg and a reproducibility of $\pm$ 0,02mg. Sample weight measurements can be performed at temperatures starting from -20ºC, which is achieved by cooling the sample cell down by a remote thermostat, up to 450ºC, which is achieved by heating the sample cell by an external electrical heater.

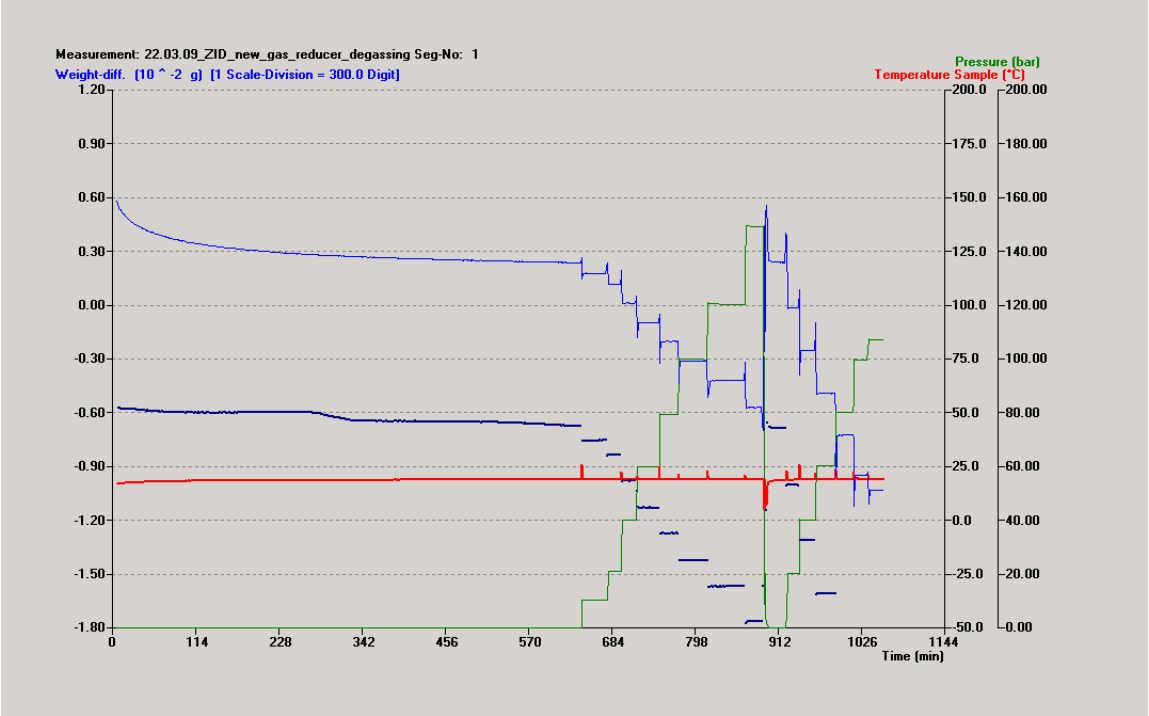

Figure 3.7. A typical example of the hydrogen adsorption experiment: red line – temperature; green line – pressure; blue line - sample weight change; dark blue - "zero point" correction.

A typical hydrogen adsorption experiment consists of several major steps (see **Figure 3.7**):

- Degassing of the sample cell at high vacuum conditions (10^{-6} - 10^{-7}bar) and at the temperature selected according to the sample thermal stability data obtained by the thermo-gravimetrical analysis. The degassing process is over when the sample weight becomes stable.

- Hydrogen adsorption measurements at constant temperature and with a step-wise pressure increase (T= from -20°C to 20°C; P_{H2}= up to 200bar) which are followed by desorption at high vacuum conditions.
- Determination of the sample total volume V_{He} (volume of the sample together with the sample cell and the holder) which is performed by measuring the sample weight at different helium pressures.
- Calculation of hydrogen adsorption considering the buoyancy effect.

Hydrogen adsorption measurements are controlled by the software which plots in situ pressure in the sample cell, temperature of the sample, the sample weight change, and a "zero-point" signal (see **Figure 3.7**).

3.2.4 Thermogravimetric measurements

Thermogravimetric analysis (TGA) is performed by precise balances which measure the sample weight as the sample is heated, cooled or kept at the constant temperature. In addition to simple weight change measurements some balances measures the temperature difference between a sample and a reference material (DTA method) or the heat flow in and out of a sample and a reference material (DSC method). Many material properties can be studied using TGA or DSC/DTA analyses (see **Table 3.1**).

TGA	**DSC**
• Adsorption and desorption of gases	• Melting
• Quantitative content analysis	• Crystallization
• Kinetics of decomposition process	• Polymorphism
• Sublimation, evaporations and vaporization	• Phase diagrams
• Thermal stability	• Glass transition
• Oxidation stability	• Reaction kinetics
• Identification of decomposition products	• Heat capacity
• Sorption and desorption of moistures	• Reaction and transition enthalpy
• Pseudopolymorphism	
• Determination of Curie temperatures	

Table 3.1. Some material properties or thermal processes which could be detected by TGA/DSC.

The major parts of any TGA analyzer are high-precision balance connected to the sample holder and thermocouples which control the temperature of the sample and the reference material. A standard TGA experiment is performed by heating the sample in a certain atmosphere (i.e. ambient air, nitrogen, argon etc are passed through the sample cell at different flow rates) and by recording the sample weight change as a function of the temperature. TGA experiments in this thesis were

performed using a L81+DTA Linseis thermobalance and a Mettler Toledo TGA/DSC1 instrument under a nitrogen flow.

3.2.5 Raman and IR spectroscopy.

Techniques which study changes of the wavelength or the intensity of light which passes through the sample are called vibrational spectroscopy, i.e. Raman and infrared (IR) spectroscopy. Photons interact with molecules of the sample and could bring them to an excited energy state. Molecular transitions from a ground energy state to an excited energy state result in photon adsorption and the intensity decrease of light that passes through the sample. As molecules relax back to the ground state new photons with the same energy as adsorbed photons are emitted. However, excited molecules could relax not back to the ground state but to another excited state with a lower energy. This will result in emission of photons with lower energy in comparison to adsorbed photons. There is also a possibility that incident photons interact with excited molecules. In this case the transition of excited molecules back to the ground energy state can increase the energy of scattered photons. As the result the wavelength of scattered light is changed.

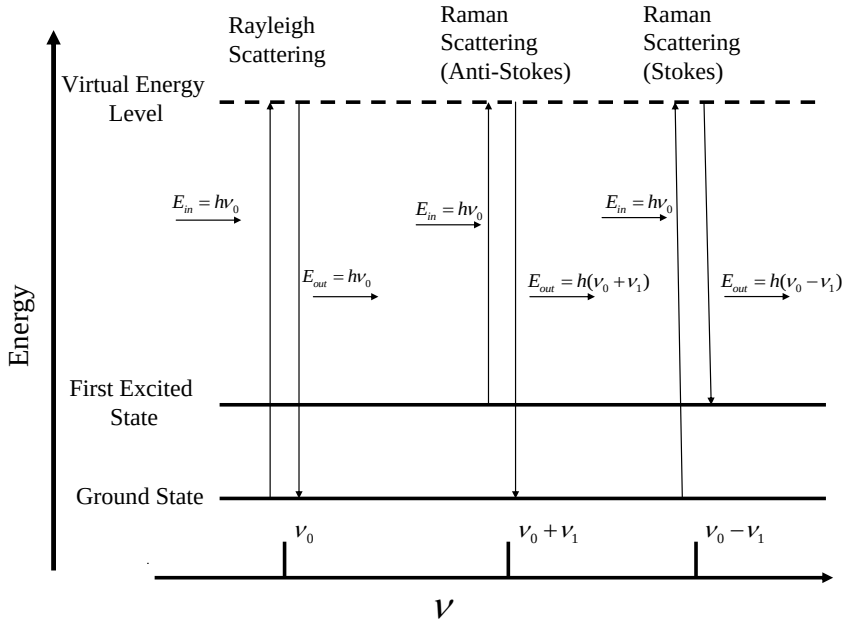

Figure 3.8. The energy level diagram which shows the basic transitions involved in spontaneous Raman scattering.

In case of Raman spectroscopy light of a certain wavelength is shone on the sample and the change in the wavelength of scattered light is measured. As a result of interaction with molecules photons can be elastically or inelastically scattered. In case of elastic scattering the adsorbed and

emitted photons have the same energy (Rayleigh scattering, see **Figure 3.8**). In case of inelastic scattering emitted phonons can have either higher (anti-Stokes scattering) or lower (Stokes scattering) energy in comparison to incident phonons. The probability of Stokes scattering is about 10^{-7} while anti-Stokes scattering has an even lower probability. Therefore, phonons scattered according to the Stokes mechanism are normally used for the Raman spectroscopy analysis.

In case of IR spectroscopy the wavelength of the incident light is changed with time in order to observe all the adsorption lines within a specific wavelength interval. IR spectra show absorbance (or transmittance) of light at different wavelengths. Despite the fact that both IR and Raman spectroscopy measure the vibrational energies of molecules they rely on different selection rules. For instance, vibrations are IR active if they change the dipole moment of the molecule (it does not imply that the molecule has a permanent dipole moment). Vibrations are Raman active if they change the polarizability of the molecule. Due to those differences Raman and IR spectroscopy are complementary techniques which are widely used to study vibrational and rotational modes of various materials.

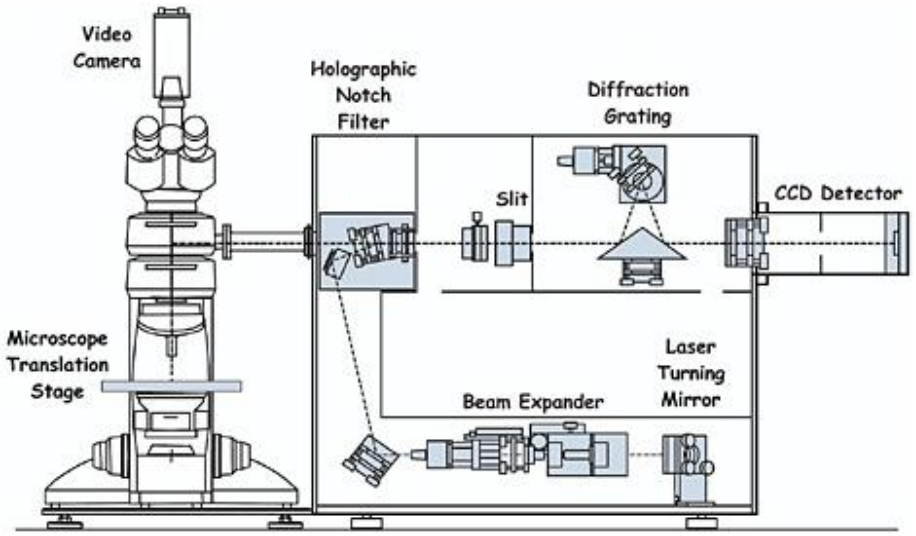

Figure 3.9.Schematic representation of the Raman spectrometer[156]. Reprinted with permission from (Stackler NAS Colloquium) Scientific Examination of Art: Modern Techniques in Conservation and Analysis, 2005, by the National Academy of Science, Courtesy of the National Academies Press, Washington, D.C.

The Raman spectrometer used in this work was the Renishaw grating spectrometer with a notch filter to remove the Rayleigh line, see **Figure 3.9**. A Peltier cooled CCD-detector was used to detect Stokes and anti-Stokes lines. Helium-neon (He-Ne, an excitation wavelength of 633nm) and argon-ion (Ar^+ ion, 514nm) lasers were used to record spectra. The resolution of the Raman

spectrometer was $2cm^{-1}$. All the IR spectra were recorded using the Perkin Elmer Spectrum BX FT-IR system.

3.2.6 Mass spectrometry

Mass spectrometry (MS) is an important analytical technique which measures the mass-to-charge ratio of charged particles. The main applications of MS are the determination of masses of particles, the determination of the elemental compositions of particles, and studies of chemical structures of particles (by controlled fragmentation).

The first step in the MS analysis is production of ions from the sample. Ions are produced in an ion source (see **Figure 3.10**). In the ion source a certain amount of energy is transferred to the sample which leads to ionization of sample molecules. Ionization sources are divided in two broad classes depending on the physical state of the sample before the ionization. For instance, electron ionization, chemical ionization, or field ionization techniques are only suitable for volatile and thermally stable samples as ionization occurs in the gas-phase. For thermally unstable samples or samples with a low vapor pressure other ionization techniques are used which ionize sample molecules in liquid or solid phase. For instance, in the case of electrospray ionization, atmospheric pressure chemical ionization, and atmospheric pressure photoionization sources samples are introduced into the ionization camera as droplets of liquid. Other ionization techniques involve irradiation of sample deposits by energetic particles or photons which lead to formation of ions near to the surface of deposits. Matrix-assisted laser desorption ionization, plasma desorption ionization, field desorption ionization techniques belong to this class of solid-state ion sources.

Figure 3.10. Block-scheme of mass spectrometer.

After ions are produced they are transferred to a mass analyzer where ions are separated according to their m/z ratio and analyzed. There are different types of mass analyzers which separate ions according to different principles, but all of them use static or dynamic electric and magnetic field for ion separation (see **Table 3.2**). Mass analyzers are divided into scanning and simultaneous

Type of mass analyzer	Principle of separation
Electric sector	Kinetic energy
Magnetic sector	Momentum
Quadrupole	Trajectory stability
Ion trap	Resonance frequency
Time-of-flight	Flight time
Fourier transform ion cyclotron resonance	Resonance frequency
Fourier transform orbitrap	Resonance frequency

Table 3.2. Types of mass analyzers and principles of ion separation[157].

transmission classes. Scanning mass analyzers scan ion with different masses over a time scale. This class of instruments includes magnetic sector mass analyzers with a flying tube in the magnetic field or quadrupole mass analyzers. Other mass analyzers transmit all ions simultaneously. This class of mass analyzers includes dispersive magnetic analyzers, time-of-flight analyzers, ion traps, ion cyclotron resonance analyzers, and orbitraps.

After ions pass through the mass analyzer they are detected by detectors which generate an electrical current proportional to ionic abundance. The detector selection for a particular instrument depends on the instrument design. Some detectors count ions of a certain mass at a time (point ion collectors) while other detectors detect ions of all masses simultaneously (photographic plates, image current detectors etc).

All mass spectra in this thesis were recorded with a MALDI TOF mass spectrometer (Voyager DE-STR, Applied Biosystems, USA) and with a high-resolution APPI FT-ICR mass spectrometer (Thermo Scientific, Bremen, Germany). Prior to the MS analysis samples were dissolved in toluene. For MALDI TOF MS toluene solutions of samples were mixed with a toluene solution of elemental sulfur, which was used as matrix, in a volume ratio 1:15.

4 Results and discussion

4.1 Hydrogen storage in some Co- and Zn-based MOFs

MOFs is a rapidly growing new class of porous materials with hundreds of new structures reported every year[158, 159]. It is important to investigate new MOFs for hydrogen adsorption properties, to reveal the most important parameters which control hydrogen storage in these materials and, possibly, to use the accumulated knowledge for more targeted design of new MOFs for hydrogen storage applications[160]. Materials studied here were synthesized within a collaboration with the group of Prof. H. Chun. They synthesized a set of new Zn- and Co-based MOFs which have different pore geometries and surface areas (see **Figure 4.1**).

Among those materials we have studied four different Zn-based MOFs (ZBDt, ZBDh, ZID, ZIDs, and $[Zn_4(O)(mip)_3]$) and one Co-based MOF (CND). ZBDt and ZBDh are two different isomers of the same MOF (chemical formula: $C_{22}H_{20}N_2O_8Zn_2$). ZBDt consists of square channels with the size of 7,5Å*7,5Å, while ZBDh consists of triangle and hexagonal channels with a van der Waals radius of the channels 4,5Å and 13,5-15Å correspondingly[161, 162]. ZID, ZIDs, and $[Zn_4(O)(mip)_3]$ were synthesized by changing the organic ligands. ZID and ZIDs are the same material (chemical formula: $C_{38}H_{32}N_2O_{18}Zn_4$), but were synthesized by different methods: ZID is synthesized by the diffusion method, while ZIDs are obtained by the solvothermal reaction[163]. The ZID structure shows three kinds of cage-like pores with diameters of 8-20Å. $[Zn_4(O)(mip)_3]$ (chemical formula: $C_{42}H_{55}N_5O_{19}Zn_4$) consists of various pores with irregular shape which are less than 10Å in diameter[164]. CND (chemical formula: $C_{73,5}H_{66}N_2O_{12}Co_3$) consists of triangular channels with a van der Waals radius of 4,5Å[165].

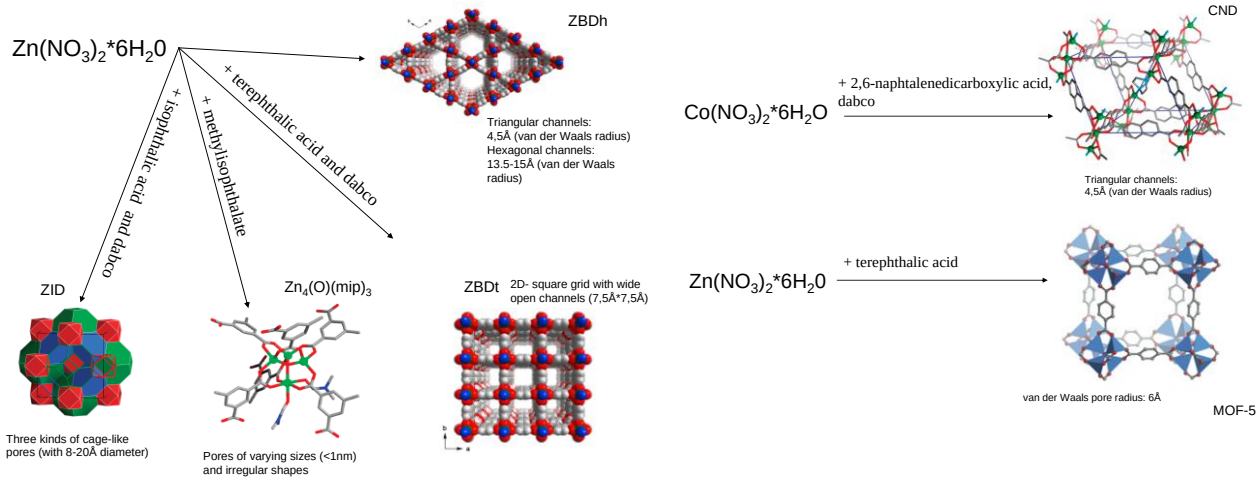

Figure 4.1. Various Zn- and Co-based MOFs studied for hydrogen adsorption at ambient temperatures.

Therefore, the samples provided to us for hydrogen adsorption experiments showed a broad variation of the main parameters: surface area, pore size and geometry, two different metals in oxide clusters and a variety of organic linker types. According to results previously published by the group of Prof H.Chun, some of these MOFs showed hydrogen uptake values in the range of 1,5-2,45wt.% at 1 bar of H_2 pressure and T=77K[161-165] which are comparable with best results reported for MOFs at those conditions[31].

Hydrogen adsorption at temperature conditions close to ambient were measured in our study.

Hydrogen adsorption isotherms: effects of pressure and surface area. At ambient temperatures the highest hydrogen uptake of 0,51wt.% was observed for ZBDh (p=120bar and T=20°C), see **Figure 4.2**. After lowering the temperature down to -4°C hydrogen uptake in ZBDh increased up to 0,63wt.% which agrees well with the fact that physisorption is a temperature dependent process. As saturation was not achieved at 120bar for either of these temperatures, pressure was further increased up to 175bar. At 175bar ZBDh adsorbed 0,75 wt.% of H_2 (see **Figure 4.2b**), but even at that pressure the adsorption curve did not reach saturation. As expected for physisorption, hydrogen adsorption was completely reversible and the equilibrium value of hydrogen uptake was established every time within a few minutes after the hydrogen pressure was stabilized. Using a Langmuir fit, the hydrogen adsorption saturation value for ZBDh was estimated to be on the level of ~1,63wt.%, but according to this fit the saturation would be achieved at extremely high pressure (4000-5000bar).

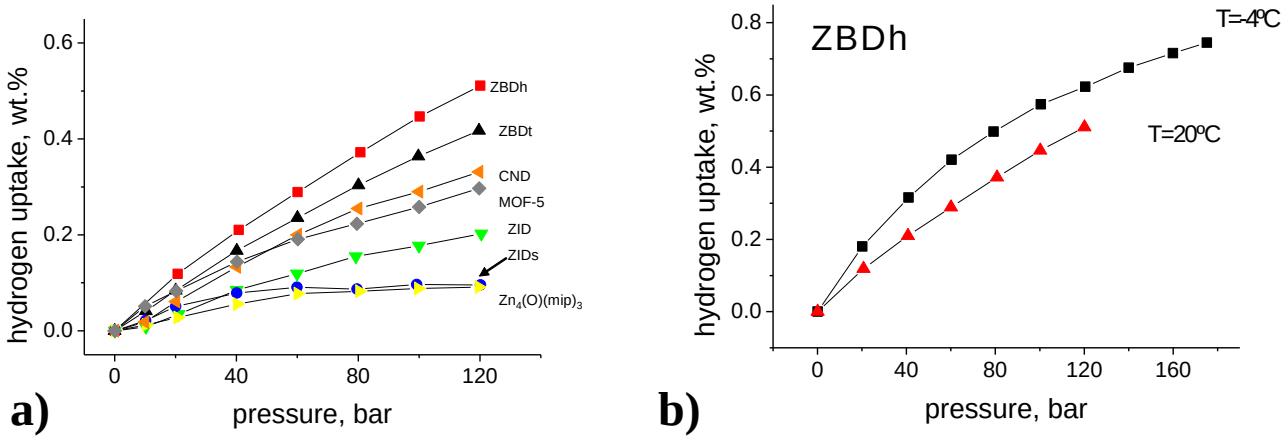

Figure 4.2. a) Hydrogen adsorption isotherms recorded at T=20°C (-■- - ZBDh, -▲- - ZBDt, -◀- - CND, -▼- ZID, -●- $Zn_4(O)(mip)_3$, -►- ZIDs, -♦- MOF-5). B) Hydrogen adsorption isotherm recorded for ZBDh at temperatures T=20°C (-▲-) and T= -4°C (-■-).

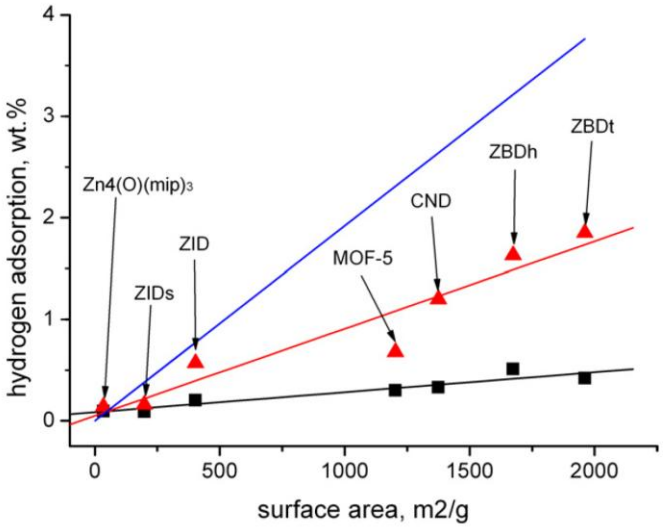

Figure 4.3. The relation between hydrogen adsorption values and BET specific surface area measured for different MOFs: ■- hydrogen adsorption at 120bar and room temperature with linear fit shown by black line, ▲- the saturation value of hydrogen adsorption obtained using Langmuir fit with linear fit shown by red line, blue line- excess hydrogen adsorption measured on MOFs at -196ºC plotted versus BET surface area[24]).

All MOFs studied in our project exhibited a hydrogen adsorption which was almost linearly proportional to the BET surface area (see **Figure 4.3** and **Table 4.1**). This result was in good agreement with known trends observed for materials which store hydrogen by physisorption. The correlation between hydrogen uptake and total pore volume was less pronounced which also agrees well with literature. Surface area was reported to be the main factor influencing hydrogen adsorption at ambient temperatures[24] while pore volume was a more important parameter at cryogenic temperatures[41].

Structural stability issues. The problem of poor structural stability is another issue which must be carefully considered while designing MOFs for hydrogen adsorption. Hydrogen adsorption measured for $Zn_4(O)(mip)_3$ was rather low, see **Table 4.1**. The reason for low hydrogen adsorption for $Zn_4(O)(mip)_3$ became obvious after analysis of powder X-ray diffraction patterns recorded before and after adsorption experiments (see **Figure 4.4**). It is obvious from **Figure 4.4** that the $Zn_4(O)(mip)_3$ structure collapsed during hydrogen adsorption measurements.

It should be noted that MOFs are rather fragile materials and are normally stored immersed into some solvents which fills the large pores and stabilizes the structure[164]. In principle, collapse of the MOF structure might either occur in the process of vacuum degassing at elevated temperature or be an effect of hydrogen pressure increase in the process of adsorption measurements. Most likely,

the collapse of the $Zn_4(O)(mip)_3$ structure occured in the process of degassing which included heating in vacuum at 110ºC.

Name	Surface area (our exp.), m^2/g	Surface area (literature), m^2/g	Pore volume (our exp.), g/cm^3	Pore volume (literature), g/cm3	Hydrogen uptake (our exp.), wt.%[a]	Hydrogen uptake (literature), wt.%[a]
ZBDt	1961	1450 [161, 162]	0,69	0,75 [161, 162]	0,42	2,0 [161, 162]
ZBDh	1674	1603 [162]	0,59	0,86 [162]	0,51	1,8 [162]
ZID	403	1609 [163]	0,56	0,86 [163]	0,2	1,5 [163]
ZIDs	198	-	0,11	-	0,09	-
$Zn4(O)(mip)_3$	34,4	1062 [164]	0,017	0,56 [164]	0,1	2,1 [164]
CND	1375	1502 [165]	0,47	0,822 [165]	0,33	2,45 [165]
MOF-5	1203	839,6 [166]	0,66	0,34 [166]	0,3	3,6 [166], [b]

[a] - data were recorded at: 1) 77K and 1 bar of hydrogen pressure (literature), 2) at RT and 120bar of hydrogen pressure (our experiment).

[b] - data were recorded at 77K and 17, 4 bar of hydrogen pressure.

Table 4.1. Summary of hydrogen adsorption experiments performed in this study compared to literature data.

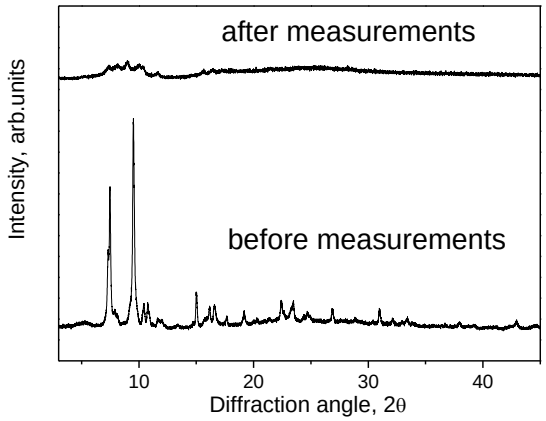

Figure 4.4. XRD patterns recorded for $[Zn_4(O)(mip)_3]$ before and after hydrogen adsorption measurements.

According to previously published TGA data the material is stable in the temperature interval of 230-400ºC[164]. However, the heat treatment used in our experiments was relatively long (12 hours) to provide more complete degassing of the material compared to the relatively short TGA

experiments. The degassing temperature should be lowered or the degassing time should be reduced in order to avoid structural decomposition of $Zn_4(O)(mip)_3$. However, in this case it could be rather difficult to remove all solvent molecules from the $Zn_4(O)(mip)_3$ structure. Therefore, the relatively weak structural stability of this material is the major obstacle for possible applications.

It can be concluded that the crystal structure of MOFs must be carefully examined after hydrogen adsorption experiments in order to make sure that MOFs did not decompose during hydrogen adsorption measurements. However, in many previously published studies the structural characterization of samples was performed only *before* hydrogen adsorption measurements and rarely *after* the experiment. Partial decomposition of the material during the experiment could be one possible reason for the discrepancy in hydrogen adsorption capacities of some MOFs reported by various groups[166-168].

Reference MOF-5 sample. Hydrogen adsorption measurements are a very delicate procedure, and small mistakes could lead to huge overestimation of hydrogen adsorption[20-22]. To validate our data we performed test measurements on MOF-5 which is one of the most studied MOFs for hydrogen adsorption. MOF-5 adsorbed 0,3wt.% of H_2 at 120bar which is in a reasonable agreement with results published for MOF-5 samples prepared and activated according to similar procedures[166].

Summarizing this chapter, hydrogen storage in MOFs is mainly governed by surface area at ambient temperatures and pressures at least up to 120bar. Pore geometry is also an important factor influencing hydrogen adsorption in MOFs, and therefore should be carefully considered while designing new MOFs for hydrogen storage. The crystal structure of MOFs must be examined after the experiment in order to verify their structural stability throughout degassing and hydrogen adsorption measurements.

4.2 Hydrogen adsorption in MOF-5 doped/bridged with Pt-catalyst

As noted in the previous section, the MOF-5 material was synthesized first as a reference sample to ensure correctness of hydrogen adsorption measurements. On the next stage of the project this material was used to verify recent exciting reports published by the group of Prof. R.T. Yang which claimed that hydrogen adsorption in MOF-5 can be significantly improved by doping with Pt-catalyst[66,59].

Hydrogen adsorption in all MOFs studied in the previous chapter did not exceed 1wt.% at ambient temperatures even if hydrogen pressure was increased up to 175bar. Therefore, new methods to increase hydrogen uptake in MOFs are of significant importance. The methods of Pt

doping described in the literature are simple[59, 66] and, if confirmed, could be further developed to optimize hydrogen storage in MOF materials.

Therefore, we performed a set of experiments aimed at studying the effect of Pt catalyst on hydrogen adsorption in MOF-5. The MOF-5 is a well-characterized material with known hydrogen adsorption properties which makes it a good model material for studies of catalyst addition effects[167].

Characterization of pristine MOF-5. Two sets of MOF-5, MOF-5_a and MOF-5_b, were synthesized following a slightly modified procedure given in the literature. The difference is related to removal of residual solvent from the pores of the structure[166, 168]. Both samples showed the expected FCC crystal structure (Fm-3m, a=25,8Å) which was in good agreement with previously published results (see **Figure 4.5**)[168].

Nitrogen sorption analysis showed that the modified drying process slightly increased surface area and total pore volume of MOF-5_b compared to MOF-5_a while both samples had the same micropore volume (see **Table 4.2**). The increase of pore volume and surface area for MOF-5_b is mainly contributed by pores in the range of 30-140Å which possibly represent cavities formed between grains of MOF-5_b during the drying process.

Doping MOF-5 with Pt catalyst. A set of Pt-doped MOF-5 was prepared by mixing MOF-5_a (or MOF-5_b) samples with Pt/AC catalysts (5wt.% or 10wt.% of Pt) in a weight ratio of 9:1. In order to improve the contact between Pt catalyst particles and MOF-5 samples, MOF-5, Pt-catalysts, and sucrose were thoroughly mixed together and subjected to heat treatment according to a slightly modified protocol published elsewhere[59]. After the heat treatment the sucrose carbonized, as was confirmed by IR spectroscopy, supposedly forming carbon bridges between Pt catalyst particles and MOF-5 (see **Figure 4.6**). Both "doped" and "bridged" MOF-5 samples retained their original crystal structure without any visual changes observed in XRD patterns (see **Figure 4.5**). A slight decrease of surface area and pore volume in the "bridged" samples can be explained by pore blockage by carbonized sucrose and was also observed in the original claim about spillover in MOFs[59].

Prior to hydrogen adsorption measurements all samples were activated at 120ºC in vacuum during 12 hours. The degassing temperature was chosen in agreement with literature[169]. Removal of solvent molecules from the MOF-5 structure was confirmed by IR spectroscopy. A broad peak at 1660cm^{-1}, which originated from the C=O band of DMF, disappeared from the IR spectra of activated samples (see **Figure 4.6**)[170].

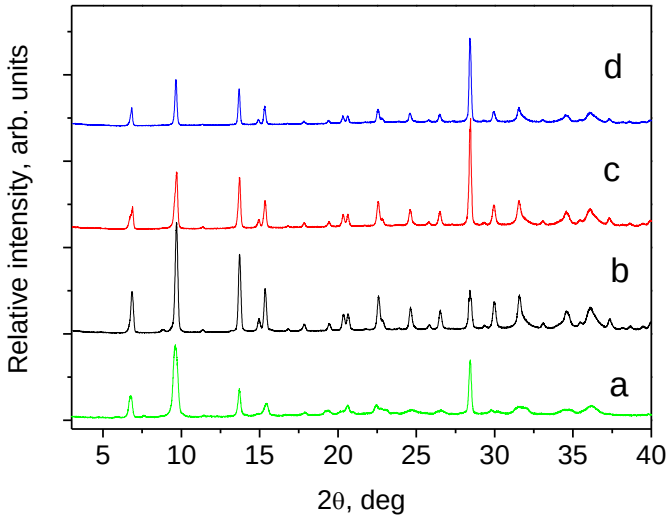

Figure 4.5. X-ray diffraction patterns of a) as-synthesized MOF-5_a; b) MOF-5_a after hydrogen adsorption measurements; c) MOF-5_a mixed with 5wt.% Pt/AC (after hydrogen adsorption measurement) d) MOF-5_a bridged with 5wt.% Pt/AC (after hydrogen adsorption measurement).

	BET, m^2/g	Langm., m^2/g	Micropore volume, cm^3/g	Pore volume, cm^3/g	H_2 uptake, wt.%
MOF-5_a	832	862	0,31	0,37	0,38
MOF-5_b	908	943	0,31	0,44	0,47
MOF-5_a Pt 5wt.% "mixed"	759	789	0,29	0,37	0,43
MOF-5_b Pt 10wt.% "mixed"	761	802	0,29	0,33	0,32
MOF-5_a Pt 5wt.% "bridged"	618	652	0,23	0,31	0,27
MOF-5_b Pt10wt.% "bridged"	441	451	0,16	0,18	0,27
Pt 5wt.% on AC	1183	1267	0,48	0,97	0,53
Pt 10wt.% on AC	595	612	0,24	0,45	0,39
MOF-5 [59]	1021	1355	0,39	0,68	0,4
MOF-5 Pt 5wt.% "mixed" [59]	n/a	n/a	n/a	n/a	~1,6
MOF-5 Pt 5wt.% "bridged" [66]	890	n/a	n/a	0,61	3,0

Table 4.2. Hydrogen/nitrogen adsorption data for samples of pristine MOF-5 samples, Pt catalysts and MOF/Pt samples synthesized by "mixing" and "bridging. H_2 uptake is for 120 Bar and 15^0C.

Hydrogen adsorption in Pt doped samples. Results of hydrogen adsorption measurements are summarized in **Table 4.2**. Pristine MOF-5_a adsorbed 0,47 wt.% of hydrogen at 15°C and 120bar which is in a rather good agreement with literature (see **Figure 4.7**). In contrast to our expectations, no Pt-doped or Pt-bridged samples showed any significant increase in hydrogen

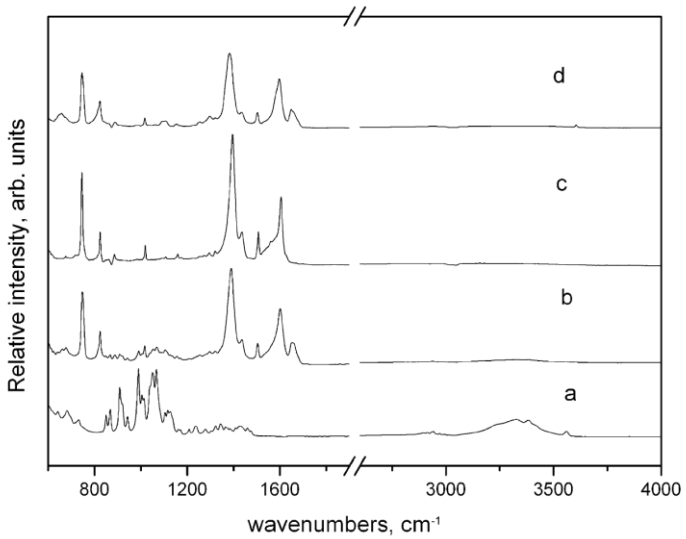

Figure 4.6. IR spectra recorded for: a) sucrose; b) mixture of sucrose, MOF-5_ a, and 5wt.% Pt/AC catalyst before the bridging process; c) mixture of sucrose, MOF-5_ a, and 5wt.% Pt/AC catalyst after the bridging process; d) pristine MOF-5_a material.

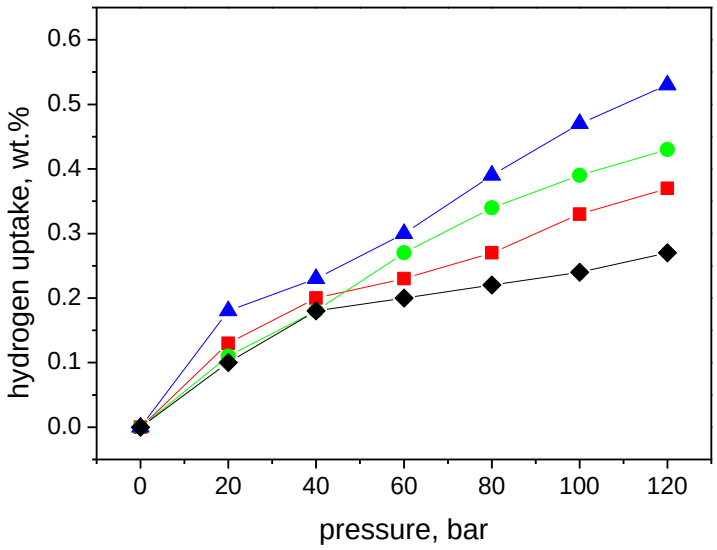

Figure 4.7. Hydrogen adsorption isotherms measured on: MOF-5_a (-■-), MOF-5_a mixed with 5wt.% Pt/AC (-●-), MOF-5_a bridged with 5wt.% Pt/AC (-♦-), 5wt.% Pt/AC (-▲-).

adsorption capacity compared to pristine samples, and no specific features typically attributed to the spillover effect were observed in our experiment (e.g. slow kinetics, linear pressure dependence of adsorption values). Hydrogen adsorption was reversible, and the maximum was achieved in a few

minutes after pressure stabilization (see **Figure 4.8a**). No difference was also observed upon increase of the Pt load in carbon supported catalyst from 5wt% to 10wt%.

Hydrogen adsorption values measured for all samples strongly correlated with BET surface area and pore volume (see **Figure 4.8b**). Correlation of hydrogen adsorption with surface area/pore volume, fast kinetics, and Langmuir type of adsorption isotherm suggests that hydrogen uptake in our samples occured solely by the physisorption mechanism.

The results reported here disagree with initial claims of a significant hydrogen adsorption enhancement due to addition of noble metal catalysts by the group of Prof. R.T Yang[59, 66]. Publication of our results started a discussion about possible reasons for the absence/presence of "spillover" in reports from different groups[22, 171-173]. The authors of the initial report provided a response to our paper citing various small variations in the synthesis procedures as a possible reason for the poor reproducibility of the results[173]. However, we did not find these arguments sufficient to explain the absence of spillover in our experiments, as discussed in details in the following correspondence[172]. A comment by Prof. M. Hirscher published following our paper also contributed to the discussion[22]. It should be noted that independent experiments performed by the group of Prof. M. Hirscher also did not reveal any spillover effect in MOFs materials[74].

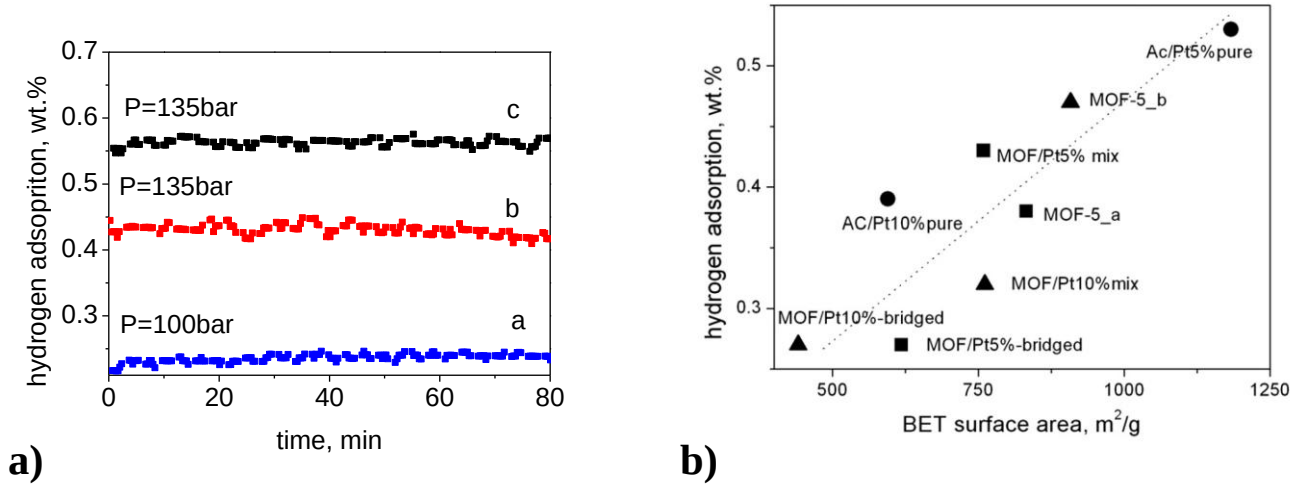

Figure 4.8. a) Hydrogen adsorption measured at 15°C as a function of time for MOF-5_a bridged with 5wt.% Pt/AC (a); MOF-5_a mixed with 5wt.% Pt/AC (b); 5wt.% Pt/AC (c). b) The relation between hydrogen adsorption and BET surface area of studied materials: Pt catalysts (-●-); as-synthesized, doped, and bridged MOF-5_a (-■-); as-synthesized, doped, and bridged MOF-5_b (-▲-).

Following our report, the group of Prof. R.T.Yang published a new study which reported that enhancement of hydrogen adsorption via spillover depends additionally on a number of factors such as size and dispersion of metal catalyst particles, the catalyst activation procedure, chemistry of the

adsorbent surface, and the number of defects induced in the adsorbent[63, 67, 68, 174-177]. It is worth to mention that none of those factors were considered in the original reports where a significant enhancement of hydrogen adsorption was observed in MOF-5 "mixed" or "bridged" with Pt-catalysts[59, 66]. In our work "mixed" and "bridged" MOF-5 samples prepared according to a similar synthesis procedure failed to show any signs of spillover. The absence of spillover in MOFs mixed/bridged with Pt-catalyst was later independently confirmed by other research groups[74, 75].

It can be concluded that the methods proposed previously, e.g. a simple mechanical mixture of Pt catalyst and MOFs powders, are not sufficient to provide room temperature spillover. The discrepancy in hydrogen adsorption measurements performed on samples with seemingly very similar structural properties can possibly be due to some unidentified additional factors or to errors in hydrogen adsorption measurements.

4.3 Hydrogen storage in nanocarbon materials prepared by the cycloaddition reaction of C_{60} with coronene and anthracene

In the solid state the C_{60} molecules are close packed forming the fullerite phase. The surface area of the fullerite phase is negligible but, nevertheless, hydrogen is able to diffuse between C_{60} molecules and occupy interstitial sites. The fullerite phase contains two types of interstitial sites but only one of them, the octahedral void, is sufficiently large to accommodate one hydrogen molecule. Therefore, hydrogen storage in fullerene C_{60} is limited to ~0,28 wt.% at ambient temperatures and moderate hydrogen pressures.

Functionalization of fullerene C_{60} aimed at synthesis of new hydrogen storage materials is focused on a significant expansion of the structure, making interstitial sites sufficiently large to accommodate more than one hydrogen molecule. Another goal would be to create some framework materials with C_{60} molecules connected by some linkers into a 3D structure (similar to MOFs) thus making all the surface area of the fullerene molecules available for hydrogen adsorption. The project described here was aimed at verification of a possibility to functionalize C_{60} by a reaction with various PAHs, e.g. coronene and anthracene.

We have studied the reaction between fullerene C_{60} and coronene in the temperature interval of 450-850ºC. The reaction resulted in expansion of the FCC fullerene C_{60} structure in the temperature interval of 500-650ºC as shown in **Figure 4.9**. Higher temperatures of the reaction (700-850ºC) resulted in amorphization of the C_{60} structure and formation of some nanostructured carbon materials, as was confirmed by Raman spectroscopy[23]. Reaction products with an increased cell parameter were tested for hydrogen adsorption.

Samples synthesized at 500-600ºC adsorbed approximately the same amount of hydrogen as pristine C_{60}. Hydrogen adsorption started to increase for samples synthesized at temperatures above 650-700ºC and reached a maximum for the sample synthesized at 800ºC (0,38wt.% at p=120bar and T=15ºC; 0,45wt.% at p=120bar and T=0ºC, see **Figure 4.10**). Higher reaction temperatures decreased hydrogen adsorption values.

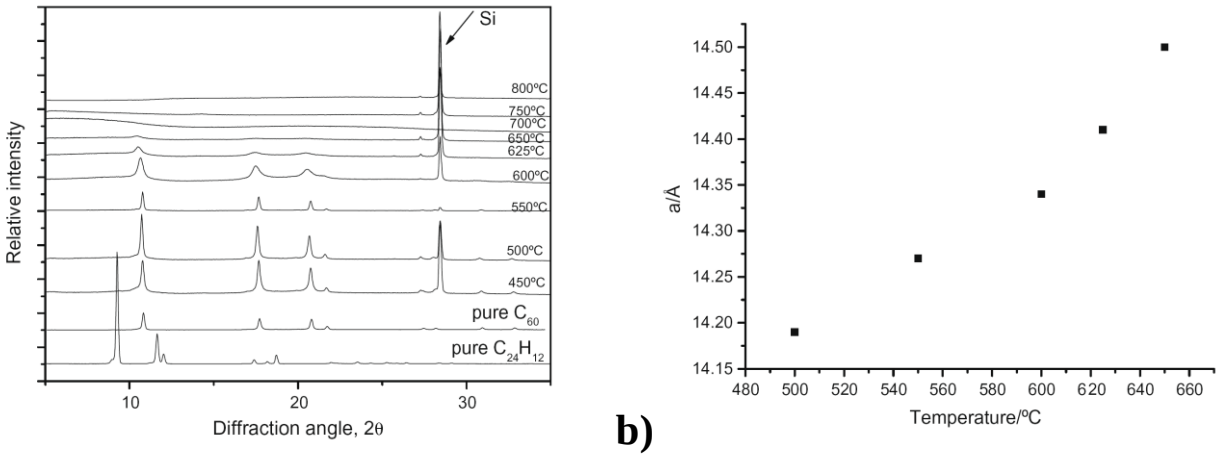

Figure 4.9. a) XRD patterns recorded for products of the C_{60} reaction with coronene at different temperatures within the interval of 450-800ºC (from the bottom to the top); b) cell parameter of C_{60}/coronene samples plotted versus reaction temperatures (reflections are indexed in the FCC structure).

The increase of hydrogen adsorption correlated with the beginning of C_{60}/coronene graphitization at ca. 700ºC and the formation of graphite-like nanoparticles. The decrease of hydrogen adsorption observed for samples synthesized at temperatures above 800ºC was possibly due to aggregation of graphite-like nanoparticles into larger grains and a general graphitization of samples. Real density measurements confirmed this assumption. The real density of pristine C_{60} is 1,7g/cm^3 and the real density of graphite is 2,25g/cm^3. During the heat treatment of C_{60}/coronene materials the real density changed from 1,7-1,8g/cm^3 typical for C_{60} to 2,07g/cm^3 which is closer to the real density of graphite. The increase of the real density, i.e. graphitization of samples, occurred at temperatures above 800ºC and correlated with the decrease of hydrogen adsorption.

It is interesting to note that despite a relatively high hydrogen adsorption no samples had any measurable surface area (<3 m^2/g), which suggests that mechanisms different from physisorption were responsible for hydrogen adsorption in these materials[10]. Possibly, hydrogen adsorption in this case was related to nano-voids in the bulk structure of the carbon material.

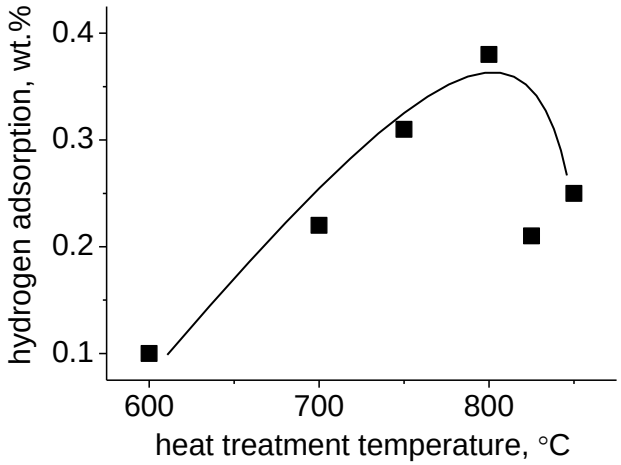

Figure 4.10. Hydrogen adsorption measured on C_{60}/coronene samples synthesized at different temperatures (120bar of H_2 pressure and T=15ºC).

We have also measured hydrogen adsorption on samples synthesized by the reaction between C_{60} and anthracene. Hydrogen adsorption was ~0,1wt.% for all tested samples and did not change for samples synthesized at 600-800ºC where formation of some nanocarbons was expected.

4.4 Hydrogenation of C_{60}

4.4.1 Hydrogenation of C_{60} as a function of the reaction temperature

Hydrogenation of C_{60} was performed at 50bar of hydrogen pressure and in the temperature interval of 350-440ºC and monitored *in situ* using the gravimetric method. The high precision balance with magnetic suspension provided us with a unique possibility to monitor the kinetics of C_{60} hydrogenation by following the weight change of the sample at high hydrogen pressures and high temperatures. As expected, the kinetics of C_{60} hydrogenation strongly depended on the temperature. At 350-400ºC hydrogenation proceeded very slowly and the gravimetric curve reached the saturation only for the sample hydrogenated at 400ºC after 6000min (see **Figure 4.11**). Hydrogenation proceeded much faster if the temperature was increased up to 420-440ºC and at a certain moment the weight increase reached a maximum. The weight decrease observed after the maximum on the gravimetric curve indicates fragmentation of C_{60} and evaporation of some light hydrocarbons formed in the process of fragmentation. According to gravimetric measurements the highest weight increase was observed for the sample hydrogenated at 400ºC (3,96wt.% after 7500min).

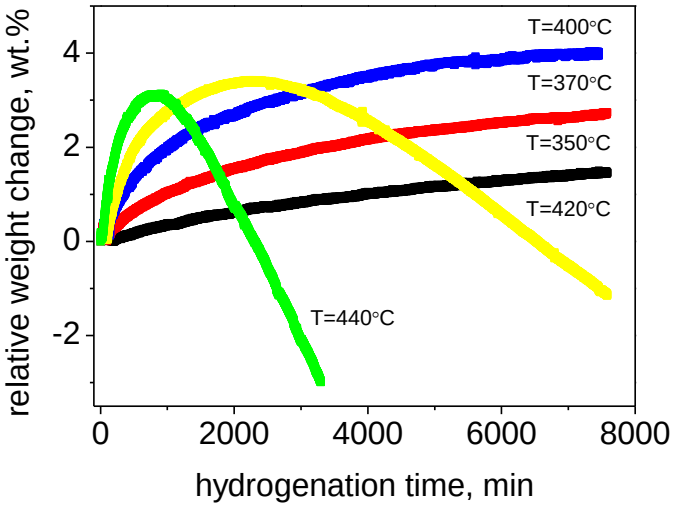

Figure 4.11. Weight change recorded *in situ* from C_{60} hydrogenated at different temperatures (p=50bar of hydrogen).

Samples produced in the hydrogenation experiments shown in **Figure 4.11** were extensively studied ex situ. Analysis of XRD patterns recorded from these samples showed that reaction products are different for experiments performed at different temperatures. Samples hydrogenated at 350-400ºC showed a FCC lattice with an increased cell parameter which is typical for hydrogenated fullerenes. For instance, the sample hydrogenated at 375ºC showed a cell parameter of a=14,60Å which is close to a=14,55Å previously reported for $C_{60}H_{18}$[114]. Prolonged hydrogenation at 400-440ºC resulted in material amorphization and disappearance of all reflections except the (111) reflection from the XRD patterns.

The chemical composition of samples subjected to prolonged hydrogenation reactions at different temperatures was determined using elemental analysis. Hydrogen content agreed very well with the results of the gravimetric analysis for samples hydrogenated at 350-375ºC and is higher than expected for samples hydrogenated at 400-440ºC. Samples hydrogenated at 420ºC and 440ºC contained 4,9wt.% and 4,7wt.% of hydrogen correspondingly despite the negative total weight change. A high hydrogen content together with a negative total weight change are expected if part of the C_{60} molecules collapse during hydrogenation with formation of large hydrocarbon molecules (fullerene fragments).

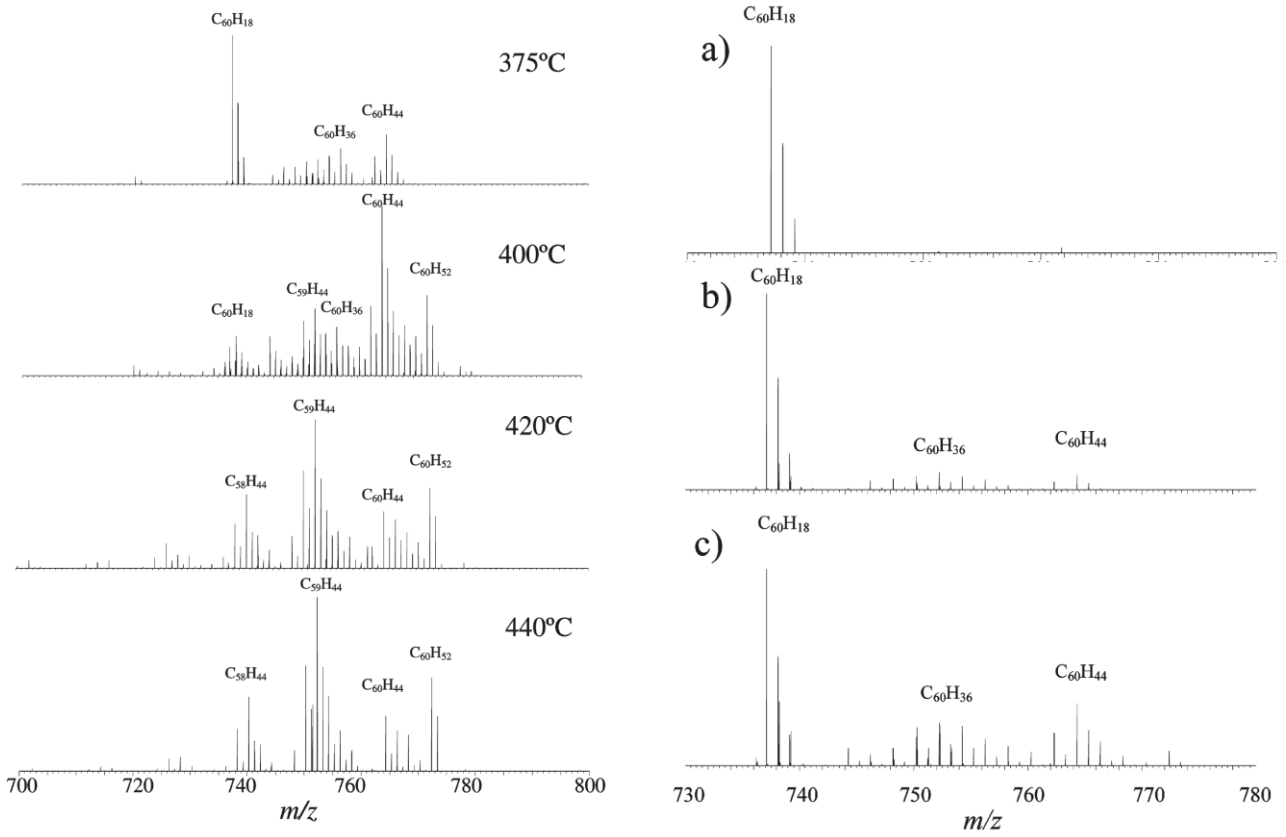

Figure 4.12. APPI FT-ICR mass spectra of C_{60} hydrogenated at different temperatures (left figure). APPI FT-ICR mass spectra of C_{60} hydrogenated at 440ºC for: a) 240min; b) 480min; and c) 750min (right figure).

Fragmentation of C_{60} in the process of hydrogenation at 400-440ºC was confirmed by MS analysis. High resolution mass spectrometry methods allow to identify exactly the compositions of hydrogenated C_{60} molecules even when they are synthesized as complex mixtures. The sample hydrogenated at 350ºC mostly consisted of $C_{60}H_{18}$ while hydrogenation at 375ºC resulted in formation of small amounts of $C_{60}H_{36}$ and $C_{60}H_{44}$ in addition to $C_{60}H_{18}$ (see **Figure 4.12**). The sample hydrogenated at 400ºC mainly consisted of highly hydrogenated fulleranes, e.g. $C_{60}H_{44}$ and $C_{60}H_{52}$, while some fragmented fullerenes with a loss of 1-2 carbon atoms from the cage appeared in MS spectra, e.g. $C_{59}H_{44}$. Samples hydrogenated at 420-440ºC mainly consisted of fragmented fullerenes, e.g. $C_{59}H_{44}$, $C_{59}H_{42}$, $C_{58}H_{44}$, $C_{58}H_{42}$, and some highly hydrogenated fulleranes. It should be noted that prior to MS measurements samples were dissolved in toluene and therefore only the soluble part of the material can be analyzed in MS spectra and the relative abundance of molecular species can be affected by possible differences in their solubility. For example, fulleranes $C_{60}H_x$ with low hydrogen content (X<18) have low solubilities in toluene and therefore can not be seen in MS spectra even if they are present in the sample.

4.4.2 Hydrogenation of C_{60} as a function of the reaction time

To gain a better understanding of C_{60} hydrogenation we prepared a set of samples hydrogenated at 440ºC with different durations of the heat treatment: 240min, 480min, and 750min. The sample hydrogenated for 240min, which corresponds to ~75% of the maximal weight gain (hereafter 440ºC_75%), had a FCC cell parameter of 14,47Å and mostly consisted of $C_{60}H_{18}$ according to MS (see **Figure 4.12**). The samples hydrogenated during 480min (~85% of the maximal weight gain, hereafter 440ºC_85%) and 750min (the maximal weight gain, hereafter 440ºC_100%) had larger FCC cell parameters, i.e. higher degrees of hydrogenation. According to MS spectra those samples were mainly composed by $C_{60}H_{18}$, $C_{60}H_{36}$, and $C_{60}H_{44}$.

It is interesting to note that products of C_{60} hydrogenation at 440ºC with different durations of hydrogenation are very similar to products of C_{60} hydrogenation at different temperatures (see the previous section). We concluded that the C_{60} hydrogenation pathway is the same for different hydrogenation temperatures and a similar set of $C_{60}H_x$ molecules is always formed. Higher temperatures only lead to faster kinetics of hydrogenation.

4.4.3 C_{60} hydrogenation and fragmentation pathways

Hydrogenation of C_{60} occurs by addition of hydrogen pairs and, in principle, all theoretically possible compositions with an even number of hydrogen atoms could be formed starting from $C_{60}H_2$ and finishing with $C_{60}H_{60}$. However, **Figure 4.12** shows that some of the fulleranes are much more abundant than others reflecting a more complex process which consists of certain steps. The existence of these steps suggests that fulleranes with certain compositions are more stable than others and that the kinetics of hydrogen addition varies very strongly for fulleranes with different compositions.

The hydrogenation pathway of C_{60} can be summarized using the following main steps: $C_{60}\rightarrow C_{60}H_{18}\rightarrow C_{60}H_{36}\rightarrow C_{60}H_{44}\rightarrow C_{60}H_{52}$. We suggest that synthesis of $C_{60}H_{52}$ is the last step of hydrogenation. Hydrogenated fullerenes with higher hydrogen content are either not formed or extremely unstable and collapse in the process of reaction. This C_{60} hydrogenation pathway is in agreement with earlier theoretical predictions by Zhao *et al*[178].

Further hydrogenation leads to formation of fragmented fullerenes. Fragmentation of C_{60} during hydrogenation is an undesirable process for hydrogen storage applications. On the other hand, fragmentation of C_{60} could lead to synthesis of some new molecules and materials. Therefore, it is important to understand fragmentation mechanisms in order to either avoid fragmentation or to use it in a controlled way for synthesis of new materials.

Fragmentation of C_{60} induced by extensive hydrogenation was best of all observed in the sample hydrogenated at 440ºC (see **Figure 4.11**). According to MS analysis this sample contained fragmented fullerenes with a loss of up to 7 carbon atoms from the C_{60} cage. Analyzing all fragmented fullerenes observed in MS spectra we proposed two possible fragmentation mechanisms (see **Figure 4.13**). Both fragmentation mechanisms can be described by steps which include the total loss of either one carbon atom or a CH_2 unit from the C_{60} cage and reformation of as-formed dangling bonds into new C-C bonds. This conclusion agrees well with previous results reported by our group[179].

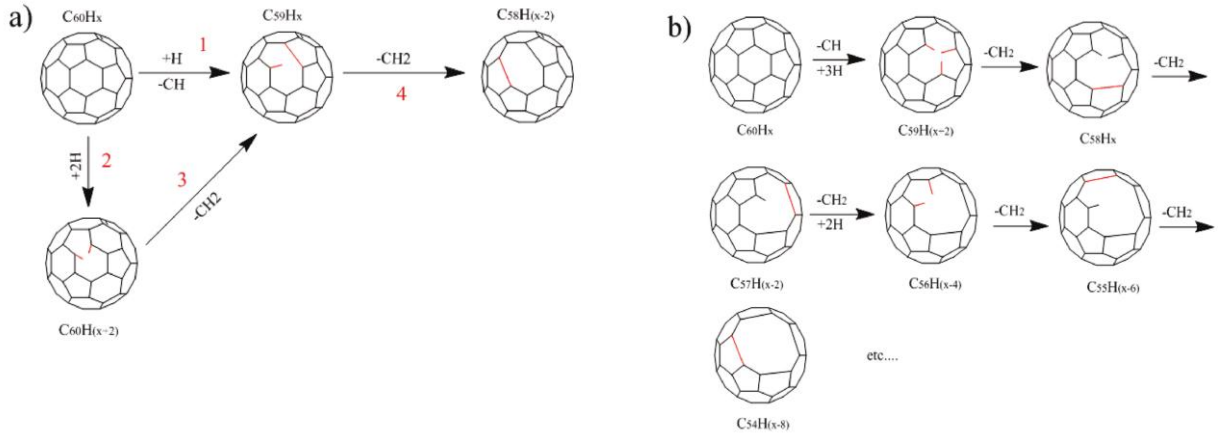

Figure 4.13. Two suggested pathways of C_{60} hydrogenation-induced fragmentation (new bonds formed on every fragmentation step are marked by red color).

Additional studies aimed at isolation and evaluation of structural and isomeric compositions of specific $C_{60}H_x$ and products of its fragmentation are required to confirm either of the proposed fragmentation models.

4.4.4 HPLC separation of hydrogenated fullerenes

We performed toluene-based HPLC separation of C_{60} hydrogenated at 440ºC with different duration of the heat treatment (see **Chapter 4.4.2**). The HPLC trace of the 440ºC_100% sample showed two main peaks with the elution times of ~8-10min and ~13,5-15min, respectively. According to MS analysis the first peak in the HPLC chromatogram was an overlap of several poorly resolved peaks originated by $C_{60}H_{44}$, $C_{60}H_{34}$, and $C_{60}H_{28}$, while the second peak was solely originated by $C_{60}H_{18}$ (see **Figure 4.14**). A similar HPLC trace was observed for the 440ºC_85% sample. The elution time was shorter for hydrogenated fullerenes with higher hydrogen content which is in good agreement with literature[107, 125]. However, complete separation of hydrogenated fullerenes was not achieved and the only well separated fullerane was $C_{60}H_{18}$.

HPLC separation was also performed for the sample hydrogenated at 440ºC for a prolonged period of time (3300min) aiming on separation of some fragmented fulleranes, e.g. $C_{59}H_{44}$ or $C_{58}H_{44}$. However, it turned out that the HPLC column was not suitable for separation of fragmented fulleranes. This column provided separation according to the number of hydrogen attached to the C_{60} cage while some fragmented fulleranes have the same number of hydrogen atoms but with a loss of 1-3 carbon atoms.

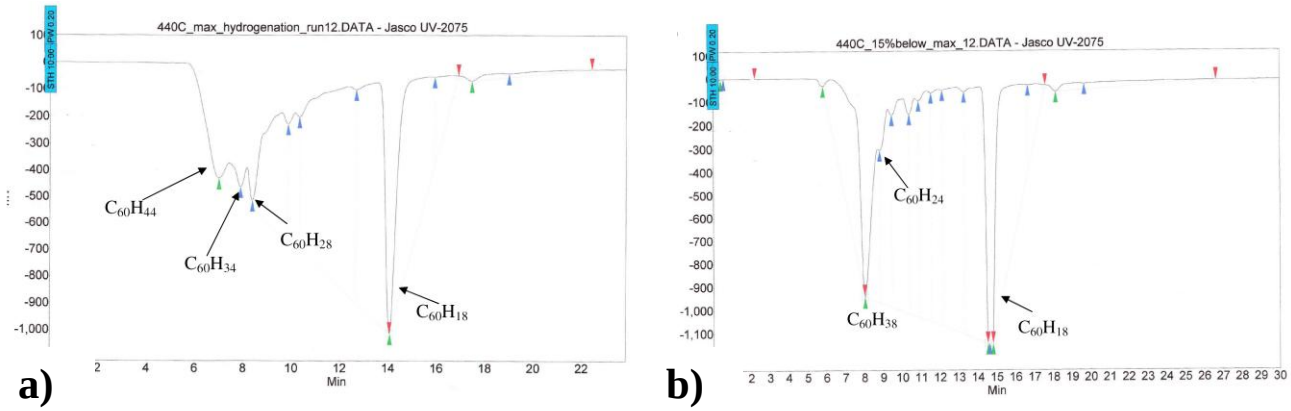

Figure 4.14. HPLC chromatogram of C_{60} hydrogenated at 440ºC for a) 750min (the maximal weight gain); b) 450min (85% of the maximal weight gain).

4.4.5 Hydrogenation of C_{60} with addition of metal catalysts

As was shown earlier (see **Chapter 4.4.3**) hydrogenation of C_{60} follows a certain pathway and, in principle, at the certain stage of hydrogenation could result in conversion of all material into a fullerane with high hydrogen content, e.g. $C_{60}H_{52}$. However, hydrogenation of C_{60} has slow kinetics, and prolonged heating at reaction temperatures leads to fragmentation of some highly hydrogenated fulleranes. Therefore, synthesis of highly hydrogenated C_{60} could be possible only if some methods to suppress fragmentation and to accelerate hydrogenation kinetics are found. Hydrogenation of C_{60} with addition of metal catalysts has faster kinetics[100, 180] and possibly will result in synthesis of fulleranes with a lower degree of fragmentation compared to non-catalytic hydrogenation.

In this work we studied hydrogenation of C_{60} at 400ºC and 50bar of H_2 pressure with addition of Pt- and Ni-catalysts and compared it with non-catalytic hydrogenation. Non-catalytic hydrogenation of C_{60} proceeds very slowly (see **Figure 4.11**), and the sample weight reaches saturation only after 6000min. Addition of Pt catalyst significantly improved hydrogenation kinetics. The maximum weight gain was achieved already after 500min while prolonged hydrogenation resulted in a total weight decrease similar to that of catalyst free samples. Two samples with hydrogenation times of 500min (hereafter, 400ºC_Pt) and 1700min (hereafter, 400ºC_Pt_long) were analyzed in detail. Some experiments were also performed with Ni catalyst supported on carbon.

The total weight of C_{60} hydrogenated with addition of Ni catalyst started to decrease already after ca. 50min of hydrogenation. However, this effect is not due to fragmentation of C_{60}. It should be attributed to hydrogen reduction of Ni catalyst which prior to hydrogenation was stored in air and oxidized.

Compositions of samples synthesized by catalytic and non-catalytic hydrogenation appeared to be similar according to MS analysis (see **Figure 4.15**). It could be assumed that in both cases hydrogenation follows the same hydrogenation pathway with sequential formation of $C_{60}H_{18}$, $C_{60}H_{36}$, $C_{60}H_{44}$, and $C_{60}H_{52}$.

Surprisingly, XRD structural characterization showed remarkable structural differences in samples synthesized by catalytic and non-catalytic hydrogenation. C_{60} hydrogenated at 400ºC without addition of metal catalysts had the same FCC lattice as pristine C_{60} but with an increased cell parameter (a=15,02Å compared to a=14,17Å for pristine C_{60}). The 400ºC_Pt sample consisted of two phases: a FCC phase with a=14,32Å and a body-centered cubic (BCC) phase with a=12,0Å. Prolonged hydrogenation left the cell parameter of the BCC phase unchanged while the cell parameter of the FCC phase increased up to 14,82Å (see **Figure 4.16**). The 400ºC_Ni sample also consisted of FCC and BCC phases with cell parameters 14,74Å and 11,93Å correspondingly.

It can be suggested that catalytic hydrogenation of samples with addition of catalyst proceeds in two steps. The first step is the same as for non-catalytic hydrogenation and begins with formation of $C_{60}H_{18}$ with the FCC lattice. This was confirmed by NMR measurements on the 400ºC_Ni sample which showed that it contained the C3v isomer of $C_{60}H_{18}$, the same $C_{60}H_{18}$ isomer as obtained by non-catalytic hydrogenation of C_{60}[114]. In the next step hydrogenation proceeds by rapid formation of the BCC phase while a part of the material still retains the original FCC lattice. Prolonged hydrogenation results in conversion of more and more material into highly hydrogenated fulleranes with the BCC lattice.

It can be suggested that even for the sample with added Pt we observed both catalytic and non-catalytic hydrogenation, possibly due to inhomogeneous distribution of Pt particles in the samples. In this case fulleranes with the FCC lattice were formed by non-catalytic hydrogenation and fulleranes with the BCC lattice by catalytic hydrogenation. It should be noted that no fulleranes with the BCC lattice were observed in any sample hydrogenated without addition of metal catalysts. Both FCC and BCC phases possibly coexisted in the sample due to a large grain size of C_{60} or due to poor contact with catalyst particles for some grains. Highly hydrogenated fulleranes with the BCC lattice were quickly formed on C_{60} grain boundaries in the vicinity to Pt catalyst particles. Pt catalyst particles served as centers for dissociation of molecular hydrogen into atomic hydrogen. Prolonged

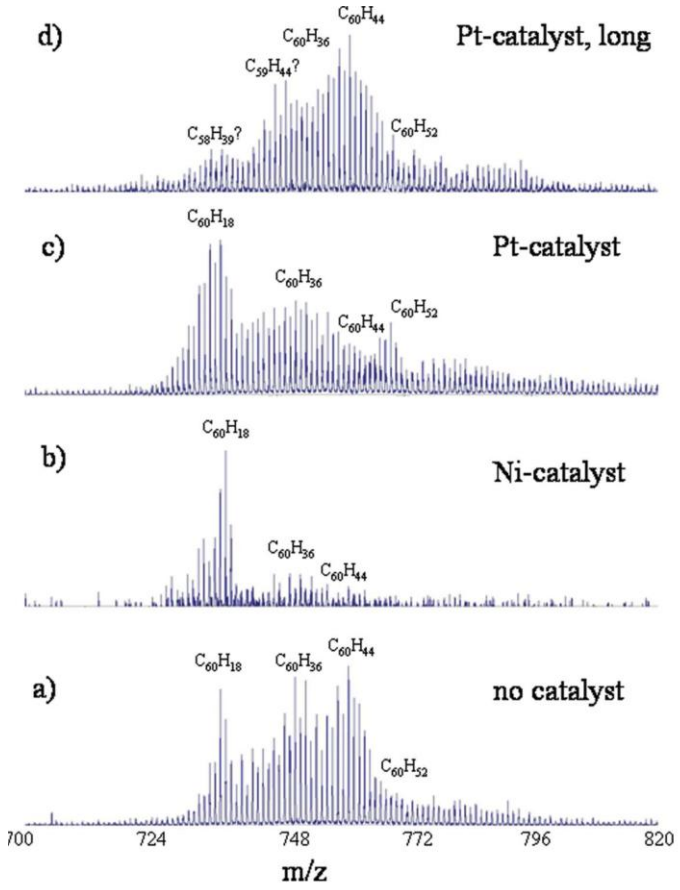

Figure 4.15. MS spectra recorded for C_{60} hydrogenated at 400ºC: a) without any catalysts (7500min); b) with addition of Ni catalyst (800min); c) with addition of Pt catalyst (500min); d) with addition of Pt catalyst (1700min).

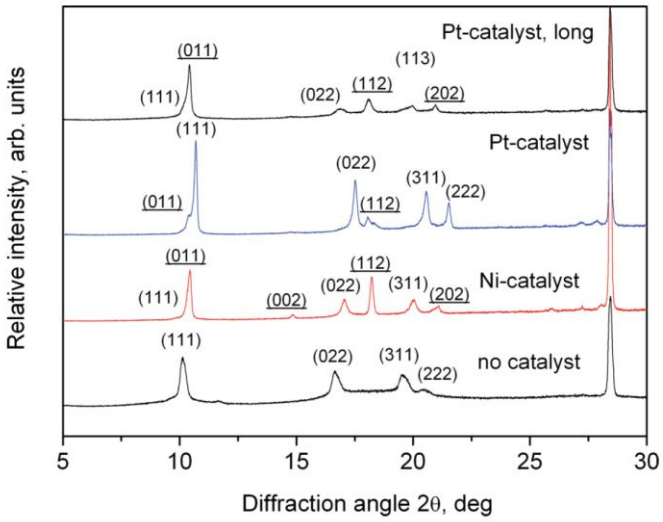

Figure 4.16. XRD patterns recorded for C_{60} hydrogenated at 400ºC and 50bar of hydrogen pressure with and without addition of metal catalysts (reflections of the BCC phase are underlined).

hydrogenation increased the fraction of hydrogenated fulleranes with the BCC lattice due to migration of atomic hydrogen further away from catalyst particles. Synthesis of fulleranes with the BCC lattice and similar cell parameters was earlier reported for C_{60} hydrogenated with atomic hydrogen[110, 181, 182].

Further experiments are required to understand how different factors such as the catalyst particle size or the contact between C_{60} and metal catalyst particles effect C_{60} hydrogenation. For instance, hydrogenation should be tested for C_{60} with reduced grain size (e.g. by ball milling) and for C_{60} mixed with different types of metal catalysts (e.g. varying catalyst dispersion or type of the support material).

4.4.6 Reversibility of C_{60} hydrogenation

Fullerene C_{60} was considered as a promising material for hydrogen storage by chemisorption. However, hydrogenation of C_{60} must be a reversible process to be useful for hydrogen storage. To check the reversibility of C_{60} hydrogenation, we studied samples hydrogenated in the temperature interval of 350-400ºC with or without addition of metal catalysts by TGA. Samples synthesized at temperatures above 400ºC fragmented already during hydrogenation and therefore reversible formation of C_{60} upon dehydrogenation was not expected for those samples.

C_{60} hydrogenation at 350ºC resulted in synthesis of mainly $C_{60}H_{18,}$ according to MS measurements (see **Figure 4.17**). During dehydrogenation the weight of the sample started to decrease at ~450ºC and stabilized after 600-650ºC with a stepwise loss of ca. 2wt% (see **Table 4.3**). A gradual decrease of the sample weight upon further heating could be explained by sublimation of recovered C_{60}. The weight loss obtained by TGA was similar to the hydrogen content estimated by elemental analysis (1,7wt%). Therefore, the weight loss in the TGA experiment was mainly attributed to hydrogen release. Products of dehydrogenation were studied by mass spectrometry and XRD analysis. According to MS analysis the dehydrogenated sample consisted of C_{60} and no other peaks were observed in MS spectra (see **Figure 4.17**). Similar results were obtained for samples hydrogenated at 375ºC and 400ºC. Weight losses obtained by TGA analysis were higher than the hydrogen content obtained from the elemental analysis which indicated partial decomposition of C_{60} upon hydrogen release (see **Table 4.3**)[106]. According to MS spectra some C_{60} was partially recovered upon dehydrogenation for both samples.

Upon hydrogenation the cell parameter of the C_{60} FCC structure expanded indicating that the molecular diameter increased due to attached hydrogen atoms. After dehydrogenation the cell parameter, i.e. the diameter of molecules, was expected to decrease. Surprisingly, after

dehydrogenation the cell parameter remained increased (a=14,40Å) and did not return back to the value a=14,17Å reported for C_{60} (see **Figure 4.18**). The same result was obtained for the sample synthesized at 375ºC while dehydrogenation of the sample synthesized at 400ºC resulted in sample amorphization.

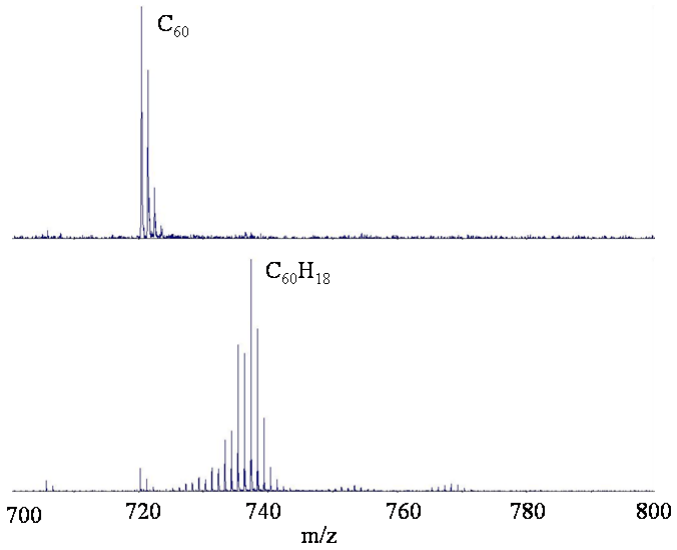

Figure 4.17. MS spectra recorded for the sample hydrogenated at 350ºC and 50bar of hydrogen pressure (7500min): before (bottom spectrum) and after (top spectrum) dehydrogenation.

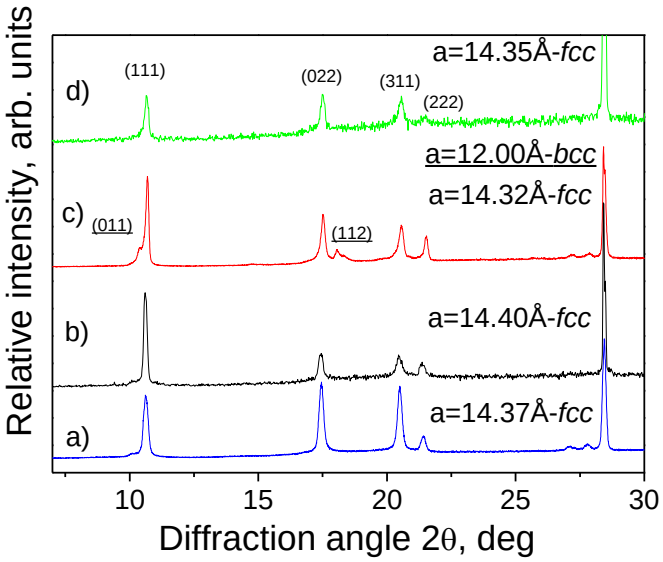

Figure 4.18. XRD patterns recorded for a) the sample hydrogenated at 350ºC (7500min); b) the sample hydrogenated at 350ºC after dehydrogenation; c) the sample hydrogenated at 400ºC with addition of Pt catalyst (500min); d) the sample hydrogenated at 400ºC with addition of Pt catalyst after dehydrogenation.

Synthesis T, ºC	C content, elemen. analysis, wt.%	H content, elemen. analysis, wt.%	H content, gravim. analysis, wt.%	TGA weight loss, wt.%
350	97,4	1,7	1,67	2,04
375	96,4	2,9	2,73	4,06
400	94,9	4,4	3,96	6,92
400_Pt*	n/a	n/a	n/a	3,85

Table 4.3. Summary of the elemental analysis performed for samples hydrogenated at 350-400ºC and its comparison with results of the TGA analysis.

*- the sample hydrogenated at 400ºC with addition of Pt catalyst (500min).

Interesting results were obtained for the sample hydrogenated with addition of Pt catalyst. After hydrogenation at 400ºC for 500min the sample consisted of two fullerane phases: FCC phase and BCC phase (see **Chapter 4.4.5** and **Figure 4.18**). As suggested in **Chapter 4.4.5** catalytic hydrogenation started with synthesis of fulleranes with the FCC lattice (with an increased cell parameter) and then the BCC phase was formed. After dehydrogenation the BCC phase was likely converted back to the FCC phase with an increased cell parameter (no BCC reflections were observed in XRD patterns after dehydrogenation). However, the cell parameter of the FCC phase remained increased after dehydrogenation and did not go back to 14,17Å as reported for pristine C_{60}.

As a hint for future research it would be interesting to check the reversibility of C_{60} hydrogenation when fulleranes with only the BCC lattice are formed. Fulleranes with the BCC lattice could be synthesized by hydrogenation of C_{60} with atomic hydrogen[181, 182]. Direct reaction of C_{60} with hydrogen gas normally results in synthesis of either pure FCC fullerane phase or a mixture of FCC and BCC fullerane phases[100]. Synthesis of fulleranes with purely BCC lattice using direct reaction of C_{60} with hydrogen gas could possibly be achieved by improving the dispersion of metal catalyst particles and their contact with C_{60} grains.

It is also interesting to understand why the cell parameter of the FCC phase did not go back to the original value of C_{60} after dehydrogenation of fulleranes. In order to answer this question we synthesized a sample which contained 95% of the $C_{60}H_{18}$ C_{3v} isomer (without addition of any metal catalysts)[114] and studied the products obtained by the heat treatment of this sample in the temperature interval of 410-600ºC.

4.4.7 Thermal decomposition of $C_{60}H_{18}$

$C_{60}H_{18}$ was heat treated at different temperatures for 12 hours and the samples were analyzed after annealing using XRD, IR and Raman spectroscopy, and TGA. The results of the XRD analysis are summarized in **Figure 4.19a**. Following the trend described in the previous chapter the FCC cell parameter of the sample heat treated at 410-500ºC remained unchanged and did not go back to the value reported for pristine C_{60}. Higher treatment temperatures of 550-600ºC resulted in amorphization of the material. Duration of the heat treatment at 550-600ºC was reduced to 30 minutes in order to reduce amorphization of the material (see **Figure 4.19b**). Surprisingly, after the heat treatment at those temperatures for 30 minutes the cell parameter did not go back to 14,17Å but increased indicating further expansion of the structure. This structural expansion can not be explained by further hydrogenation or oxidation of the material as the annealing experiment was conducted in vacuum.

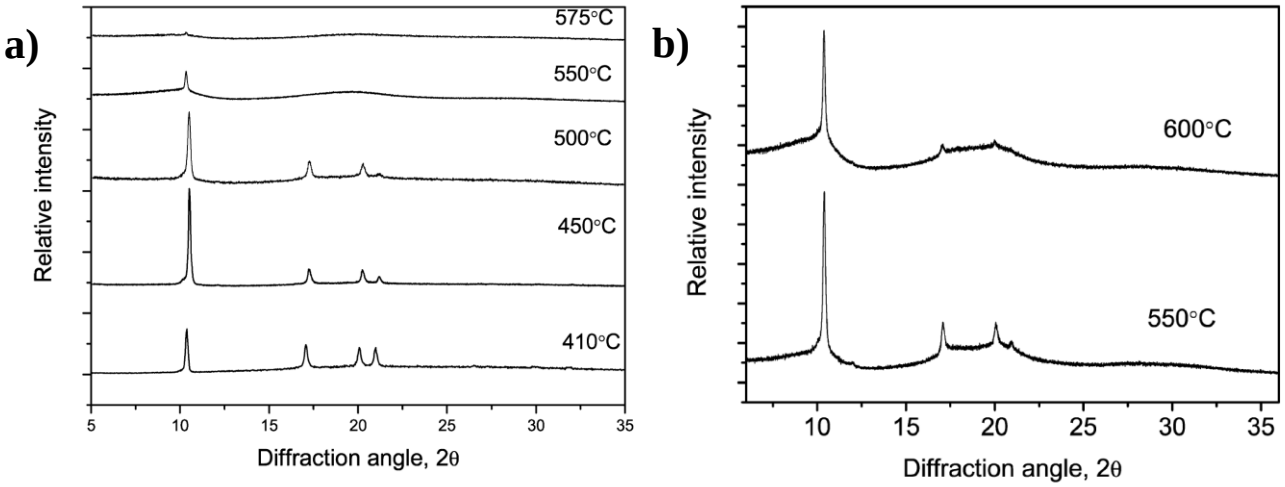

Figure 4.19. XRD patterns recorded for samples heat treated at different temperatures for: a) 12hours; b) 30min.

IR spectra recorded from annealed samples showed that peaks which correspond to C-H vibrations in pristine $C_{60}H_{18}$ had disappeared after annealing, indicating hydrogen release. Some spectral features from pristine C_{60} were recovered. Additionally, some new features were observed in IR spectra after the heat treatment indicating partial decomposition of the material during dehydrogenation (e.g. the broad peak at 3041cm^{-1} assigned to C-H vibrations from PAHs, see **Figure 4.20**).

Dehydrogenation of $C_{60}H_{18}$ was also verified using TGA which showed a step-like weight loss at 450-600ºC. The weight loss measured by TGA analysis (5,7wt.%) was much larger than the

hydrogen content in $C_{60}H_{18}$ (2,5wt%) which was another evidence of partial C_{60} decomposition during dehydrogenation.

Partial recovery of fullerene C_{60} was confirmed by Raman spectroscopy. However, the position of the $A_g(2)$ mode for recovered C_{60} was downshifted compared to the position reported for pristine C_{60} which is an indication of chemical modification or polymerization of C_{60}[183, 184]. However, polymerization of C_{60} typically results in denser materials and can not explain the increase of the cell parameter observed in annealed samples and therefore should be ruled out.

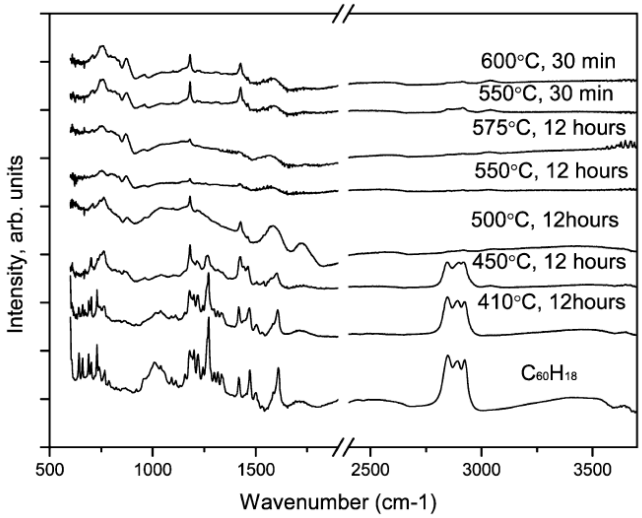

Figure 4.20. IR spectra recorded for $C_{60}H_{18}$ heat treated at different temperature and for pristine $C_{60}H_{18}$.

Summarizing this chapter, dehydrogenation of $C_{60}H_{18}$ resulted in hydrogen release and partial recovery of some C_{60}. On another hand, some C_{60} molecules collapsed during dehydrogenation, most likely forming some PAHs and larger fullerene fragments. The expansion of the structure observed for samples annealed at higher temperatures can be possibly explained by intercalation or functionalization of recovered C_{60} with products of C_{60} molecules collapse and fragmentation. It is worth to mention that a similar effect was observed earlier after heat treatment of the C_{60}-cubane compound[185].

4.5 Hydrogenation of SWCNTs

Hydrogenation of SWCNTs was extensively studied over the past decade[131, 133, 134, 186]. However, most of the studies were performed using the reaction with atomic hydrogen. Atomic hydrogen readily reacts with nanotube walls at elevated temperatures, while it was believed that molecular hydrogen does not. No SWCNTs hydrogenation was observed in our previous experiments which were performed under similar conditions on C_{60}@SWCNTs purified from the

metal catalyst[187]. Similarly, no hydrogenation was observed in this work for SWCNTs purified from Fe-catalyst.

Experiments performed in this study demonstrated that SWNTs react with hydrogen gas if the metallic catalysts which are typically used for synthesis of nanotubes (e.g. Fe) are not removed from the samples. The catalytic effect of Fe particles is likely connected with dissociation of molecular hydrogen into atomic species with subsequent migration of atomic hydrogen on SWNTs (spillover effect). Thus, reaction of SWNTs with hydrogen gas becomes possible when atomic hydrogen is produced on catalyst particles. The importance of metal catalysts for hydrogenation of CNTs was also recently shown by Bhowmick *et al* who reported that SWCNTs doped with Pt-nanoparticles can be hydrogenated with molecular hydrogen even at ambient tempeartures[188].

In this work we studied the reaction of hydrogen gas with SWCNTs in the temperature interval of 400-550ºC and hydrogen pressure of 50bar. SWCNTs annealed in hydrogen at various temperatures were analyzed ex situ by IR and Raman spectroscopy, scanning electron microscopy (SEM) and transmission electron microscopy (TEM), and X-ray photoelectron spectroscopy (XPS) analysis.

SWCNTs hydrogenation. SWCNTs did react with molecular hydrogen at 400-550ºC as was confirmed by Raman spectroscopy, IR spectroscopy, and XPS analysis. The process of hydrogenation depended on hydrogenation temperature. At T=400-450ºC hydrogenation proceeded by side wall functionalization and formation of C-H covalent bonds which are stable at those temperatures and resulted in a relatively high degree of SWCNTs hydrogenation. At T=550ºC, which exceeds the stability limit of C-H bonds in hydrogenated SWCNTs, hydrogenation of SWCNTs proceeded as etching. Etching of SWCNTs at 550ºC resulted in a relatively low degree of hydrogenation and a large number of defects induced on nanotube walls.

Hydrogen annealing at 400-450ºC: side wall hydrogenation. After hydrogenation at 400-450ºC Raman spectra of SWCNTs were substantially modified: some new peaks appeared in the 1100-1400cm^{-1} interval (not observed in the pristine material), the RBM mode was up-shifted, and the G/D ratio decreased (see **Figure 4.21**). The shape of the G-band changed due to conversion of some metallic SWCNTs into semiconducting SWCNTs. The metallic-semiconducting conversion of hydrogenated SWCNTs was observed earlier as a result of hydrogenation by atomic hydrogen [189]. Hydrogenation of SWCNTs was also confirmed by IR spectroscopy. After hydrogenation of SWCNTs a set of strong peaks in the region of C-H vibrations appeared in IR spectra, i.e. peaks at 2851, 2920, and 2955cm^{-1}. XPS spectra were used to estimate the degree of SWCNT hydrogenation

(see **Figure 4.22**). According to XPS measurements ca. 36 ± 9% of carbon atoms were hydrogenated at 450ºC.

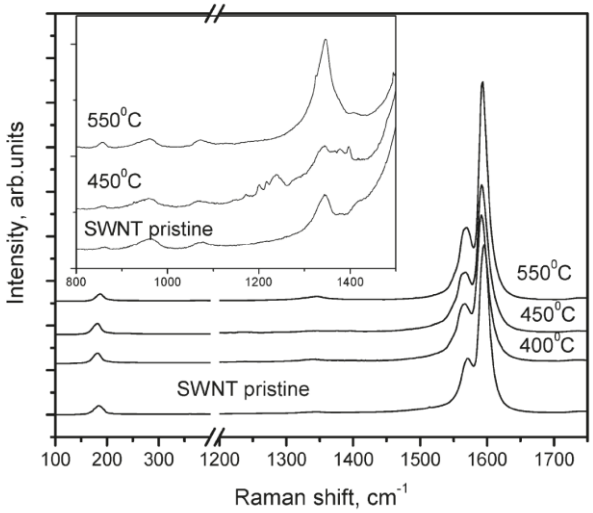

Figure 4.21. Raman spectra (514nm) recorded from SWCNTs hydrogenated at different temperatures. The inset shows a zoomed-in region where new peaks appeared as the result of hydrogenation.

Hydrogen annealing at 550ºC: etching. After hydrogenation at 550ºC Raman spectra of SWCNTs were different from both Raman spectra of pristine SWCNTs and Raman spectra of SWCNTs after hydrogenation at 400-450ºC. Hydrogenation of SWCNTs at 550ºC resulted in an up-shift of the RBM mode, in a modification of the G-band shape, and in a significant change of the G/D ratio (by ~20 times) which was much stronger than after hydrogenation at 400-450ºC, see **Figure 4.21**. According to XPS measurements the fraction of hydrogenated carbon atoms at 550ºC did not exceed 6 ± 3%, see **Figure 4.22**.

SWCNTs purification from the Fe catalyst SWCNTs samples are synthesized using a reaction which includes a Fe catalyst and as a result, SWCNTs are contaminated by Fe nanoparticles. These particles can not be removed by direct acid treatment of samples since they are encapsulated into graphitic carbon shells. These shells also protect Fe nanoparticles against oxidation. Fe nanoparticles remain unoxidized (as can be revealed e.g. by XPS) even after prolonged exposure of samples to air. The standard procedure of Fe removal from SWCNT samples includes an oxidation treatment at elevated temperatures to remove more reactive carbon shells and leaving nanotubes intact. When protective carbon shells are removed the Fe particles can easily be removed by acid treatment. Removal of carbon shells can also be easily verified by XPS since the catalyst particles get oxidized after exposure to air.

As revealed in our study, a combination of hydrogenation and acid treatment can be proposed as an alternative tool for purification of SWCNTs from residual metal catalyst. This is especially interesting for experiments where oxidation of SWCNTs is not desirable. Carbon shells which cover Fe nanoparticles in pristine samples could be removed by annealing of SWCNTs in hydrogen, as

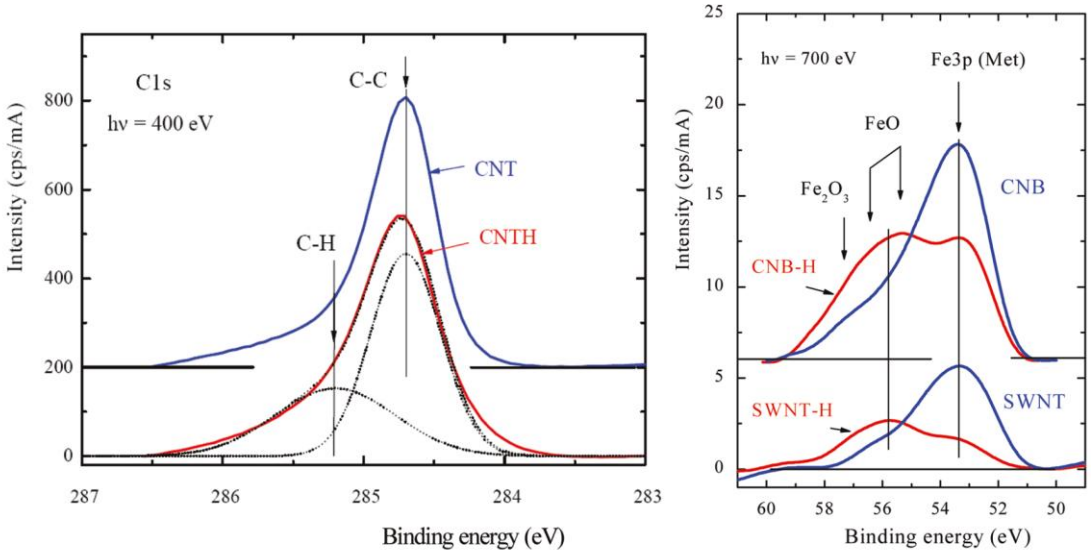

Figure 4.22. Left plot shows C1s XPS spectra of SWCNTs before (CNT) and after (CNTH) hydrogenation at 450ºC recorded with photon energy of 400eV. Right plot shows Fe3p XPS spectra of SWCNTs before and after hydrogenation at 450ºC recorded with photon energy of 700eV.

confirmed by XPS measurements which demonstrated oxidation of Fe nanoparticles in air (see **Figure 4.22**). Exposed Fe nanoparticles could be washed out by subsequent HCl treatment. Combining hydrogenation and HCl treatment, the Fe content in SWCNTs was reduced by a factor of 40-45 on average (see **Figure 4.23**).

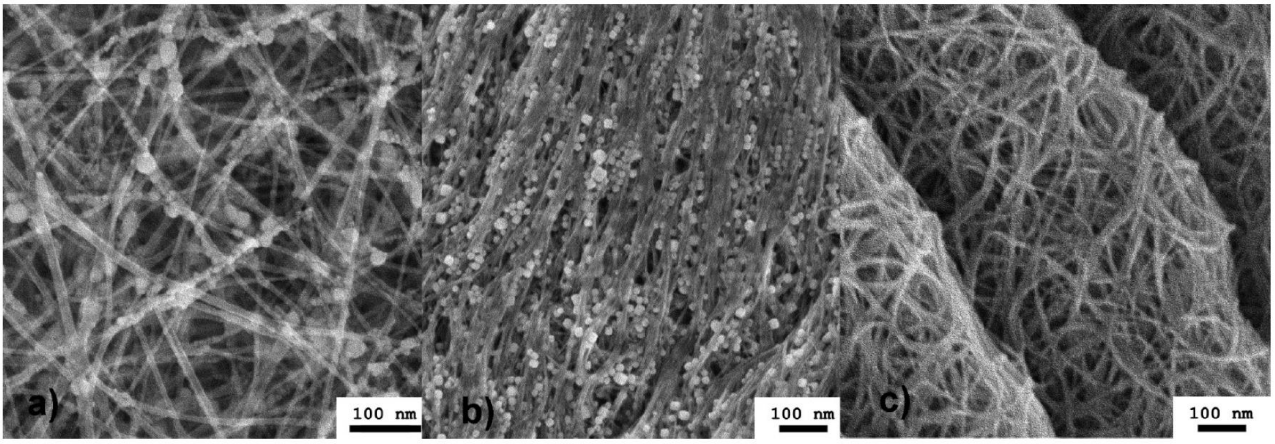

Figure 4.23. SEM images recorded from: a) pristine SWCNTs; b) SWCNTs after hydrogenation; c) hydrogenated SWCNTs after removal of Fe particles by HCl treatment.

Opening and unzipping of SWCNTs by hydrogenation. Hydrogen annealing of SWCNTs results in removal of fullerene-like cups from nanotube tips (nanotube opening) and partial unzipping of nanotube walls along the tube axis. Fullerene-like cups were expected to react with hydrogen to the point of complete removal at the conditions of our experiments, similar to reactions of fullerene C_{60} described in **Chapter 4.4** of this thesis. This effect was seen especially clearly for hydrogenation experiments on carbon nanobuds, i.e. SWCNTs which have different fullerene-like forms of carbon attached to the nanotube walls[190]. Hydrogen annealing of carbon nanobuds resulted in separation of some fullerenes from SWCNTs walls and their encapsulation into the inner space of nanotubes which could be possible only if nanotubes become open as a result of hydrogenation.

Hydrogenation also resulted in unzipping of some SWCNTs. Cone- and balloon-like features could be seen at the tips of SWCNTs after hydrogenation at 400-550ºC and are attributed to unzipped parts of SWCNTs (see **Figure 4.24**). Some nanoribbons showed a very specific wave-like shape of edges which are expected if nanoribbons are formed by SWCNTs rippling (see **Figure 4.24**). It is not clear at the moment why some SWCNTs were unzipped while other SWCNTs remained intact at certain experimental conditions. Possibly, unzipping of SWCNTs somehow depends on the properties of SWCNTs themselves (e.g. SWCNTs chirality) or on the position of Fe particles. Fe particles are normally attached at SWCNTs end parts where unzipping was observed. We believe that Fe particles serve as starting points for the unzipping of SWCNTs (see **Figure 4.24**).

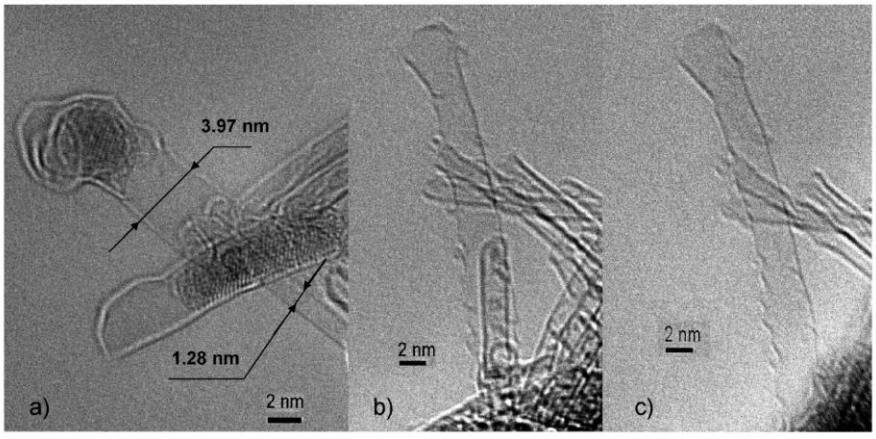

Figure 4.24. TEM images recorded from SWCNTs after hydrogenation: a)SWCNTs and attached to them graphene nanoribbons; b) another graphene nanoribbons; c) the same graphene nanoribbons as in (b) but tilted by 20º.

4.6 Hydrogenation of fullerene C_{60} inside SWCNTs

As was discovered in earlier studies from our group, fullerene C_{60} reacts with molecular hydrogen in the temperature interval of 350-450ºC and hydrogenation results in formation of fulleranes $C_{60}H_x$ (with x up to 52)[113], see also **Chapter 4.4** of this thesis. It is interesting to check whether the same hydrogenation reaction of C_{60} will occur in peapods (i.e. C_{60}@SWCNTs) where C_{60} is confined within the internal 1D-space of SWCNTs. In this thesis we studied the reaction of hydrogen with C_{60}@SWCNTs in two temperature intervals. Temperature intervals were chosen according to our knowledge about hydrogenation of bulk C_{60}: 1) T=450ºC where C_{60} hydrogenates; 2) T=500-550ºC where C_{60} is expected to collapse and to form some large hydrocarbon molecules. We compared hydrogenation of C_{60} confined within SWCNTs with hydrogenation of bulk C_{60}. The products of hydrogenation were studied with Raman spectroscopy and TEM microscopy.

C_{60}@SWCNTs hydrogenation at 450ºC. Our experiments revealed that hydrogen is able to penetrate into the inner space of SWCNTs even when SWCNTs are filled with C_{60}. Hydrogenation of C_{60}@SWCNTs at 450ºC resulted in synthesis of hydrogenated $C_{60}H_x$ inside SWCNTs similarly to hydrogenation of bulk C_{60}.

After hydrogenation of C_{60}@SWCNTs the $A_g(2)$ mode of C_{60} disappeared from Raman spectra (see **Figure 4.25**). The same result was earlier observed for hydrogenation of C_{60}@SWCNTs at 400ºC[187] and was a sign of C_{60} hydrogenation. Similarly to bulk material, the C_{60} inside SWCNTs was partially recovered during annealing of hydrogenated C_{60}@SWCNTs at 950ºC in argon. The fact of C_{60} hydrogenation was also explicitly proven by TEM analysis. Hydrogenated C_{60} molecules with an increased diameter were observed inside of SWCNTs.

C_{60}@SWCNTs hydrogenation at 500-550ºC. Reaction of hydrogen with C_{60}@SWCNTs at 500-550ºC resulted in massive collapse of C_{60} inside SWCNTs and formation of a large variety of unidentified hydrocarbon products (see **Figure 4.26**). While the major part of fullerene molecules was transformed into carbon "debris", a rather minor fraction of nanotubes appeared to be less accessible to hydrogen and some intermediate reaction steps could also be studied. For example, a TEM study revealed some C_{60} in the dimerized and polymerized states while some other images revealed C_{60} fused into short nanotubes of irregular shapes. Formation of some helical objects which visually resembled GNRs was also observed inside SWCNTs even though fusion of C_{60} fragments into GNRs was not expected at the reaction conditions.

Collapse of C_{60} inside SWCNTs during hydrogenation at 500-550ºC was also confirmed by Raman spectroscopy. Raman spectra of C_{60}@SWCNTs hydrogenated at 500-550ºC showed a number of new peaks with the most prominent peaks found at 1239 and 1272cm^{-1} (see **Figure 4.25**).

No fullerene C_{60} was recovered during annealing of hydrogenated C_{60}@SWCNTs at 950ºC in argon. New peaks in the Raman spectra of C_{60}@SWCNTs after hydrogenation were similar to new peaks observed in the products from hydrogenation of bulk C_{60}. It is worth mentioning that products of

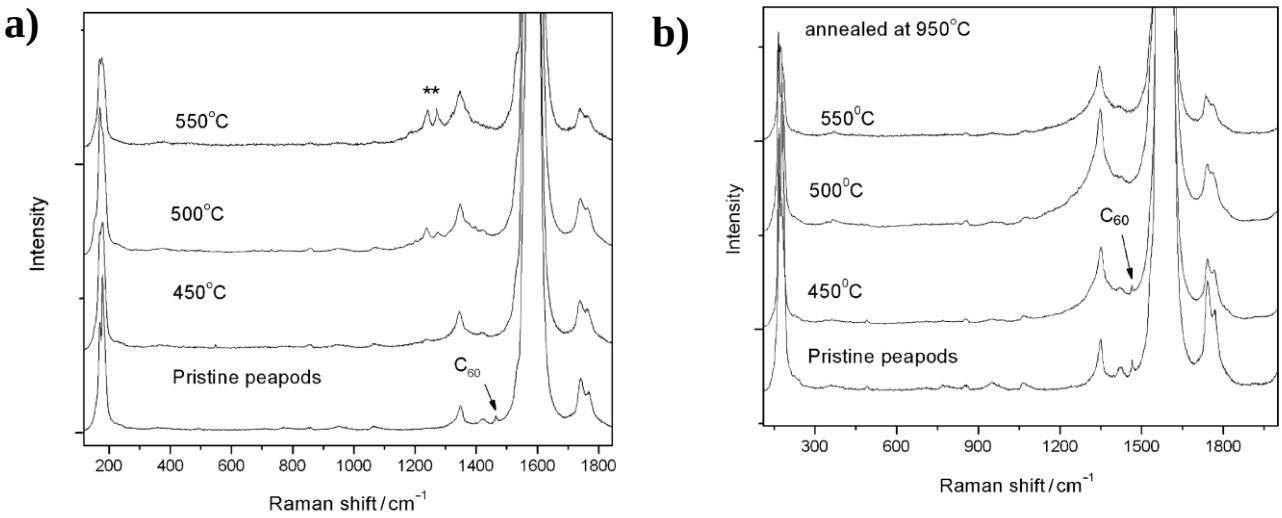

Figure 4.25. Raman spectra recorded from a) pristine C_{60}@SWCNTs and C_{60}@SWCNTs hydrogenated at different temperatures. New peaks at 1239 and 1272cm^{-1} are marked with asterisks. b) Pristine C_{60}@SWCNTs and C_{60}@SWCNTs hydrogenated at different temperatures after annealing in argon at 950ºC.

bulk C_{60} hydrogenation performed at the same temperature showed no hydrogenated fullerenes. C_{60} molecules completely collapsed in this control sample and only a broad range of hydrocarbons (molecular weight of 250-400amu) was found in MALDI-TOF MS spectra recorded from the toluene extract.

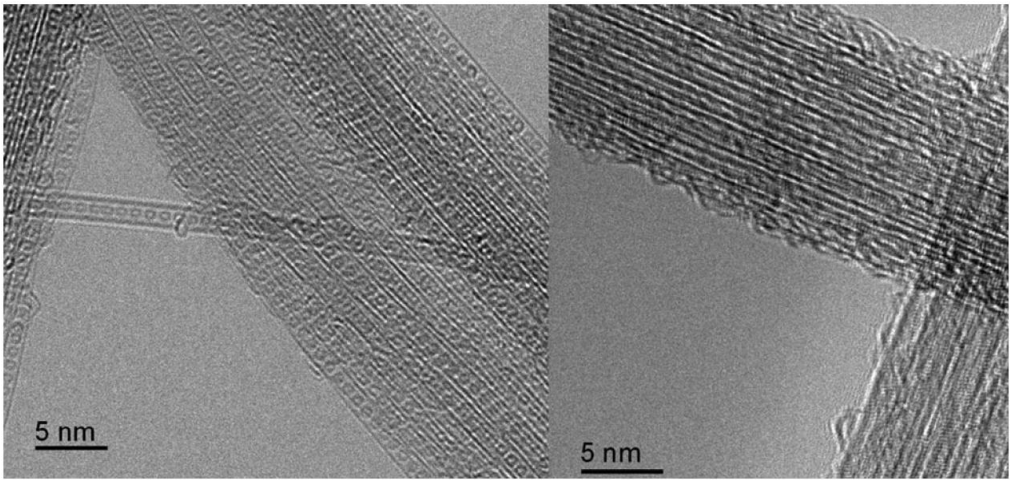

Figure 4.26. TEM images recorded from pristine peapods (left image) and peapods after hydrogenation at 550ºC (right image).

To summarize this section, we found the first direct evidence of a surprising ability of hydrogen to react with C_{60} molecules encapsulated inside SWCNTs. Hydrogen is likely to penetrate into SWCNTs through the nanotube openings on the tips and through defects in nanotube walls. Therefore, our study provides the first example of gas-molecule chemistry inside the 1D-space of nanotubes. It opens a road for exploration of many other possible kinds of gas-molecule reactions in the confined space of SWCNTs.

5 Conclusions

In this thesis I presented our results on hydrogen adsorption in some MOFs and non-porous nanocarbon materials as well as our results on hydrogen reactions with various carbon materials such as fullerene C_{60}, SWCNTs, and C_{60}@SWCNTs. As shown in this thesis, the reaction resulted in the synthesis of several new interesting materials.

Hydrogen adsorption in MOFs correlated well with surface area: MOFs with larger surface area adsorbed more hydrogen. Logically, to improve hydrogen adsorption MOFs with even higher surface area must be synthesized. In the recent article by the group of Prof. O. Yaghi MOFs with BET(Langmuir) surface area of 6240m^2/g (10 400m^2/g) were reported, but even these extremely porous MOFs had excess hydrogen adsorption below 1wt.% at room temperatures[32]. Synthesis of MOFs with even higher porosity is complicated due to the reduced stability of these materials. Highly porous MOFs become more fragile and can collapse as a result of solvent molecule removal during the activation step, or as a result of high hydrogen pressure during hydrogen adsorption measurements. Some other methods to improve hydrogen adsorption in MOFs must be developed.

In this thesis we also presented results of hydrogen adsorption studies in MOF-5 mixed or ”bridged” with Pt catalysts. Contrary to previous reports, hydrogen adsorption in MOF materials did not increase after addition of catalysts and the hydrogen spillover effect was not confirmed. Hydrogen adsorption in MOF-5 mixed/modified with Pt catalysts correlated well with surface area, showed fast kinetics, and was on the same level as for pristine catalysts free MOF-5. In the future, it would be interesting to check hydrogen adsorption in materials where the contact between MOFs and metal catalysts is improved (i.e. in MOFs impregnated with metal catalysts).

Nanocarbon materials, which were synthesized by the reaction of C_{60} with coronene/anthracene, represent another class of materials with a hydrogen adsorption mechanism different from that of MOFs. In contrast to MOFs, where hydrogen adsorption is surface related, these nanocarbon materials did not have any measurable surface area but still adsorbed up to 0,45wt.% of hydrogen. Hydrogen molecules were not adsorbed on the surface but they rather diffused into the nano-voids formed between grains of nanocarbon materials.

A large part of this thesis is dedicated to studies of hydrogen reactions with fullerene C_{60}. *In situ* gravimetric studies of fullerene C_{60} hydrogenation revealed that the kinetics of the reaction strongly depends on the temperature. In contrast, the reaction pathway was the same for different hydrogenation temperatures: $C_{60}\rightarrow C_{60}H_{18}\rightarrow C_{60}H_{36}\rightarrow C_{60}H_{44}\rightarrow C_{60}H_{52}$. Prolonged hydrogenation resulted in fullerane fragmentation which was followed by fullerane collapse and the formation of a

large variety of PAHs. It was found that fulleranes are separated in the HPLC column according to the number of hydrogen atoms, but complete isolation of new fulleranes or fragmented fulleranes using the HPLC column was not achieved. Dehydrogenation of fulleranes resulted in hydrogen release and partial recovery of fullerene C_{60} which, however, had an increased FCC cell parameter. The expansion of the FCC fullerene structure upon dehydrogenation was explained by the "self-doping" effect.

Addition of Pt or Ni metal catalysts significantly improved the kinetics of C_{60} hydrogenation. Catalytic hydrogenation of C_{60} followed the same reaction pathway as for non-catalytic hydrogenation, but resulted in synthesis of a mixture of fulleranes with FCC and BCC lattices. After dehydrogenation fulleranes with the BCC lattice were not observed, and the only dehydrogenation products were fullerene C_{60} with an expanded FCC lattice. In the future, it would be interesting to check dehydrogenation of fulleranes with a pure BCC lattice. Such fulleranes can possibly be synthesized choosing other catalysts, improving the dispersion of catalysts within fullerene C_{60}, and improving the contact between catalyst particles and fullerene C_{60}.

The reaction of SWCNTs with hydrogen gas at elevated temperatures was strongly affected by Fe catalyst nanoparticles. The reaction resulted in opening, purification, side-wall hydrogenation, and partial unzipping of SWCNTs. Some GNRs were formed as the results of SWCNTs unzipping. The reason for the selective unzipping of SWCNTs as well as the effect of various metal catalysts and SWCNTs diameters/chiralities on the reaction process remain unclear. It would be interesting to repeat these hydrogenation experiments for freestanding SWCNTs of different diameters/chiralities and for SWCNTs synthesized or impregnated with different catalysts.

Studying the reaction of hydrogen with C_{60}@SWCNTs we showed that hydrogen can penetrate inside SWCNTs and react with encapsulated fullerene C_{60} at 450-550ºC. At 450ºC the reaction resulted in the synthesis of hydrogenated fullerenes, similarly to the hydrogenation of bulk C_{60}, while at 500-550ºC the reaction resulted in massive collapse of C_{60} inside SWCNTs and formation of large variety of products (i.e. dimerized and polymerized fullerenes, short nanotubes of irregular shapes, and some helical objects visually resembling GNRs).

6 Summary of the included papers and my contribution to these papers

6.1 Paper 1

In **paper 1**, "*Thermal decomposition of $C_{60}H_{18}$*", we studied thermal decomposition of the pure C_{3v} isomer of $C_{60}H_{18}$ in the temperature interval of 410-600ºC. We found that fullerene C_{60} was partially recovered upon heat treatment at 410-500ºC as evidenced by IR spectroscopy, Raman spectroscopy, and X-ray diffraction measurements. Partial collapse of the fullerene C_{60} structure was observed during the heat treatment at temperatures above 500ºC which correlated with a slight structure expansion. Partial collapse of the fullerene structure was confirmed by TGA analysis, by XRD measurements, and by Raman spectroscopy. The expansion of the FCC fullerene structure upon dehydrogenation was explained by the "self-doping" effect.

My contribution: heat treatment of $C_{60}H_{18}$ at different temperatures; XRD measurements, IR and Raman measurements; analysis of the data; writing the manuscript.

6.2 Paper 2

In **paper 2**, "*Hydrogen storage in Co- and Zn-based metal-organic frameworks at ambient temperature*", we studied hydrogen adsorption in some Co- and Zn-based MOFs. These MOFs have different pore structures and surface areas and as a results have different hydrogen adsorption properties. Hydrogen adsorption correlated almost linearly with BET surface area. The maximum uptake of 0,75wt.% of hydrogen was measured for the ZBDh material (a Zn-based MOF which consist of triangular and hexagonal channels). Structural stability of the materials upon activation and hydrogen adsorption measurements was pointed out as an important factor which could limit the application of certain MOFs as materials for hydrogen storage.

My contribution: hydrogen adsorption measurements; nitrogen adsorption measurements; recording X-ray diffraction patterns; analysis of the data; writing the manuscript.

6.3 Paper 3

In **paper 3**, "*High-temperature reactions of C_{60} with polycyclic aromatic hydrocarbons*", we studied the reaction of C_{60} with polycyclic aromatic hydrocarbons (i.e. anthracene and coronene) and measured hydrogen adsorption in nanocarbons synthesized by this reaction. The reaction between C_{60} and anthracene at temperatures above 650ºC resulted in C_{60} collapse and formation of some nanocarbons. Hydrogen adsorption in these nanocarbons did not exceed 0,1wt.% and was on the same level as for pristine C_{60}.

The reaction between C_{60} and coronene resulted in C_{60} structural expansion with the FCC cell parameter increasing from a=14.17Å (for the reaction temperature of 500ºC) to a=14.50Å (T=650ºC). The structural expansion correlates with collapse of some fraction of C_{60} molecules induced by fusion and with carbonization of coronene molecules. Heat treatment of the C_{60}/coronene mixture above 650^0C results in complete fullerene collapse and the formation of nanocarbons. Hydrogen adsorption in these nanocarbons did not correlate with BET surface area and a maximum hydrogen adsorption of 0,45wt% was measured for nanocarbons synthesized at 800ºC.

My contribution: hydrogen adsorption measurements; nitrogen adsorption measurements; analysis of the data; discussion of the manuscript.

6.4 Paper 4

In **paper 4**, "*Hydrogen adsorption in Pt-catalyst/MOF-5" materials*", we studied hydrogen adsorption in MOFs doped/modified with Pt catalysts. We did not observe any features of hydrogen "spillover" effect, the effect which according to some previous publications led to a tremendous increase of hydrogen adsorption in MOF-5 doped/modified with Pt-catalysts[59, 66]. On the contrary, we showed that hydrogen adsorption in MOF-5 mixed/modified with Pt catalysts correlated well with BET surface area of those materials and had very fast kinetics. The highest hydrogen adsorption was measured for the Pt catalyst itself. None of the features attributed to the hydrogen "spillover" effect were observed in this study (e.g. slow kinetics, absence of correlation with BET surface area, linear pressure dependence of adsorption). This article initiated a discussion in the literature regarding reasons behind the absence of "spillover"[22, 172, 173].

My contribution: synthesis of samples; hydrogen adsorption measurements; nitrogen adsorption measurements; recording X-ray diffraction patterns; recording IR spectra; analysis of the data; writing the manuscript.

6.5 Paper 5

In **paper 5**, "*Reaction of C_{60} with Hydrogen Gas: In Situ Monitoring and Pathways*", we studied hydrogenation of C_{60} at T=350-440ºC and a hydrogen pressure of 50bar. The weight change of the sample during hydrogenation was monitored in situ using a gravimetric method and the products of hydrogenation were studied by MS spectrometry and XRD analysis. Hydrogenation kinetics depended strongly on the reaction temperature. At 350-400ºC hydrogenation proceeded slowly and the sample weight saturated after days of hydrogenation. At 420-440ºC hydrogenation proceeded with improved kinetics and after the initial increase the sample weight started to decrease

indicating C_{60} fragmentation and collapse. Independently of the reaction temperature hydrogenation of C_{60} followed the same hydrogenation pathway: $C_{60} \rightarrow C_{60}H_{18} \rightarrow C_{60}H_{36} \rightarrow C_{60}H_{44} \rightarrow C_{60}H_{52}$. Higher reaction temperature resulted in a faster conversion rate of fulleranes with low hydrogen content (e.g. $C_{60}H_{18}$) into fulleranes with a high hydrogen content (e.g. $C_{60}H_{44}$, $C_{60}H_{52}$). Prolonged hydrogenation at 400-440ºC resulted in C_{60} fragmentation and synthesis of fragmented fullerenes with loss of up to seven carbon atoms. Analyzing the products of C_{60} fragmentation we proposed two possible fragmentation models. We performed HPLC experiments aiming at separation and isolation of fulleranes with high hydrogen contents and fragmented fullerenes. Fulleranes were eluted according to the number of hydrogen atoms attached to the C_{60} cage but the complete isolation was not achieved due to the high complexity of the hydrogenation products. The only isolated fullerane was $C_{60}H_{18}$.

My contribution: synthesis of hydrogenated and fragmented C_{60}, participated in high resolution MS measurements; XRD measurements; HPLC separation; analysis of the data; discussion of the data; writing the manuscript.

6.6 Paper 6

In **paper 7**, "*Hydrogenation, Purification, and Unzipping of Carbon Nanotubes by Reaction with Molecular Hydrogen: Road to Graphane Nanoribbons*", we studied hydrogenation of SWCNTs by the direct reaction with molecular hydrogen at 400-550ºC and 50bar of hydrogen pressure. We found that SWCNTs hydrogenated at the conditions of the experiment and that the mechanism of hydrogenation depended on the hydrogenation temperature. At 400-450ºC hydrogenation occurred by formation of C-H covalent bonds and resulted in hydrogenation of ca. $36 \pm 9\%$ of carbon atoms. At 550ºC hydrogenation occurred as etching and resulted in hydrogenation of only ca. $6 \pm 3\%$ of carbon atoms.

As a result of hydrogenation SWCNTs were opened and purified from other forms of carbon. Hydrogenation also removed fullerene-like shells covering Fe catalyst particles. Exposed Fe catalyst particles could be removed by the acid treatment, significantly reducing Fe content in SWCNTs.

Fe catalyst particles were very important for SWCNTs hydrogenation and no hydrogenation was observed for catalyst-free SWCNTs. Hydrogenation also resulted in unzipping of SWCNTs which supposedly started on Fe catalyst particles and progressed further along the tube axis.

My contribution: synthesis of hydrogenated SWCNTs; participating in discussion of the data.

6.7 Paper 7

In **paper 7**, "*Effect of Catalysts on the Reaction of C_{60} with Hydrogen*", we studied hydrogenation of C_{60} at T=400ºC and hydrogen pressure of 50bar with addition of metal catalysts (e.g. Ni, Pt) and compared it with non-catalytic C_{60} hydrogenation. Addition of metal catalysts significantly accelerated hydrogenation kinetics and resulted in synthesis of fulleranes with a different crystal structure. Non-catalytic hydrogenation of C_{60} resulted in synthesis of fulleranes with the FCC crystal structure while addition of metal catalysts resulted in synthesis of fullerane mixtures consisting of FCC and BCC phases. Catalytic hydrogenation started with synthesis of C_{3v} isomer of $C_{60}H_{18}$, the same isomer as synthesized by non-catalytic hydrogenation, and proceeded by formation of fulleranes with higher hydrogen content which had the BCC structure.

My contribution: synthesis of hydrogenated C_{60}, MS measurements; XRD measurements; analysis of the data; discussion of the data; writing the manuscript.

6.8 Paper 8

In **paper 8**, "*Hydrogen-Driven Collapse of C_{60} Inside Single-Walled Carbon Nanotubes*", we studied hydrogenation of C_{60} inserted inside SWCNTs (C_{60}@SWCNTs) at 450-550ºC and 50bar of hydrogen pressure. At 450ºC encapsulated C_{60} reacted with hydrogen forming fulleranes similarly to bulk C_{60}. Pristine C_{60} were partially recovered by annealing of C_{60}@SWCNTs in argon at 950ºC. At 500-550ºC hydrogenation resulted in dimerization and polymerization of C_{60} molecules which was followed by their collapse into some smaller molecules. Formation of only a few inner nanotubes and graphene nanoribbons was observed in our experiments. We assume that after fragmentation, C_{60} fragments were immediately terminated by hydrogen which prohibited their fusion into larger structures.

My contribution: synthesis of hydrogenated C_{60}@SWCNTs; participating in discussion of the data.

7 Acknowledgements

At the end of this thesis I would like to thank all people without whom this work would not be done. First of all, I would like to thank my supervisors Alexandr Talyzin and Bertil Sundqvist for their help during the PhD studies. Many hours of scientific discussions that I had with you are priceless, and they made a huge impact on this Thesis.

During my PhD studies I was supervising lab courses for undergraduate students which was a unique and unforgettable experience. I would like to thank Hans Forsman for giving me the opportunity to teach and Leif Hassmyr for his help with all technical problems related to the lab equipment. As the lab supervisor I had a pleasure to work with many interesting people who can not be forgotten. I would like to thank to all my lab co-supervisors, namely to Mats Forsberg, Alberto Cetoli, Junchun Yu, Mikhail Modestov, Dmitry Kobyakov, with whom I spent many hours in the lab educating undergraduate students.

Of course, I would like to thank Katarina Hassler, Lena Burström, Jörgen Eriksson, and Ann-Charlot Dalberg who solved all science not-related problems letting me concentrate on the research. I would also like to thank Lena Åström and Thomas Gustafsson who were always ready to help if I needed some help in the workshop. I would like to thank all employees at the department of physics who created an inspiring and very positive working atmosphere. It was my pleasure to work with you!

I would like to thank the J.C. Kempe Minnes foundation for providing the financial support.

I am very grateful to our collaborators: Prof. Y. Tsybin for his help with MS measurements, Prof. H. Chun for providing us with MOFs, Prof. F. Cataldo for his help with TGA measurements, Dr. A. Nasibulin and Dr. I. Anoshkin for providing us with SWCNTs and for their help with TEM measurements. Special thank to Dr. T. Kieselbach for his very helpful introduction course into the field of mass spectrometry and for letting me work with MALDI-TOF MS. I would like to thank Dr. A. Gorzsas, who is a lab manager of the vibrational spectroscopy platform at KBC, for his help with IR and Raman measurements.

I would like to thank all my friends and my girlfriend Elwira who were always supporting me in a tough time and sharing my happiness in a good moment.

Finally, I would like to thank my parents, my grandparents, and my brother Andrey who are the most important people in my life. Your love and your support mean a lot to me, and there are no words which can help to express my deepest gratitude to you!

8 References

1. Schlapbach, L.; Zuttel, A., Hydrogen-storage materials for mobile applications. *Nature* **2001,** 414, (6861), 353-358.
2. Schlapbach, L., Technology: Hydrogen-fuelled vehicles. *Nature* **2009,** 460, (7257), 809-811.
3. *http://www.mechanicalengineeringblog.com/wp-content/uploads/2011/03/01- fuelcell_vehicle-FCV-ultimate-Eco-car-Hybrid-technology.jpg*.
4. *http://green.autoblog.com/2007/04/11/first-fuel-cell-hybrid-bus-hits-the-road-in-connecticut/*.
5. *https://www1.eere.energy.gov/hydrogenandfuelcells/mypp/pdfs/storage.pdf*.
6. Fierro, V.; Szczurek, A.; Zlotea, C.; Mareche, J. F.; Izquierdo, M. T.; Albiniak, A.; Latroche, M.; Furdin, G.; Celzard, A., Experimental evidence of an upper limit for hydrogen storage at 77 K on activated carbons. *Carbon* **2010,** 48, (7), 1902-1911.
7. Jin, H.; Lee, Y. S.; Hong, I., Hydrogen adsorption characteristics of activated carbon. *Catalysis Today* **2007,** 120, (3-4), 399-406.
8. Iijima, S., Helical Microtubules of Graphitic Carbon. *Nature* **1991,** 354, (6348), 56-58.
9. Ye, Y.; Ahn, C. C.; Witham, C.; Fultz, B.; Liu, J.; Rinzler, A. G.; Colbert, D.; Smith, K. A.; Smalley, R. E., Hydrogen adsorption and cohesive energy of single-walled carbon nanotubes. *Applied Physics Letters* **1999,** 74, (16), 2307-2309.
10. Xu, W. C.; Takahashi, K.; Matsuo, Y.; Hattori, Y.; Kumagai, M.; Ishiyama, S.; Kaneko, K.; Iijima, S., Investigation of hydrogen storage capacity of various carbon materials. *International Journal of Hydrogen Energy* **2007,** 32, (13), 2504-2512.
11. Panella, B.; Hirscher, M.; Roth, S., Hydrogen adsorption in different carbon nanostructures. *Carbon* **2005,** 43, (10), 2209-2214.
12. Zhang, X. R.; Cao, D. P.; Chen, J. F., Hydrogen adsorption storage on single-walled carbon nanotube arrays by a combination of classical potential and density functional theory. *Journal of Physical Chemistry B* **2003,** 107, (21), 4942-4950.
13. Xia, Y. Y.; Zhu, J. Z. H.; Zhao, M. W.; Li, F.; Huang, B. D.; Ji, Y. J.; Liu, X. D.; Tan, Z. Y.; Song, C.; Yin, Y. Y., Enhancement of hydrogen physisorption on single-walled carbon nanotubes resulting from defects created by carbon bombardment. *Physical Review B* **2005,** 71, (7), 075412 - 075412-8.
14. Chen, C. H.; Huang, C. C., Hydrogen adsorption in defective carbon nanotubes. *Separation and Purification Technology* **2009,** 65, (3), 305-310.
15. Zhu, H. W.; Chen, A.; Mao, Z. Q.; Xu, C. L.; Xiao, X.; Wei, B. Q.; Liang, J.; Wu, D. H., The effect of surface treatments on hydrogen storage of carbon nanotubes. *Journal of Materials Science Letters* **2000,** 19, (14), 1237-1239.
16. Liu, F.; Zhang, X. B.; Cheng, J. P.; Tu, J. P.; Kong, F. Z.; Huang, W. Z.; Chen, C. P., Preparation of short carbon nanotubes by mechanical ball milling and their hydrogen adsorption behavior. *Carbon* **2003,** 41, (13), 2527-2532.
17. Mu, S. C.; Tang, H. L.; Qian, S. H.; Pan, M.; Yuan, R. Z., Hydrogen storage in carbon nanotubes modified by microwave plasma etching and Pd decoration. *Carbon* **2006,** 44, (4), 762-767.
18. Lin, K. Y.; Chang, J. K.; Chen, C. Y.; Tsai, W. T., Effects of heat treatment on materials characteristics and hydrogen storage capability of multi-wall carbon nanotubes. *Diamond and Related Materials* **2009,** 18, (2-3), 553-556.
19. Takagi, H.; Soneda, Y.; Hatori, H.; Zhu, Z. H.; Lu, G. Q., Effects of nitric acid and heat treatment on hydrogen adsorption of single-walled carbon nanotubes. *Australian Journal of Chemistry* **2007,** 60, (7), 519-523.
20. Dillon, A. C.; Jones, K. M.; Bekkedahl, T. A.; Kiang, C. H.; Bethune, D. S.; Heben, M. J., Storage of hydrogen in single-walled carbon nanotubes. *Nature* **1997,** 386, (6623), 377-379.
21. Chambers, A.; Park, C.; Baker, R. T. K.; Rodriguez, N. M., Hydrogen storage in graphite nanofibers. *Journal of Physical Chemistry B* **1998,** 102, (22), 4253-4256.
22. Hirscher, M., Remarks about spillover and hydrogen adsorption - Comments on the contributions of AV Talyzin and RT Yang. *Microporous and Mesoporous Materials* **2010,** 135, (1-3), 209-210.
23. Martin, N. M.; Luzan, S. M.; Talyzin, A. V., High-temperature reactions of C-60 with polycyclic aromatic hydrocarbons. *Chemical Physics* **2010,** 368, (1-2), 49-57.
24. Zhao, D.; Yuan, D. Q.; Zhou, H. C., The current status of hydrogen storage in metal-organic frameworks. *Energy & Environmental Science* **2008,** 1, (2), 222-235.
25. FitzGerald, S. A.; Yildirim, T.; Santodonato, L. J.; Neumann, D. A.; Copley, J. R. D.; Rush, J. J.; Trouw, F., Quantum dynamics of interstitial H-2 in solid C-60. *Physical Review B* **1999,** 60, (9), 6439-6451.
26. FitzGerald, S. A.; Forth, S.; Rinkoski, M., Induced infrared absorption of molecular hydrogen in solid C-60. *Physical Review B* **2002,** 65, (14), 140302 – 140302-4.
27. Talyzin, A. V.; Klyamkin, S., Hydrogen adsorption in C60 at pressures up to 2000 atm. *Chemical Physics Letters* **2004,** 397, (1–3), 77-81.

28. Talyzin, A. V.; Jacob, A., Hydrogen adsorption by ball milled C-60. *Journal of Alloys and Compounds* **2005,** 395, (1-2), 154-158.
29. Talyzin, A. V.; Szabo, T.; Dekany, I.; Langenhorst, F.; Sokolov, P. S.; Solozhenko, V. L., Nanocarbons by High-Temperature Decomposition of Graphite Oxide at Various Pressures. *Journal of Physical Chemistry C* **2009,** 113, (26), 11279-11284.
30. Srinivas, G.; Zhu, Y. W.; Piner, R.; Skipper, N.; Ellerby, M.; Ruoff, R., Synthesis of graphene-like nanosheets and their hydrogen adsorption capacity. *Carbon* **2010,** 48, (3), 630-635.
31. Murray, L. J.; Dinca, M.; Long, J. R., Hydrogen storage in metal-organic frameworks. *Chemical Society Reviews* **2009,** 38, (5), 1294-1314.
32. Furukawa, H.; Ko, N.; Go, Y. B.; Aratani, N.; Choi, S. B.; Choi, E.; Yazaydin, A. O.; Snurr, R. Q.; O'Keeffe, M.; Kim, J.; Yaghi, O. M., Ultrahigh Porosity in Metal-Organic Frameworks. *Science* **2010,** 329, (5990), 424-428.
33. Wang, Z. Q.; Cohen, S. M., Postsynthetic covalent modification of a neutral metal-organic framework. *Journal of the American Chemical Society* **2007,** 129, (41), 12368-12369.
34. Song, Y. F.; Cronin, L., Postsynthetic covalent modification of metal-organic framework (MOF) materials. *Angewandte Chemie-International Edition* **2008,** 47, (25), 4635-4637.
35. Hirscher, M., Hydrogen Storage by Cryoadsorption in Ultrahigh-Porosity Metal-Organic Frameworks. *Angewandte Chemie-International Edition* **2011,** 50, (3), 581-582.
36. Perez, E. V.; Balkus, K. J.; Ferraris, J. P.; Musselman, I. H., Mixed-matrix membranes containing MOF-5 for gas separations. *Journal of Membrane Science* **2009,** 328, (1-2), 165-173.
37. Saha, D.; Wei, Z. J.; Deng, S. G., Equilibrium, kinetics and enthalpy of hydrogen adsorption in MOF-177. *International Journal of Hydrogen Energy* **2008,** 33, (24), 7479-7488.
38. Garrone, E.; Bonelli, B.; Arean, C. O., Enthalpy-entropy correlation for hydrogen adsorption on zeolites. *Chemical Physics Letters* **2008,** 456, (1-3), 68-70.
39. Suh, M. P.; Park, H. J.; Prasad, T. K.; Lim, D. W., Hydrogen Storage in Metal-Organic Frameworks. *Chemical Reviews* **2012,** 112, (2), 782-835.
40. Luzan, S. M.; Jung, H.; Chun, H.; Talyzin, A. V., Hydrogen storage in Co-and Zn-based metal-organic frameworks at ambient temperature. *International Journal of Hydrogen Energy* **2009,** 34, (24), 9754-9759.
41. Frost, H.; Duren, T.; Snurr, R. Q., Effects of surface area, free volume, and heat of adsorption on hydrogen uptake in metal-organic frameworks. *Journal of Physical Chemistry B* **2006,** 110, (19), 9565-9570.
42. Panella, B.; Hones, K.; Muller, U.; Trukhan, N.; Schubert, M.; Putter, H.; Hirscher, M., Desorption studies of hydrogen in metal-organic frameworks. *Angewandte Chemie-International Edition* **2008,** 47, (11), 2138-2142.
43. Rowsell, J. L. C.; Yaghi, O. M., Effects of functionalization, catenation, and variation of the metal oxide and organic linking units on the low-pressure hydrogen adsorption properties of metal-organic frameworks. *Journal of the American Chemical Society* **2006,** 128, (4), 1304-1315.
44. Rowsell, J. L. C.; Yaghi, O. M., Strategies for hydrogen storage in metal-organic frameworks. *Angewandte Chemie-International Edition* **2005,** 44, (30), 4670-4679.
45. Frost, H.; Snurr, R. Q., Design requirements for metal-organic frameworks as hydrogen storage materials. *Journal of Physical Chemistry C* **2007,** 111, (50), 18794-18803.
46. Thornton, A. W.; Nairn, K. M.; Hill, J. M.; Hill, A. J.; Hill, M. R., Metal-Organic Frameworks Impregnated with Magnesium-Decorated Fullerenes for Methane and Hydrogen Storage. *Journal of the American Chemical Society* **2009,** 131, (30), 10662-10669.
47. Chae, H. K.; Siberio-Perez, D. Y.; Kim, J.; Go, Y.; Eddaoudi, M.; Matzger, A. J.; O'Keeffe, M.; Yaghi, O. M., A route to high surface area, porosity and inclusion of large molecules in crystals. *Nature* **2004,** 427, (6974), 523-527.
48. Rowsell, J. L. C.; Eckert, J.; Yaghi, O. M., Characterization of H-2 binding sites in prototypical metal-organic frameworks by inelastic neutron scattering. *Journal of the American Chemical Society* **2005,** 127, (42), 14904-14910.
49. Yildirim, T.; Hartman, M. R., Direct observation of hydrogen adsorption sites and nanocage formation in metal-organic frameworks. *Physical Review Letters* **2005,** 95, (21), 215504 – 215504-4.
50. Hirscher, M.; Panella, B., Hydrogen storage in metal-organic frameworks. *Scripta Materialia* **2007,** 56, (10), 809-812.
51. Botas, J. A.; Calleja, G.; Sanchez-Sanchez, M.; Orcajo, M. G., Cobalt Doping of the MOF-5 Framework and Its Effect on Gas-Adsorption Properties. *Langmuir* **2010,** 26, (8), 5300-5303.
52. Dinca, M.; Han, W. S.; Liu, Y.; Dailly, A.; Brown, C. M.; Long, J. R., Observation of Cu2+-H-2 interactions in a fully desolvated sodalite-type metal-organic framework. *Angewandte Chemie-International Edition* **2007,** 46, (9), 1419-1422.
53. Han, S. S.; Deng, W. Q.; Goddard, W. A., Improved designs of metal-organic frameworks for hydrogen storage. *Angewandte Chemie-International Edition* **2007,** 46, (33), 6289-6292.
54. Mulder, F. M.; Dingemans, T. J.; Wagemaker, M.; Kearley, G. J., Modelling of hydrogen adsorption in the metal organic framework MOF5. *Chemical Physics* **2005,** 317, (2-3), 113-118.
55. Conner, W. C.; Falconer, J. L., Spillover in Heterogeneous Catalysis. *Chemical Reviews* **1995,** 95, (3), 759-788.

56. Contescu, C. I.; Brown, C. M.; Liu, Y.; Bhat, V. V.; Gallego, N. C., Detection of Hydrogen Spillover in Palladium-Modified Activated Carbon Fibers during Hydrogen Adsorption. *Journal of Physical Chemistry C* **2009,** 113, (14), 5886-5890.
57. Sinfelt, J. H.; Lucchesi, P. J., Kinetic Evidence for Migration of Reactive Intermediates in Surface Catalysis. *Journal of the American Chemical Society* **1963,** 85, (21), 3365-3367.
58. Robell, A. J.; Ballou, E. V.; Boudart, M., Surface Diffusion of Hydrogen on Carbon. *Journal of Physical Chemistry* **1964,** 68, (10), 2748-2753.
59. Li, Y. W.; Yang, R. T., Hydrogen storage in metal-organic frameworks by bridged hydrogen spillover. *Journal of the American Chemical Society* **2006,** 128, (25), 8136-8137.
60. Srinivas, S. T.; Rao, P. K., Direct Observation of Hydrogen Spillover on Carbon-Supported Platinum and Its Influence on the Hydrogenation of Benzene. *Journal of Catalysis* **1994,** 148, (2), 470-477.
61. Braunschweig, T.; Roland, U.; Winkler, H., Electrical-Conductivity Study of Hydrogen Spillover on Tio2. *Studies in Surface Science and Catalysis* **1993,** 77, 183-188.
62. Wang, L. F.; Yang, R. T., Hydrogen storage properties of carbons doped with ruthenium, platinum, and nickel nanoparticles. *Journal of Physical Chemistry C* **2008,** 112, (32), 12486-12494.
63. Lachawiec, A. J.; Qi, G. S.; Yang, R. T., Hydrogen storage in nanostructured carbons by spillover: Bridge-building enhancement. *Langmuir* **2005,** 21, (24), 11418-11424.
64. Li, Y. W.; Yang, R. T., Hydrogen storage in low silica type X zeolites. *Journal of Physical Chemistry B* **2006,** 110, (34), 17175-17181.
65. Huang, C. C.; Pu, N. W.; Wang, C. A.; Huang, J. C.; Sung, Y.; Ger, M. D., Hydrogen storage in graphene decorated with Pd and Pt nano-particles using an electroless deposition technique. *Separation and Purification Technology* **2011,** 82, 210-215.
66. Li, Y. W.; Yang, R. T., Significantly enhanced hydrogen storage in metal-organic frameworks via spillover. *Journal of the American Chemical Society* **2006,** 128, (3), 726-727.
67. Stuckert, N. R.; Wang, L. F.; Yang, R. T., Characteristics of Hydrogen Storage by Spillover on Pt-Doped Carbon and Catalyst-Bridged Metal Organic Framework. *Langmuir* **2010,** 26, (14), 11963-11971.
68. Tsao, C. S.; Yu, M. S.; Wang, C. Y.; Liao, P. Y.; Chen, H. L.; Jeng, U. S.; Tzeng, Y. R.; Chung, T. Y.; Wut, H. C., Nanostructure and Hydrogen Spillover of Bridged Metal-Organic Frameworks. *Journal of the American Chemical Society* **2009,** 131, (4), 1404-1406.
69. Wang, L. F.; Stuckert, N. R.; Yang, R. T., Unique Hydrogen Adsorption Properties of Graphene. *Aiche Journal* **2011,** 57, (10), 2902-2908.
70. Ma, L. P.; Wu, Z. S.; Li, J.; Wu, E. D.; Ren, W. C.; Cheng, H. M., Hydrogen adsorption behavior of graphene above critical temperature. *International Journal of Hydrogen Energy* **2009,** 34, (5), 2329-2332.
71. Wang, C. Y.; Tsao, C. S.; Yu, M. S.; Liao, P. Y.; Chung, T. Y.; Wu, H. C.; Miller, M. A.; Tzeng, Y. R., Hydrogen storage measurement, synthesis and characterization of metal-organic frameworks via bridged spillover. *Journal of Alloys and Compounds* **2010,** 492, (1-2), 88-94.
72. Lee, S. Y.; Park, S. J., Effect of platinum doping of activated carbon on hydrogen storage behaviors of metal-organic frameworks-5. *International Journal of Hydrogen Energy* **2011,** 36, (14), 8381-8387.
73. Miller, M. A.; Wang, C. Y.; Merrill, G. N., Experimental and Theoretical Investigation Into Hydrogen Storage via Spillover in IRMOF-8. *Journal of Physical Chemistry C* **2009,** 113, (8), 3222-3231.
74. Campesi, R.; Cuevas, F.; Latroche, M.; Hirscher, M., Hydrogen spillover measurements of unbridged and bridged metal-organic frameworks-revisited. *Physical Chemistry Chemical Physics* **2010,** 12, (35), 10457-10459.
75. Ardelean, O.; Blanita, G.; Borodi, G.; Mihet, M.; Coros, M.; Lupu, D., On the enhancement of hydrogen uptake by IRMOF-8 composites with Pt/carbon catalyst. *International Journal of Hydrogen Energy* **2012,** 37, (9), 7378-7384.
76. Li, Y. W.; Yang, F. H.; Yang, R. T., Kinetics and mechanistic model for hydrogen spillover on bridged metal-organic frameworks. *Journal of Physical Chemistry C* **2007,** 111, (8), 3405-3411.
77. Campesi, R.; Cuevas, F.; Gadiou, R.; Leroy, E.; Hirscher, M.; Vix-Guterl, C.; Latroche, M., Hydrogen storage properties of Pd nanoparticle/carbon template composites. *Carbon* **2008,** 46, (2), 206-214.
78. Li, Y. W.; Yang, F. H.; Yang, R. T., Reply to "Comment on 'Kinetics and Mechanistic Model for Hydrogen Spillover on Bridged Metal-Organic Frameworks'". *Journal of Physical Chemistry C* **2008,** 112, (8), 3155-3156.
79. Mavrandonakis, A.; Klopper, W., Comment on “Kinetics and Mechanistic Model for Hydrogen Spillover on Bridged Metal-Organic Frameworks”. *The Journal of Physical Chemistry C* **2008,** 112, (8), 3152-3154.
80. Psofogiannakis, G. M.; Froudakis, G. E., DFT Study of the Hydrogen Spillover Mechanism on Pt-Doped Graphite. *Journal of Physical Chemistry C* **2009,** 113, (33), 14908-14915.
81. Jain, P.; Fonseca, D. A.; Schaible, E.; Lueking, A. D., Hydrogen uptake of platinum-doped graphite nanoribers and stochastic analysis of hydrogen spillover. *Journal of Physical Chemistry C* **2007,** 111, (4), 1788-1800.
82. Anson, A.; Lafuente, E.; Urriolabeitia, E.; Navarro, R.; Benito, A. M.; Maser, W. K.; Martinez, M. T., Hydrogen capacity of palladium-loaded carbon materials. *Journal of Physical Chemistry B* **2006,** 110, (13), 6643-6648.
83. Prins, R., Hydrogen Spillover. Facts and Fiction. *Chemical Reviews* **2012,** 112, (5), 2714-2738.

84. Zaluska, A.; Zaluski, L.; Strom-Olsen, J. O., Nanocrystalline magnesium for hydrogen storage. *Journal of Alloys and Compounds* **1999,** 288, (1-2), 217-225.
85. Grochala, W.; Edwards, P. P., Thermal decomposition of the non-interstitial hydrides for the storage and production of hydrogen. *Chemical Reviews* **2004,** 104, (3), 1283-1315.
86. Wagemans, R. W. P.; van Lenthe, J. H.; de Jongh, P. E.; van Dillen, A. J.; de Jong, K. P., Hydrogen storage in magnesium clusters: Quantum chemical study. *Journal of the American Chemical Society* **2005,** 127, (47), 16675-16680.
87. Loutfy, R. O.; Wexler, E. M., Gas-phase hydrogenation of fullerenes. *Perspectives of Fullerene Nanotechnology* **2002**, 281-287.
88. Loutfy, R. O.; Wexler, E. M., Hydrogenation of alkali metal-doped fullerenes. *Perspectives of Fullerene Nanotechnology* **2002**, 289-292.
89. Kroto, H. W.; Heath, J. R.; Obrien, S. C.; Curl, R. F.; Smalley, R. E., C-60 - Buckminsterfullerene. *Nature* **1985,** 318, (6042), 162-163.
90. Henderson, C. C.; Cahill, P. A., C60h2 - Synthesis of the Simplest C60 Hydrocarbon Derivative. *Science* **1993,** 259, (5103), 1885-1887.
91. Ballenweg, S.; Gleiter, R.; Kratschmer, W., Hydrogenation of Buckminsterfullerene C-60 Via Hydrozirconation - a New Way to Organofullerenes. *Tetrahedron Letters* **1993,** 34, (23), 3737-3740.
92. Ruchardt, C.; Gerst, M.; Ebenhoch, J.; Beckhaus, H. D.; Campbell, E. E. B.; Tellgmann, R.; Schwarz, H.; Weiske, T.; Pitter, S., Bimolecular Radical Formation through H-Transfer .3. Transfer Hydrogenation and Deuteration of Buckminsterfullerene C-60 by 9,10-Dihydroanthracene and 9,9',10,10'[D(4)]Dihydroanthracene. *Angewandte Chemie-International Edition in English* **1993,** 32, (4), 584-586.
93. Cliffel, D. E.; Bard, A. J., Electrochemical Studies of the Protonation of C-60- and C-60(2-). *Journal of Physical Chemistry* **1994,** 98, (33), 8140-8143.
94. Darwish, A. D.; Abdulsada, A. K.; Langley, G. J.; Kroto, H. W.; Taylor, R.; Walton, D. R. M., Polyhydrogenation of [60]-Fullerenes and [70]-Fullerenes. *Journal of the Chemical Society-Perkin Transactions 2* **1995**, (12), 2359-2365.
95. Avent, A. G.; Darwish, A. D.; Heimbach, D. K.; Kroto, H. W.; Meidine, M. F.; Parsons, J. P.; Remars, C.; Roers, R.; Ohashi, O.; Taylor, R.; Walton, D. R. M., Formation of Hydrides of Fullerene-C-60 and Fullerene-C-70. *Journal of the Chemical Society-Perkin Transactions 2* **1994**, (1), 15-22.
96. Attalla, M. I.; Vassallo, A. M.; Tattam, B. N.; Hanna, J. V., Preparation of Hydrofullerenes by Hydrogen Radical-Induced Hydrogenation. *Journal of Physical Chemistry* **1993,** 97, (24), 6329-6331.
97. Fukuzumi, S.; Suenobu, T.; Kawamura, S.; Ishida, A.; Mikami, K., Selective two-electron reduction of C-60 by 10-methyl-9,10-dihydroacridine via photoinduced electron transfer. *Chemical Communications* **1997**, (3), 291-292.
98. Jin, C. M.; Hettich, R.; Compton, R.; Joyce, D.; Blencoe, J.; Burch, T., Direct Solid-Phase Hydrogenation of Fullerenes. *Journal of Physical Chemistry* **1994,** 98, (16), 4215-4217.
99. Petrie, S.; Javahery, G.; Wang, J.; Bohme, D. K., Derivatization of the Fullerene Dications C-60(2+) and C-70(2+) by Ion Molecule Reactions in the Gas-Phase. *Journal of the American Chemical Society* **1992,** 114, (23), 9177-9181.
100. Talyzin, A. V.; Shulga, Y. M.; Jacob, A., Comparative study of hydrofullerides C60Hx synthesized by direct and catalytic hydrogenation. *Applied Physics a-Materials Science & Processing* **2004,** 78, (7), 1005-1010.
101. Talyzin, A. V.; Tsybin, Y. O.; Peera, A. A.; Schaub, T. M.; Marshall, A. G.; Sundqvist, B.; Mauron, P.; Zuttel, A.; Billups, W. E., Synthesis of C59Hx and C58Hx fullerenes stabilized by hydrogen. *Journal of Physical Chemistry B* **2005,** 109, (12), 5403-5405.
102. Talyzin, A. V.; Tsybin, Y. O.; Schaub, T. M.; Mauron, P.; Shulga, Y. M.; Zuttel, A.; Sundqvist, B.; Marshall, A. G., Composition of hydrofullerene mixtures produced by go reaction with hydrogen gas revealed by high-resolution mass spectrometry. *Journal of Physical Chemistry B* **2005,** 109, (26), 12742-12747.
103. Talyzin, A. V.; Tsybin, Y. O.; Purcell, J. M.; Schaub, T. M.; Shulga, Y. M.; Noreus, D.; Sato, T.; Dzwilewski, A.; Sundqvist, B.; Marshall, A. G., Reaction of hydrogen gas with C-60 at elevated pressure and temperature: Hydrogenation and cage fragmentation. *Journal of Physical Chemistry A* **2006,** 110, (27), 8528-8534.
104. Luzan, S. M.; Tsybin, Y. O.; Talyzin, A. V., Reaction of C(60) with Hydrogen Gas: In Situ Monitoring and Pathways. *Journal of Physical Chemistry C* **2011,** 115, (23), 11484-11492.
105. Tarasov, B. P.; Shul'ga, Y. M.; Fokin, V. N.; Vasilets, V. N.; Shul'ga, N. Y.; Schur, D. V.; Yartys, V. A., Deuterofullerene C60D24 studied by XRD, IR and XPS. *Journal of Alloys and Compounds* **2001,** 314, (1-2), 296-300.
106. Shul'ga, Y. M.; Tarasov, B. P.; Fokin, V. N.; Martynenko, V. M.; Schur, D. V.; Volkov, G. A.; Rubtsov, V. I.; Krasochka, G. A.; Chapusheva, N. V.; Shevchenko, V. V., Deuterofullerenes. *Carbon* **2003,** 41, (7), 1365-1368.
107. Darwish, A. D.; Avent, A. G.; Taylor, R.; Walton, D. R. M., Structural characterisation of C60H18; a C-3v symmetry crown. *Journal of the Chemical Society-Perkin Transactions 2* **1996**, (10), 2051-2054.
108. Cataldo, F., Iglesias-Groth, S., Fulleranes: The Hydrogenated Fullerenes. *Springer* **2010,** ISSN 1875-0745.

109. Itaka, K.; Yamashiro, M.; Yamaguchi, J.; Haemori, M.; Yaginuma, S.; Matsumoto, Y.; Kondo, M.; Koinuma, H., High-mobility C-60 field-effect molecular-wetting controlled transistors fabricated on substrates. *Advanced Materials* **2006,** 18, (13), 1713-1716.
110. Antonov, V. E.; Bashkin, I. O.; Khasanov, S. S.; Moravsky, A. P.; Morozov, Y. G.; Shulga, Y. M.; Ossipyan, Y. A.; Ponyatovsky, E. G., Magnetic ordering in hydrofullerite C60H24. *Journal of Alloys and Compounds* **2002,** 330, 365-368.
111. Tarasov, B. P.; Fokin, V. N.; Moravskii, A. P.; Shulga, Y. M., Reactions of fullerenes with deuterium in the presence of palladium. *Russian Chemical Bulletin* **1996,** 45, (7), 1778-1779.
112. Luzan, S. M.; Talyzin, A. V., Effect of Catalysts on the Reaction of C-60 with Hydrogen. *Fullerenes Nanotubes and Carbon Nanostructures* **2012,** 20, (4-7), 319-323.
113. Luzan, S. M.; Tsybin, Y. O.; Talyzin, A. V., Reaction of C-60 with Hydrogen Gas: In Situ Monitoring and Pathways. *Journal of Physical Chemistry C* **2011,** 115, (23), 11484-11492.
114. Wagberg, T.; Johnels, D.; Peera, A.; Hedenstrom, M.; Schulga, Y. M.; Tsybin, Y. O.; Purcell, J. M.; Marshall, A. G.; Noreus, D.; Sato, T.; Talyzin, A. V., Selective synthesis of the C-3v isomer of C60H18. *Organic Letters* **2005,** 7, (25), 5557-5560.
115. Hall, L. E.; Mckenzie, D. R.; Attalla, M. I.; Vassallo, A. M.; Davis, R. L.; Dunlop, J. B.; Cockayne, D. J. H., The Structure of C60h36. *Journal of Physical Chemistry* **1993,** 97, (21), 5741-5744.
116. Schur, D. V.; Zaginaichenko, S. Y.; Savenko, A. F.; Bogolepov, V. A.; Anikina, N. S.; Zolotarenko, A. D.; Matysina, Z. A.; Veziroglu, T. N.; Skryabina, N. E., Experimental evaluation of total hydrogen capacity for fullerite C(60). *International Journal of Hydrogen Energy* **2011,** 36, (1), 1143-1151.
117. Peera, A. A.; Alemany, L. B.; Billups, W. E., Hydrogen storage in hydrofullerides. *Applied Physics a-Materials Science & Processing* **2004,** 78, (7), 995-1000.
118. Teprovich, J. A.; Wellons, M. S.; Lascola, R.; Hwang, S. J.; Ward, P. A.; Compton, R. N.; Zidan, R., Synthesis and Characterization of a Lithium-Doped Fullerane (Li-x-C-60-H-y) for Reversible Hydrogen Storage. *Nano Letters* **2012,** 12, (2), 582-589.
119. Nossal, J.; Saini, R. K.; Alemany, L. B.; Meier, M.; Billups, W. E., The synthesis and characterization of fullerene hydrides. *European Journal of Organic Chemistry* **2001**, (22), 4167-4180.
120. Haufler, R. E.; Conceicao, J.; Chibante, L. P. F.; Chai, Y.; Byrne, N. E.; Flanagan, S.; Haley, M. M.; Obrien, S. C.; Pan, C.; Xiao, Z.; Billups, W. E.; Ciufolini, M. A.; Hauge, R. H.; Margrave, J. L.; Wilson, L. J.; Curl, R. F.; Smalley, R. E., Efficient Production of C60 (Buckminsterfullerene), C60h36, and the Solvated Buckide Ion. *Journal of Physical Chemistry* **1990,** 94, (24), 8634-8636.
121. Popov, A. A.; Senyavin, V. V.; Granovsky, A. A.; Lobach, A. S., Vibrational spectra and molecular structure of the hydrofullerenes C60H18, C60D18, and C60H36 as studied by IR and Raman spectroscopy and first-principle calculations. *Hydrogen Materials Science and Chemistry of Carbon Nanomaterials* **2004,** 172, 347-356.
122. Balasubramanian, K., Enumeration of Isomers of Polysubstituted C60 and Application to Nmr. *Chemical Physics Letters* **1991,** 182, (3-4), 257-262.
123. Clare, B. W.; Kepert, D. L., The structures of C60F36 and new possible structures for C60H36. *Journal of Molecular Structure-Theochem* **1999,** 466, 177-186.
124. Nossal, J.; Saini, R. K.; Sadana, A. K.; Bettinger, H. F.; Alemany, L. B.; Scuseria, G. E.; Billups, W. E.; Saunders, M.; Khong, A.; Weisemann, R., Formation, isolation, spectroscopic properties, and calculated properties of some isomers of C60H36. *Journal of the American Chemical Society* **2001,** 123, (35), 8482-8495.
125. Bucsi, I.; Szabo, P.; Aniszfeld, R.; Prakash, G. K. S.; Olah, G. A., HPLC separation of hydrogenated derivatives of buckminsterfullerene. *Chromatographia* **1998,** 48, (1-2), 59-64.
126. Talyzin, A. V.; Sundqvist, B.; Shulga, Y. M.; Peera, A. A.; Imus, P.; Billups, W. E., Gentle fragmentation of C-60 by strong hydrogenation: a route to synthesizing new materials. *Chemical Physics Letters* **2004,** 400, (1-3), 112-116.
127. Sakurai, H.; Daiko, T.; Hirao, T., A synthesis of sumanene, a fullerene fragment. *Science* **2003,** 301, (5641), 1878-1878.
128. Steinberg, B. D.; Jackson, E. A.; Filatov, A. S.; Wakamiya, A.; Petrukhina, M. A.; Scott, L. T., Aromatic pi-Systems More Curved Than C(60). The Complete Family of All Indenocorannulenes Synthesized by Iterative Microwave-Assisted Intramolecular Arylations. *Journal of the American Chemical Society* **2009,** 131, (30), 10537-10545.
129. Wu, T. C.; Hsin, H. J.; Kuo, M. Y.; Li, C. H.; Wu, Y. T., Synthesis and Structural Analysis of a Highly Curved Buckybowl Containing Corannulene and Sumanene Fragments. *Journal of the American Chemical Society* **2011,** 133, (41), 16319-16321.
130. Wu, Y. T.; Siegel, J. S., Aromatic molecular-bowl hydrocarbons: Synthetic derivatives, their structures, and physical properties. *Chemical Reviews* **2006,** 106, (12), 4843-4867.
131. Miller, G. P.; Kintigh, J.; Kim, E.; Weck, P. F.; Berber, S.; Tomanek, D., Hydrogenation of single-wall carbon nanotubes using polyamine reagents: Combined experimental and theoretical study. *Journal of the American Chemical Society* **2008,** 130, (7), 2296-2303.

132. Zhang, G. Y.; Qi, P. F.; Wang, X. R.; Lu, Y. R.; Mann, D.; Li, X. L.; Dai, H. J., Hydrogenation and hydrocarbonation and etching of single-walled carbon nanotubes. *Journal of the American Chemical Society* **2006,** 128, (18), 6026-6027.
133. Nikitin, A.; Ogasawara, H.; Mann, D.; Denecke, R.; Zhang, Z.; Dai, H.; Cho, K.; Nilsson, A., Hydrogenation of single-walled carbon nanotubes. *Physical Review Letters* **2005,** 95, (22), 225507 – 225507-4.
134. Nikitin, A.; Li, X. L.; Zhang, Z. Y.; Ogasawara, H.; Dai, H. J.; Nilsson, A., Hydrogen storage in carbon nanotubes through the formation of stable C-H bonds. *Nano Letters* **2008,** 8, (1), 162-167.
135. Kosynkin, D. V.; Higginbotham, A. L.; Sinitskii, A.; Lomeda, J. R.; Dimiev, A.; Price, B. K.; Tour, J. M., Longitudinal unzipping of carbon nanotubes to form graphene nanoribbons. *Nature* **2009,** 458, (7240), 872-876.
136. Cataldo, F.; Compagnini, G.; Patane, G.; Ursini, O.; Angelini, G.; Ribic, P. R.; Margaritondo, G.; Cricenti, A.; Palleschi, G.; Valentini, F., Graphene nanoribbons produced by the oxidative unzipping of single-wall carbon nanotubes. *Carbon* **2010,** 48, (9), 2596-2602.
137. Kosynkin, D. V.; Lu, W.; Sinitskii, A.; Pera, G.; Sun, Z. Z.; Tour, J. M., Highly Conductive Graphene Nanoribbons by Longitudinal Splitting of Carbon Nanotubes Using Potassium Vapor. *Acs Nano* **2011,** 5, (2), 968-974.
138. Jiao, L. Y.; Zhang, L.; Wang, X. R.; Diankov, G.; Dai, H. J., Narrow graphene nanoribbons from carbon nanotubes. *Nature* **2009,** 458, (7240), 877-880.
139. Zhao, N. Q.; He, C. N.; Li, J. J.; Jiang, Z. Y.; Li, Y. D., Study on purification and tip-opening of CNTs fabricated by CVD. *Materials Research Bulletin* **2006,** 41, (12), 2204-2209.
140. Okazaki, T.; Iizumi, Y.; Okubo, S.; Kataura, H.; Liu, Z.; Suenaga, K.; Tahara, Y.; Yudasaka, M.; Okada, S.; Iijima, S., Coaxially Stacked Coronene Columns inside Single-Walled Carbon Nanotubes. *Angewandte Chemie-International Edition* **2011,** 50, (21), 4853-4857.
141. Takenobu, T.; Takano, T.; Shiraishi, M.; Murakami, Y.; Ata, M.; Kataura, H.; Achiba, Y.; Iwasa, Y., Stable and controlled amphoteric doping by encapsulation of organic molecules inside carbon nanotubes. *Nature Materials* **2003,** 2, (10), 683-688.
142. Guan, L. H.; Shi, Z. J.; Li, M. X.; Gu, Z. N., Ferrocene-filled single-walled carbon nanotubes. *Carbon* **2005,** 43, (13), 2780-2785.
143. Yao, M. G.; Stenmark, P.; Abou-Hamad, E.; Nitze, F.; Qin, J. A.; Goze-Bac, C.; Wagberg, T., Confined adamantane molecules assembled to one dimension in carbon nanotubes. *Carbon* **2011,** 49, (4), 1159-1166.
144. Talyzin, A. V.; Anoshkin, I. V.; Krasheninnikov, A. V.; Nieminen, R. M.; Nasibulin, A. G.; Jiang, H.; Kauppinen, E. I., Synthesis of Graphene Nanoribbons Encapsulated in Single-Walled Carbon Nanotubes. *Nano Letters* **2011,** 11, (10), 4352-4356.
145. Abou-Hamad, E.; Kim, Y.; Talyzin, A. V.; Goze-Bac, C.; Luzzi, D. E.; Rubio, A.; Wagberg, T., Hydrogenation of C(60) in Peapods: Physical Chemistry in Nano Vessels. *Journal of Physical Chemistry C* **2009,** 113, (20), 8583-8587.
146. Moisala, A.; Nasibulin, A. G.; Brown, D. P.; Jiang, H.; Khriachtchev, L.; Kauppinen, E. I., Single-walled carbon nanotube synthesis using ferrocene and iron pentacarbonyl in a laminar flow reactor. *Chemical Engineering Science* **2006,** 61, (13), 4393-4402.
147. Kataura, H.; Maniwa, Y.; Kodama, T.; Kikuchi, K.; Hirahara, K.; Iijima, S.; Suzuki, S.; Kratschmer, W.; Achiba, Y., Fullerene-peapods: Synthesis, structure, and Raman spectroscopy. *Electronic Properties of Molecular Nanostructures* **2001,** 591, 251-255.
148. Sing, K. S. W.; Everett, D. H.; Haul, R. A. W.; Moscou, L.; Pierotti, R. A.; Rouquerol, J.; Siemieniewska, T., Reporting Physisorption Data for Gas Solid Systems with Special Reference to the Determination of Surface-Area and Porosity (Recommendations 1984). *Pure and Applied Chemistry* **1985,** 57, (4), 603-619.
149. Dubinin, M. M., The Potential Theory of Adsorption of Gases and Vapors for Adsorbents with Energetically Nonuniform Surfaces. *Chemical Reviews* **1960,** 60, (2), 235-241.
150. Horvath, G.; Kawazoe, K., Method for the Calculation of Effective Pore-Size Distribution in Molecular-Sieve Carbon. *Journal of Chemical Engineering of Japan* **1983,** 16, (6), 470-475.
151. Saito, A.; Foley, H. C., Curvature and Parametric Sensitivity in Models for Adsorption in Micropores. *Aiche Journal* **1991,** 37, (3), 429-436.
152. Cheng, L. S.; Yang, R. T., Improved Horvath-Kawazoe Equations Including Spherical Pore Models for Calculating Micropore Size Distribution. *Chemical Engineering Science* **1994,** 49, (16), 2599-2609.
153. Barrett, E. P.; Joyner, L. G.; Halenda, P. P., The Determination of Pore Volume and Area Distributions in Porous Substances .1. Computations from Nitrogen Isotherms. *Journal of the American Chemical Society* **1951,** 73, (1), 373-380.
154. Ravikovitch, P. I.; Vishnyakov, A.; Russo, R.; Neimark, A. V., Unified approach to pore size characterization of microporous carbonaceous materials from N-2, Ar, and CO2 adsorption isotherms. *Langmuir* **2000,** 16, (5), 2311-2320.
155. Tarazona, P., Free-Energy Density Functional for Hard-Spheres. *Physical Review A* **1985,** 31, (4), 2672-2679.
156. *(Sackler NAS Colloquium) Scientific Examination of Art: Modern Techniques in Conservation and Analysis*. The National Academies Press: 2005.

157. Stroobant, E. H. V., Mass Spectrometry Principles and Applications. *ISBN 978-0-470-03311-1 - John Wiley & Sons* **2008**, (Third Edition).
158. Xuan, W. M.; Zhu, C. F.; Liu, Y.; Cui, Y., Mesoporous metal-organic framework materials. *Chemical Society Reviews* **2012,** 41, (5), 1677-1695.
159. Meek, S. T.; Greathouse, J. A.; Allendorf, M. D., Metal-Organic Frameworks: A Rapidly Growing Class of Versatile Nanoporous Materials. *Advanced Materials* **2011,** 23, (2), 249-267.
160. Sculley, J.; Yuan, D. Q.; Zhou, H. C., The current status of hydrogen storage in metal-organic frameworks-updated. *Energy & Environmental Science* **2011,** 4, (8), 2721-2735.
161. Dybtsev, D. N.; Chun, H.; Kim, K., Rigid and flexible: A highly porous metal-organic framework with unusual guest-dependent dynamic behavior. *Angewandte Chemie-International Edition* **2004,** 43, (38), 5033-5036.
162. Chun, H.; Moon, J., Discovery, synthesis, and characterization of an isomeric coordination polymer with pillared kagome net topology. *Inorganic Chemistry* **2007,** 46, (11), 4371-4373.
163. Chun, H.; Jung, H. J.; Seo, J. W., Isoreticular Metal-Organic Polyhedral Networks Based on 5-Connecting Paddlewheel Motifs. *Inorganic Chemistry* **2009,** 48, (5), 2043-2047.
164. Chun, H.; Jung, H., Targeted Synthesis of a prototype MOF Based on Zn-4(O)(O2C)(6) Units and a Nonlinear Dicarboxylate Ligand. *Inorganic Chemistry* **2009,** 48, (2), 417-419.
165. Chun, H.; Jung, H.; Koo, G.; Jeong, H.; Kim, D. K., Efficient hydrogen sorption in 8-connected MOFs based on trinuclear pinwheel motifs. *Inorganic Chemistry* **2008,** 47, (12), 5355-5359.
166. Li, J. P.; Cheng, S. J.; Zhao, Q.; Long, P. P.; Dong, J. X., Synthesis and hydrogen-storage behavior of metal-organic framework MOF-5. *International Journal of Hydrogen Energy* **2009,** 34, (3), 1377-1382.
167. Li, H.; Eddaoudi, M.; O'Keeffe, M.; Yaghi, O. M., Design and synthesis of an exceptionally stable and highly porous metal-organic framework. *Nature* **1999,** 402, (6759), 276-279.
168. Panella, B.; Hirscher, M., Hydrogen physisorption in metal-organic porous crystals. *Advanced Materials* **2005,** 17, (5), 538-541.
169. Saha, D. P. D.; Deng, S. G.; Yang, Z. G., Hydrogen adsorption on metal-organic framework (MOF-5) synthesized by DMF approach. *Journal of Porous Materials* **2009,** 16, (2), 141-149.
170. Biliskov, N.; Baranovic, G., Infrared spectroscopy of liquid water-N,N-dimethylformamide mixtures. *Journal of Molecular Liquids* **2009,** 144, (3), 155-162.
171. Luzan, S. M.; Talyzin, A. V., Hydrogen adsorption in Pt catalyst/MOF-5 materials. *Microporous and Mesoporous Materials* **2010,** 135, (1-3), 201-205.
172. Luzan, S. M.; Talyzin, A. V., Comment to the "Response to "Hydrogen adsorption in Pt catalyst/MOF-5 materials"" by Li et al. [1]. *Microporous and Mesoporous Materials* **2011,** 139, (1-3), 216-218.
173. Li, Y. W.; Wang, L. F.; Yang, R. T., Response to "hydrogen adsorption in Pt catalyst/MOF-5 materials" by Luzan and Talyzin. *Microporous and Mesoporous Materials* **2010,** 135, (1-3), 206-208.
174. Wang, L. F.; Stuckert, N. R.; Chen, H.; Yang, R. T., Effects of Pt Particle Size on Hydrogen Storage on Pt-Doped Metal-Organic Framework IRMOF-8. *Journal of Physical Chemistry C* **2011,** 115, (11), 4793-4799.
175. Wang, L.; Yang, R. T., Hydrogen Storage Properties of Carbons Doped with Ruthenium, Platinum, and Nickel Nanoparticles. *The Journal of Physical Chemistry C* **2008,** 112, (32), 12486-12494.
176. Wang, L. F.; Yang, F. H.; Yang, R. T.; Miller, M. A., Effect of Surface Oxygen Groups in Carbons on Hydrogen Storage by Spillover. *Industrial & Engineering Chemistry Research* **2009,** 48, (6), 2920-2926.
177. Liu, Y. Y.; Ju-Lan, Z.; Jian, Z.; Xu, F.; Sun, L. X., Improved hydrogen storage in the modified metal-organic frameworks by hydrogen spillover effect. *International Journal of Hydrogen Energy* **2007,** 32, (16), 4005-4010.
178. Zhao, Y. F.; Heben, M. J.; Dillon, A. C.; Simpson, L. J.; Blackburn, J. L.; Dorn, H. C.; Zhang, S. B. B., Nontrivial tuning of the hydrogen-binding energy to fullerenes with endohedral metal dopants. *Journal of Physical Chemistry C* **2007,** 111, (35), 13275-13279.
179. Talyzin, A. V.; Tsybin, Y. O.; Purcell, J. M.; Schaub, T. M.; Shulga, Y. M.; Noréus, D.; Sato, T.; Dzwilewski, A.; Sundqvist, B.; Marshall, A. G., Reaction of Hydrogen Gas with C60 at Elevated Pressure and Temperature: Hydrogenation and Cage Fragmentation†. *The Journal of Physical Chemistry A* **2006,** 110, (27), 8528-8534.
180. Lobach, A. S.; Tarasov, B. P.; Shulga, Y. M.; Perov, A. A.; Stepanov, A. N., Reaction of D-2 with palladium fulleride C60Pd4.9. *Russian Chemical Bulletin* **1996,** 45, (2), 464-465.
181. Meletov, K. P.; Kourouklis, G. A., High-pressure hydrogenated fullerenes: Optical spectra and stability of C60H36 at high pressure. *Journal of Experimental and Theoretical Physics* **2005,** 100, (4), 760-774.
182. Talyzin, A.; Dzwilewski, A.; Sundqvist, B.; Tsybin, Y. O.; Purcell, J. M.; Marshall, A. G.; Shulga, Y. M.; McCammon, C.; Dubrovinsky, L., Hydrogenation Of C-60 at 2 GPa pressure and high temperature. *Chemical Physics* **2006,** 325, (2), 445-451.
183. Talyzin, A. V.; Dzwilewski, A.; Pudelko, M., Formation of palladium fullerides and their thermal decomposition into palladium nanoparticles. *Carbon* **2007,** 45, (13), 2564-2569.
184. Talyzin, A. V.; Dubrovinsky, L. S.; Le Bihan, T.; Jansson, U., Pressure-induced polymerization of C-60 at high temperatures: An in situ Raman study. *Physical Review B* **2002,** 65, (24), 245413 – 245413-10.

185. Pekker, S.; Kovats, E.; Oszlanyi, G.; Benyei, G.; Klupp, G.; Bortel, G.; Jalsovszky, I.; Jakab, E.; Borondics, F.; Kamaras, K.; Bokor, M.; Kriza, G.; Tompa, K.; Faigel, G., Rotor-stator molecular crystals of fullerenes with cubane. *Nature Materials* **2005,** 4, (10), 764-767.
186. Pekker, S.; Salvetat, J. P.; Jakab, E.; Bonard, J. M.; Forro, L., Hydrogenation of carbon nanotubes and graphite in liquid ammonia. *Journal of Physical Chemistry B* **2001,** 105, (33), 7938-7943.
187. Abou-Hamad, E.; Kim, Y.; Talyzin, A. V.; Goze-Bac, C.; Luzzi, D. E.; Rubio, A.; Wagberg, T., Hydrogenation of C-60 in Peapods: Physical Chemistry in Nano Vessels. *Journal of Physical Chemistry C* **2009,** 113, (20), 8583-8587.
188. Bhowmick, R.; Rajasekaran, S.; Friebel, D.; Beasley, C.; Jiao, L. Y.; Ogasawara, H.; Dai, H. J.; Clemens, B.; Nilsson, A., Hydrogen Spillover in Pt-Single-Walled Carbon Nanotube Composites: Formation of Stable C-H Bonds. *Journal of the American Chemical Society* **2011,** 133, (14), 5580-5586.
189. Kim, K. S.; Park, K. A.; Kim, H. J.; Bae, D. J.; Lim, S. C.; Lee, Y. H., Band gap modulation of a carbon nanotube by hydrogen functionalization. *Journal of the Korean Physical Society* **2003,** 42, S137-S142.
190. Nasibulin, A. G.; Pikhitsa, P. V.; Jiang, H.; Brown, D. P.; Krasheninnikov, A. V.; Anisimov, A. S.; Queipo, P.; Moisala, A.; Gonzalez, D.; Lientschnig, G.; Hassanien, A.; Shandakov, S. D.; Lolli, G.; Resasco, D. E.; Choi, M.; Tomanek, D.; Kauppinen, E. I., A novel hybrid carbon material. *Nature Nanotechnology* **2007,** 2, (3), 156-161.